Aeroradiometric Measurements in the Framework of the Swiss Exercises ARM15, GNU15 and the International Exercise AGC15

Gernot Butterweck, Benno Bucher, Ladislaus Rybach, Georg Schwarz,
Bénédicte Hofstetter-Boillat, Eike Hohmann, Sabine Mayer,
Cristina Danzi, Gerald Scharding

PSI Bericht Nr. 15-04
December 2015
ISSN 1019-0643

PAUL SCHERRER INSTITUT

Aeroradiometric Measurements in the Framework of the Swiss Exercises ARM15, GNU15 and the International Exercise AGC15

Gernot Butterweck[1], Benno Bucher[2], Ladislaus Rybach[3], Georg Schwarz[2], Bénédicte Hofstetter-Boillat [1], Eike Hohmann [1], Sabine Mayer[1], Cristina Danzi[4], Gerald Scharding[4]

1 Division for Radiation Safety and Security, Paul Scherrer Institute (PSI), 5232 Villigen PSI, Switzerland
2 Swiss Federal Nuclear Safety Inspectorate (ENSI), Industriestrasse 19, 5200 Brugg, Switzerland
3 Institute of Geophysics, Swiss Federal Institute of Technology Zürich (ETHZ), 8092 Zürich, Switzerland
4 Swiss National Emergency Operations Center (NEOC), 8044 Zürich, Switzerland

Paul Scherrer Institut (PSI)
5232 Villigen PSI, Switzerland
Tel. +41 56 310 21 11
Fax +41 56 310 21 99
www.psi.ch

PSI Bericht Nr. 15-04
December 2015
ISSN 1019-0643

Abstract

The exercise ARM15 started with measurements in Switzerland performed on June 11th and 12th, 2015 organized by the National Emergency Operations Centre (NEOC) under coordination from the Expert Group for Aeroradiometrics (FAR). According to the alternating schedule of the annual ARM exercises, the environs of the nuclear power plants Gösgen (KKG) and Mühleberg (KKM) were surveyed. Additionally, the environs of KKG were inspected on September 16th during the emergency drill GNU15.
Following a request of the University of Basel additional measurements were performed in the Urseren and Piora Valleys.
Further tests with the prototype of a new airborne gammaspectrometry system and the associated data evaluation software were performed, showing performance improvements since 2014 and indicating areas, where further advancement is necessary.
The major part of the exercise consisted of the participation in the International Airborne Gamma Counting exercise AGC15 organized by the Bundesamt für Strahlenschutz (BfS) in Germany from June 14th to 19th, 2015. The results of the intercomparison will be evaluated, interpreted and published in detail by BfS. Thus, the presented report is limited to the documentation of the measurements performed by the Swiss team.

Contents

List of Figures

List of Tables

1 Introduction

Swiss airborne gamma spectrometry measurements started in 1986. Methodology and software for calibration, data acquisition and mapping were developed at the Institute of Geophysics of the Swiss Federal Institute of Technology Zurich (ETHZ). Between 1989 and 1993 the environs of Swiss nuclear installations were measured annually on behalf of the Swiss Federal Nuclear Safety Inspectorate (ENSI). This schedule was changed to biannual inspections in 1994, together with an organizational inclusion of the airborne gamma-spectrometric system into the Emergency Organization Radioactivity (EOR) of the Federal Office for Civil Protection (FOCP). The deployment of the airborne gamma-spectrometric system is organized by the National Emergency Operations Centre (NEOC). NEOC is also responsible for the recruitment and instruction of the measurement team and the operational readiness of the system. Aerial operations are coordinated and performed by the Swiss Air Force. The gamma-spectrometric equipment is stationed at the military airfield of Dübendorf. The gamma-spectrometry system can be airborne within four hours. Responsibility for scientific support, development and maintenance of the aeroradiometric measurement equipment passed from ETHZ to the Radiation Metrology Section of the Paul Scherrer Institute (PSI) in 2003 in cooperation with ENSI. General scientific coordination and planning of the annual measuring flights is provided by the Expert Group for Aeroradiometrics (FAR). FAR was a working group of the Swiss Federal Commission for NBC-protection (ComNBC) and consists of experts from all Swiss institutions concerned with aeroradiometry. FAR was re-organized as an expert group of the NEOC in 2008. Additional information can be found at `http://www.far.ensi.ch/`. This report focuses on methodological aspects and thus complements the short report of NEOC about the annual flight surveys (available from the NEOC website `https://www.naz.ch`).

1.1 Measuring System

The measuring system consists of four NaI-detectors with a total volume of 16.8 l. The measurements were performed with detector package (Detector D, Radiation Solutions RSX4) which includes digital spectrometers with a maximum resolution of 1024 channels for each detector. To render the data evaluation compatible to the old systems, the spectral resolution is reduced to 256 channels. The measurement control, data acquisition and storage are performed with an industrial grade personal computer. A second, identically configured PC is present in the electronics rack (Figure 1) as redundancy. Under normal operation conditions, this PC is used for real-time evaluation and mapping of the data. The positioning uses GPS (Global Positioning System) in the improved EGNOS (European Geostationary Navigation Overlay Service) mode. Together with spectrum and position, air pressure, air temperature and radar altitude are registered. The measuring system is mounted in an Aerospatiale AS 332 Super Puma helicopter of the Swiss Air Force (Figure 2). This helicopter has excellent navigation properties and allows emergency operation during bad weather conditions and nighttime. The detector is mounted in the cargo bay below the center of the helicopter. The cargo bay is covered with a lightweight honeycomb plate to minimize photon absorption losses.

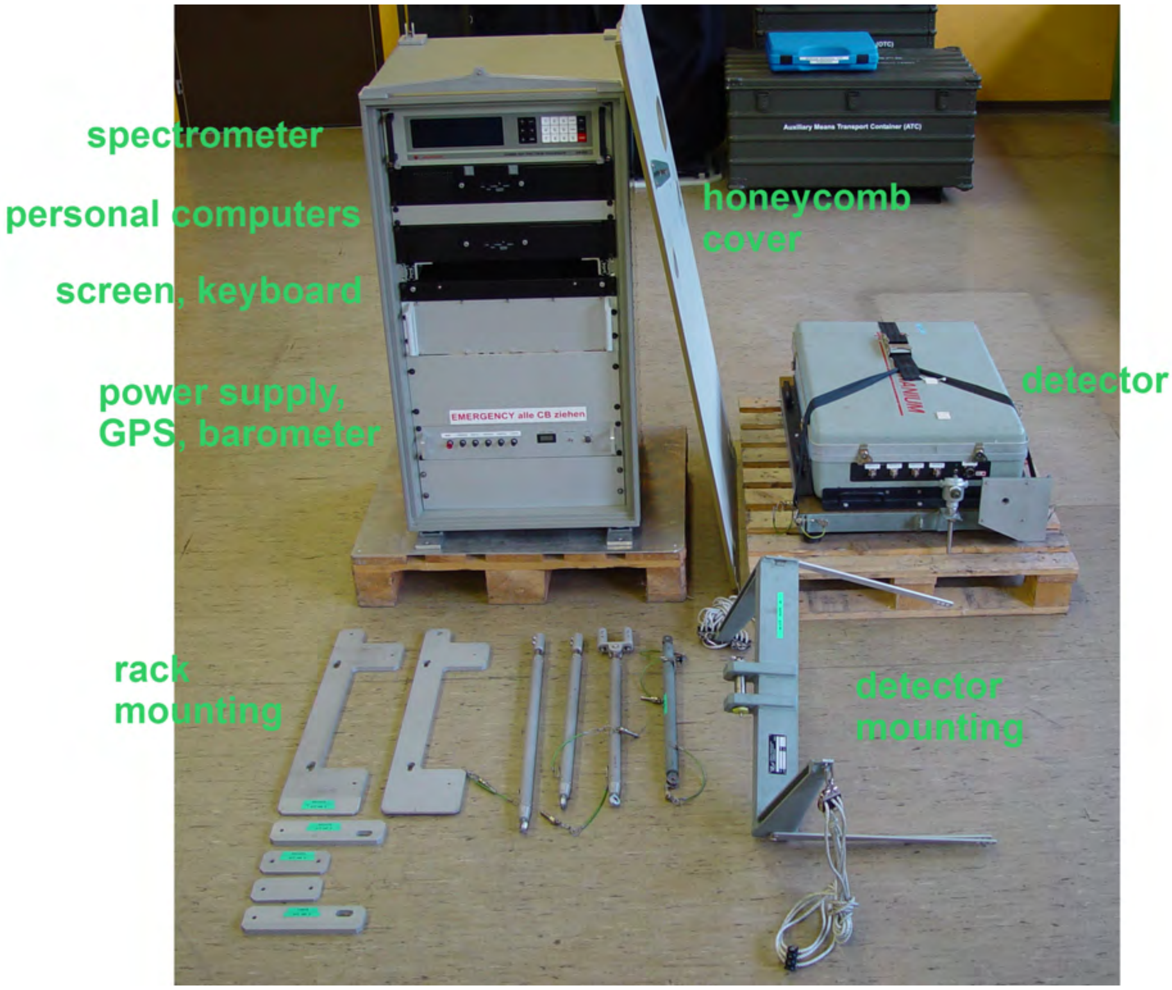

Figure 1: Measurement system of the Swiss team.

Figure 2: Super Puma helicopter of the Swiss Air Force.

1.2 Characterisation of spectroscopic performance

The evaluation of the spectra uses energy windows to determine activities or activity concentrations of different radionuclides. Due to emission characteristics, Compton-Scattering and the energy resolution of the detectors, photons originating from a specific radionuclide may be registered in energy windows assigned for a different radionuclide. For illustration, Figure 3 shows the spectrum of a ^{232}Th-source including the background of the irradiation room (black curve) and the different energy windows used for the spectrum evaluation (vertical lines). The influence of a given radionuclide to a specific energy window has to be determined experimentally for the quantification of correction factors of the measured count rates (stripping correction matrix). The ratio of the measured counts from each source in each energy window to the counts in the energy windows assigned to the radionuclide (Table 1) are the basis for the stripping correction matrix stored in the detector definition file (see section 6). A re-evaluation of the stripping correction matrix for all detectors performed in 2014 leads to observable different results compared to the previous years. Nevertheless, these differences are well within the measurement and evaluation uncertainties.

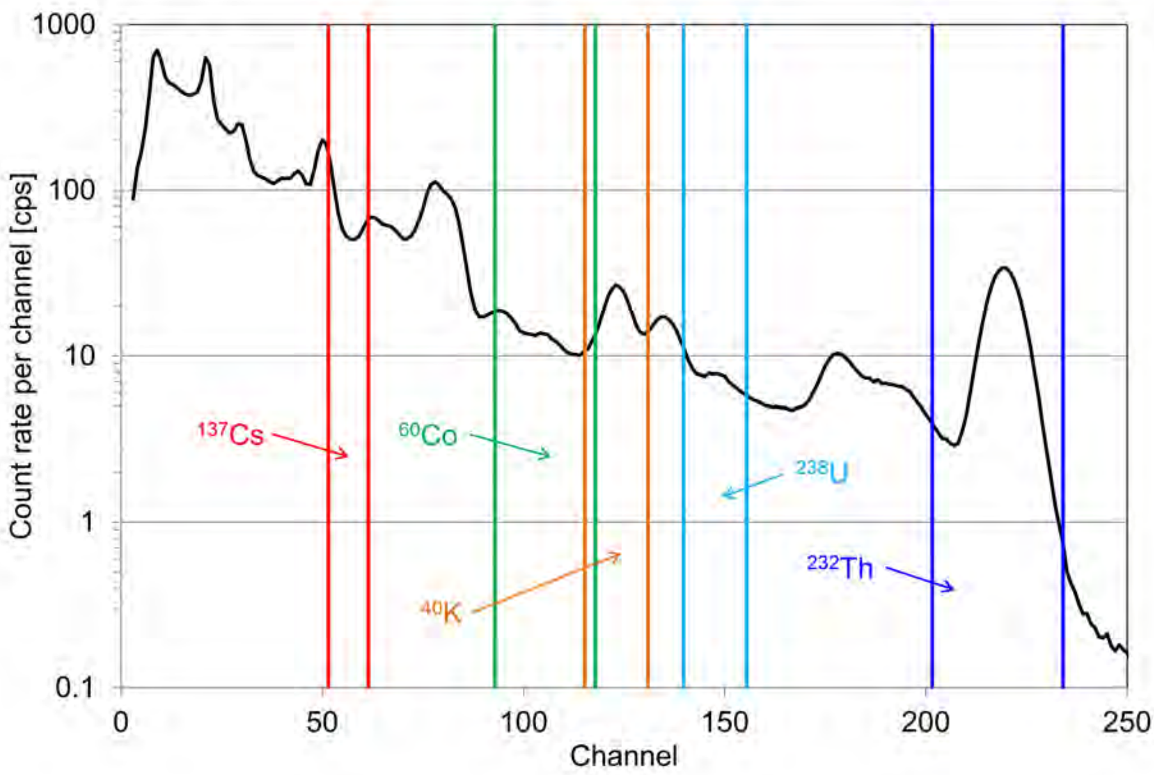

Figure 3: Spectrum of ^{232}Th and energy windows for the evaluation.

	Radionuclide				
Energy window	Potassium	Uranium	Thorium	Caesium	Cobalt
Potassium	1.0	0.8	0.3	0.0	0.1
Uranium	0.0	1.0	0.2	0.0	0.0
Thorium	0.0	0.1	1.0	0.0	0.0
Caesium	0.1	3.0	1.4	1.0	0.2
Cobalt	0.3	2.2	0.5	0.0	1.0

Table 1: Ratio of counts in the energy windows.

1.3 Measuring flights

The advantage of aeroradiometric measurements lies in the high velocity of measurements in a large area, even over rough terrain. Uniform radiological information of an area is obtained from a regular grid of measuring points. This grid is composed from parallel flight lines which are 100 m to 500 m apart, depending on the scope of the measurement. The flight altitude above ground is aspired to be constant during the measuring flight. Typical values lie between 50 m and 100 m above ground. The spectra are recorded in regular time intervals of typical one second, yielding integration over 28 meters of the flight line at a velocity of 100 km/h.

1.4 Data evaluation

The data evaluation follows the methodology described in Schwarz (1991). Since the year 2000, software developed by the Research Group for Geothermics and Radiometry of the Institute of Geophysics of the Swiss Federal Institute of Technology Zurich (ETHZ) with on-line mapping options (Bucher, 2001) is used.

1.5 Data presentation

A first brief report (Kurzbericht) of the measurement results is compiled by the measurement team and published immediately after the end of the exercise on the homepage of NEOC. These reports are archived at `http://www.far.ensi.ch`. Results of a further data evaluation are published in the form of a PSI-report. For all measuring areas, a map of the total dose rate (measuring quantity H*(10) at 1 m above ground) and the flight lines is presented together with a map of the Man-Made-Gross-Count (MMGC) ratio. A map of the ^{232}Th activity concentration (measuring quantity activity per dry mass) yields quality information as it can be expected that this quantity is constant over time. As an additional quality measure, an appendix with the basic parameters of the data evaluation is added to simplify a re-evaluation of the data in the future. If the MMGC-ratio indicates elevated values, maps of individual radionuclides are added based on the average photon spectrum over the affected area. In the case of large changes of topography in the measured area, a map of the terrestrial dose rate consisting of the total dose rate reduced of the altitude dependent cosmic component is included. In the case of measuring flights with the main purpose of mapping natural radionuclide concentrations, a supplementary map of the ^{40}K activity concentration (measuring quantity activity per wet mass) is presented. All maps use a gradual color scale from blue for low values to red for high values. The maximum and minimum values are specified in the legend together with the measurement unit of the depicted quantity. The colors for 10 percent steps between minimum and maximum values of the scale are given in Table 2. Minimum and maximum of the color scale for the measured quantity are generally set to standard values to facilitate easier comparison of maps. Maps with different value ranges are added if considered helpful to the reader.

Percentage	$\leq$0	10	20	30	40	50	60	70	80	90	$\geq$100
Color											

Table 2: Quantification of the color scale.

2 Results of the measuring flights during the exercises ARM15, AGC15 and GNU15

The flights of the exercises ARM15 and AGC15 were performed with a Super Puma helicopter of the Swiss Air Force between June 11th and 19th, 2015. Flight velocity of all measuring flights was around 30 m/s with a ground clearance of 90 m. The counting interval of the spectra was one second.
Personnel of the military unit Stab BR NAZ performed the measurements supported by experts from ENSI, PSI and NEOC. A short report of the measurement results was placed on the NEOC website `https://www.naz.ch/` on June 19th, 2015.
Representatives of KomZenABC-Kamir participated in the comparison measurements between different detectors at PSI in March 2015.
The environs of KKG were additionally inspected on September 16th during the emergency drill GNU15.
Flight parameters of the comparison measurements and the exercises ARM15, AGC15 and GNU15 are listed in Table 3.

Location	Flight number	Date	Measuring time [s]	Length of run [km]	Area [km^2]
KKG	2015008	12.6.2015	7764	359	86
KKG (GNU15)	2015030	16.9.2015	7808	458	87
KKM	2015006	11.6.2015	6449	298	68
Urseren Valley	2015005	11.6.2015	1292	50	13
Piora Valley	2015004	11.6.2015	1344	49	11
Intercomparison	2015003	18.3.2015	1941	129	17
Reference area	2015016	15.6.2015	2627	120	38
Composite mapping	2015017 2015018	16.6.2015	8889	474	459
Source search	2015022	17.6.2015	2340	87	2
Joint mapping E	2015024	17.6.2015	5285	244	63
Joint mapping F	2015025	18.6.2015	4865	224	58
Joint mapping D	2015027	18.6.2015	5049	214	54

Table 3: Flight data of ARM15, AGC15 and GNU15.

2.1 Missing and faulty spectra

The evaluation of the data revealed problems in the spectrum acquisition during the measurements of June 11th and June 12th. About one to two percent of the spectra were transmitted empty to the data acquisition computer. Two percent of the missing spectra were associated with a faulty spectrum in the successive data point. Figure 4 shows an example of a faulty spectrum. It depicts a sudden shift in the count rate at channel 55, which increases from normal 10 to 20 counts per channel to over 5000 counts per channel and can be clearly attributed to a measurement artifact. The cause of the missing and faulty spectra could be attributed to a malfunction of the serial port of the data acquisition computer. The system design with two redundant computers allowed a re-routing of data acquisition to the data evaluation computer prior to the international intercomparison exercise. No missing or faulty spectra were observed after the modification.

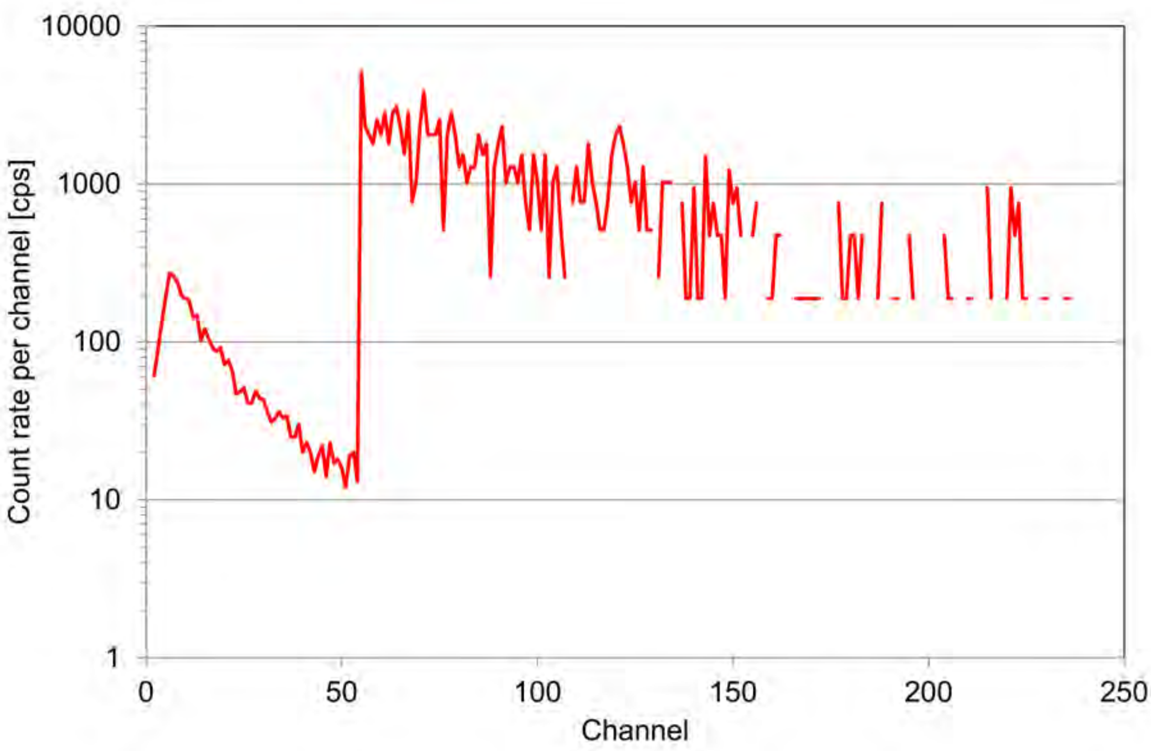

Figure 4: Faulty spectrum.

2.2 Recurrent measurement area KKG

According to a biannual rotation of routine measurements, the environs of the nuclear power plant Gösgen (KKG) were inspected in 2015. KKG was in maintenance shutdown during the measuring flight. Additionally, the environs of KKG were inspected on September 16th during the emergency drill GNU15. A new flight pattern with variable spacing of flight lines in dependence on the distance to KKG was tested during GNU15. The existing gridding algorithm uses a uniform cell size, which was set to 250 meters to compromise between the different line spacings. This algorithm should be adapted to take into account variable flight line spacing to optimize mapping performance. The dose rate maps (Figures 5 and 8) and the maps of the ^{232}Th-activity concentration (Figures 7 and 10) show normal values in the vicinity of KKG. The pattern due to the reduced values caused by the attenuation of photons in water bodies is the only distinguishable feature in these maps. No indication of artificial radionuclides is visible as higher values of the MMGC-ratio (Figures 6 and 9).

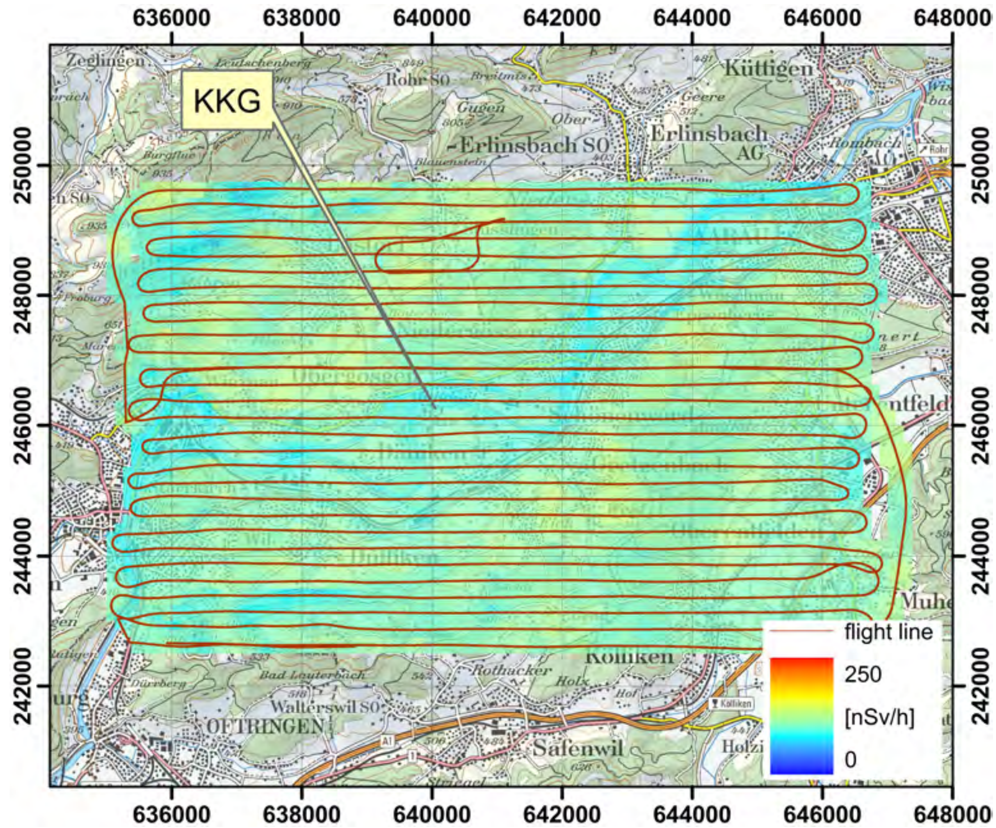

Figure 5: Dose rate in the vicinity of KKG. PK100 ©2015 swisstopo (JD100042).

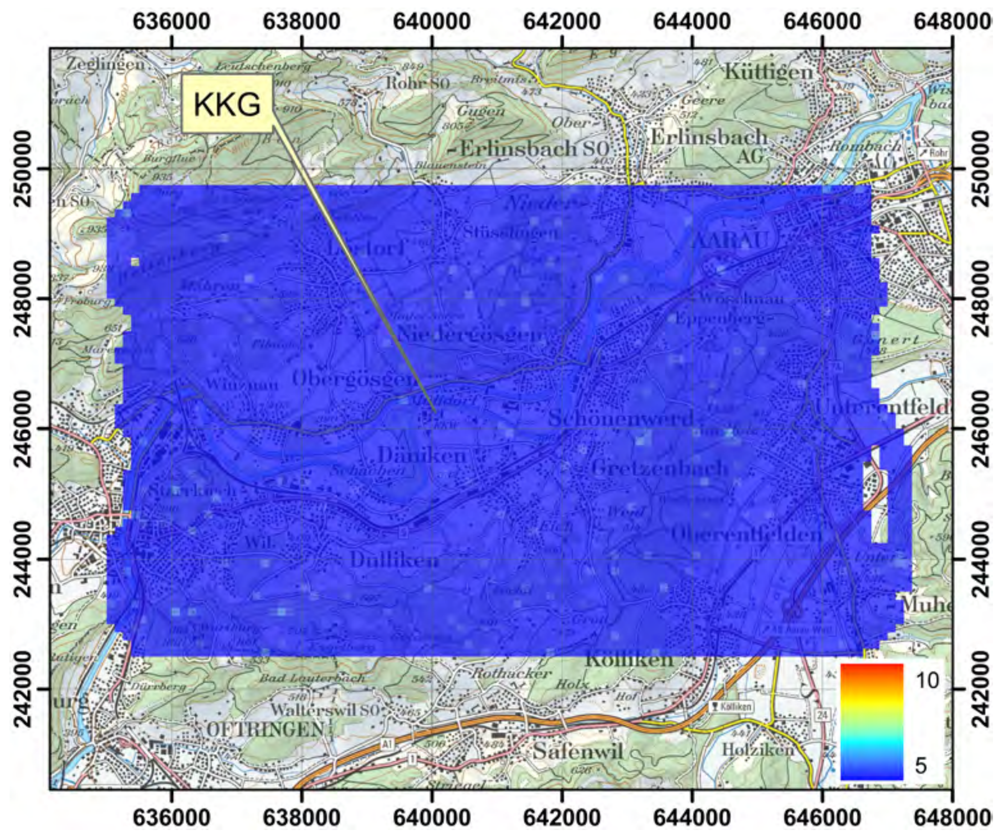

Figure 6: MMGC-ratio in the vicinity of KKG. PK100 ©2015 swisstopo (JD100042).

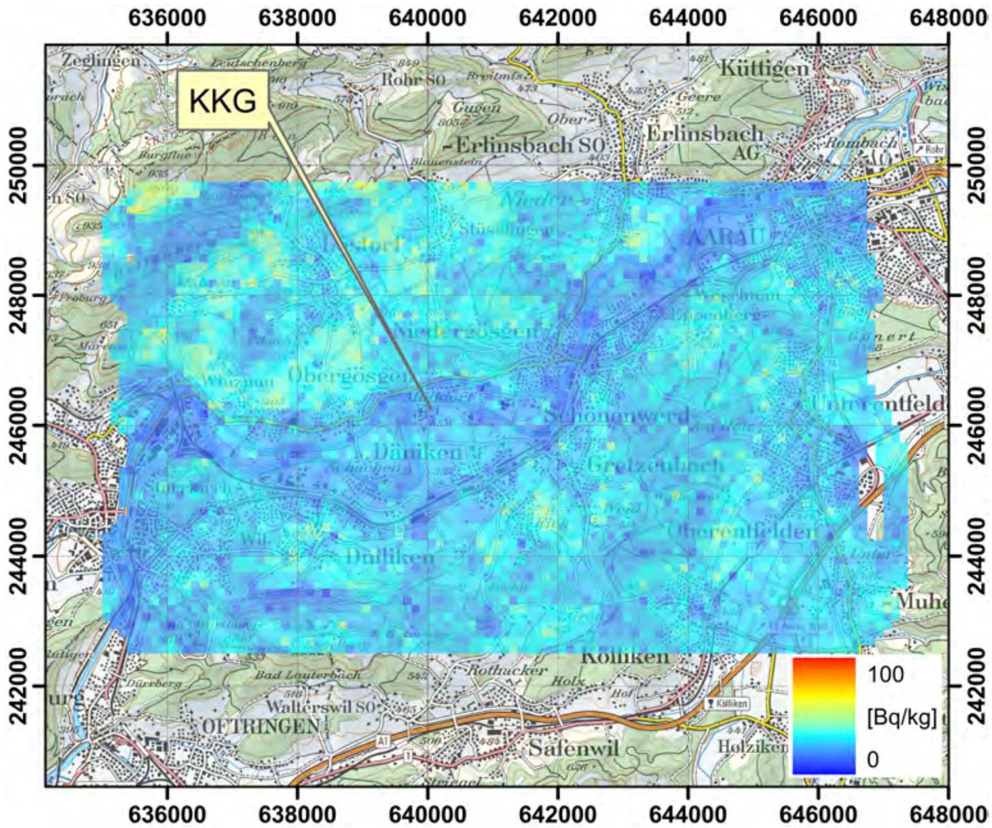

Figure 7: ^{232}Th activity concentration in the vicinity of KKG.
PK100 ©2015 swisstopo (JD100042).

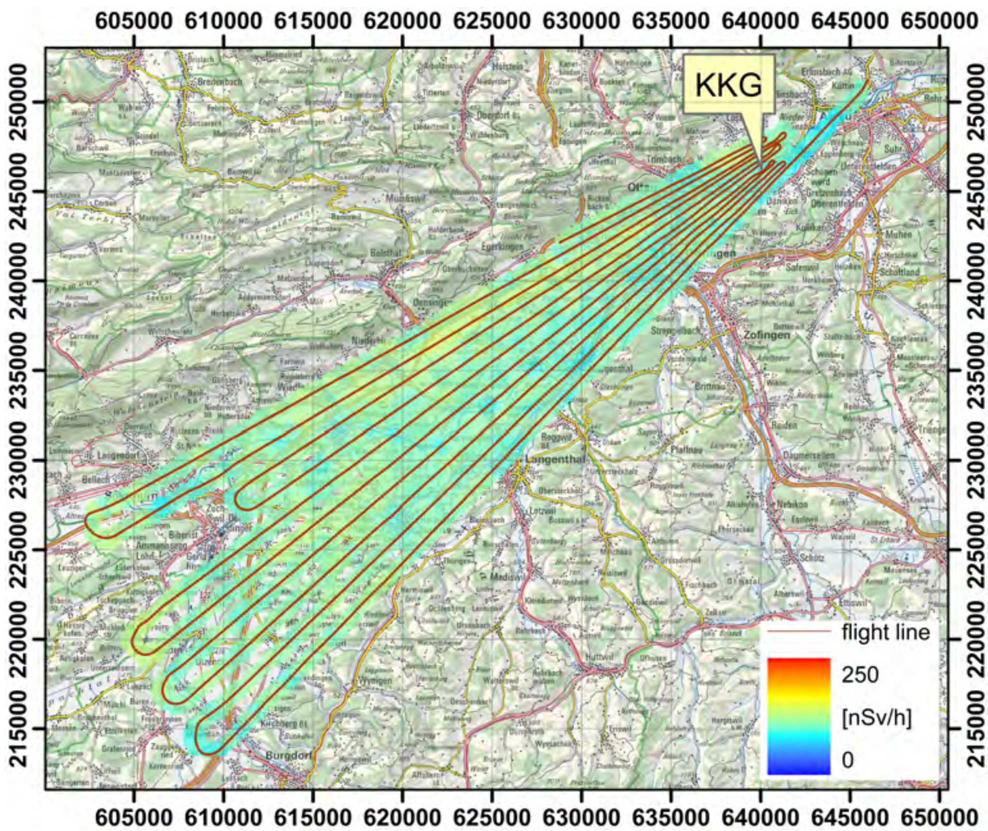

Figure 8: Dose rate in the vicinity of KKG. PK200 ©2015 swisstopo (JD100042).

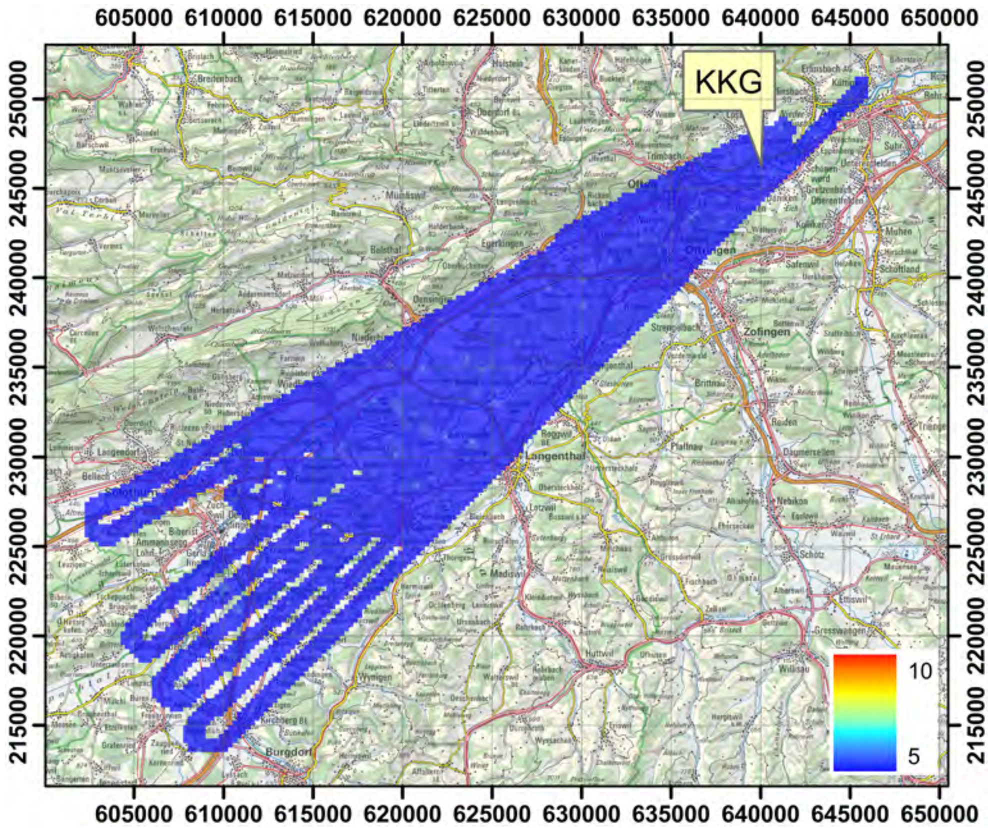

Figure 9: MMGC-ratio in the vicinity of KKG. PK200 ©2015 swisstopo (JD100042).

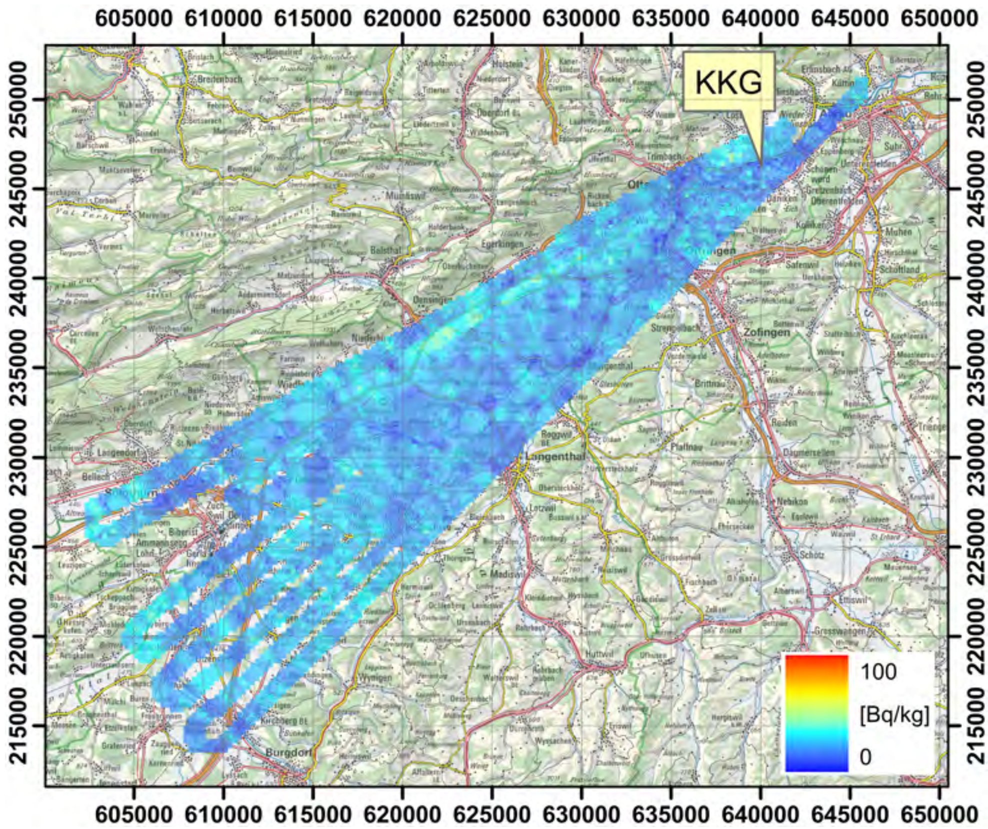

Figure 10: ^{232}Th activity concentration in the vicinity of KKG.
PK200 ©2015 swisstopo (JD100042).

2.3 Recurrent measurement area KKM

According to a biannual rotation of routine measurements, the environs of the nuclear power plant Mühleberg (KKM) were inspected in 2015. The dose rate map (Figure 11) and the maps of the MMGC-ratio (Figure 12) and ^{232}Th activity concentration (Figure 13) show values in the normal background range outside of the plant premises. Elevated values over the plant are due to the nuclide ^{16}N. This nuclide is transported in a boiling water reactor with the primary steam to the turbines in the engine building. The roof of the engine building is less shielded than the reactor building and the high energy photon radiation of ^{16}N can thus be detected from above. Due to Compton scattering in the engine building, air and detector, increased count rates are produced over the whole energy range of the spectrum leading to misinterpretations by the data evaluation algorithms. The apparently high ^{232}Th values at KKM (Figure 13) are one example.

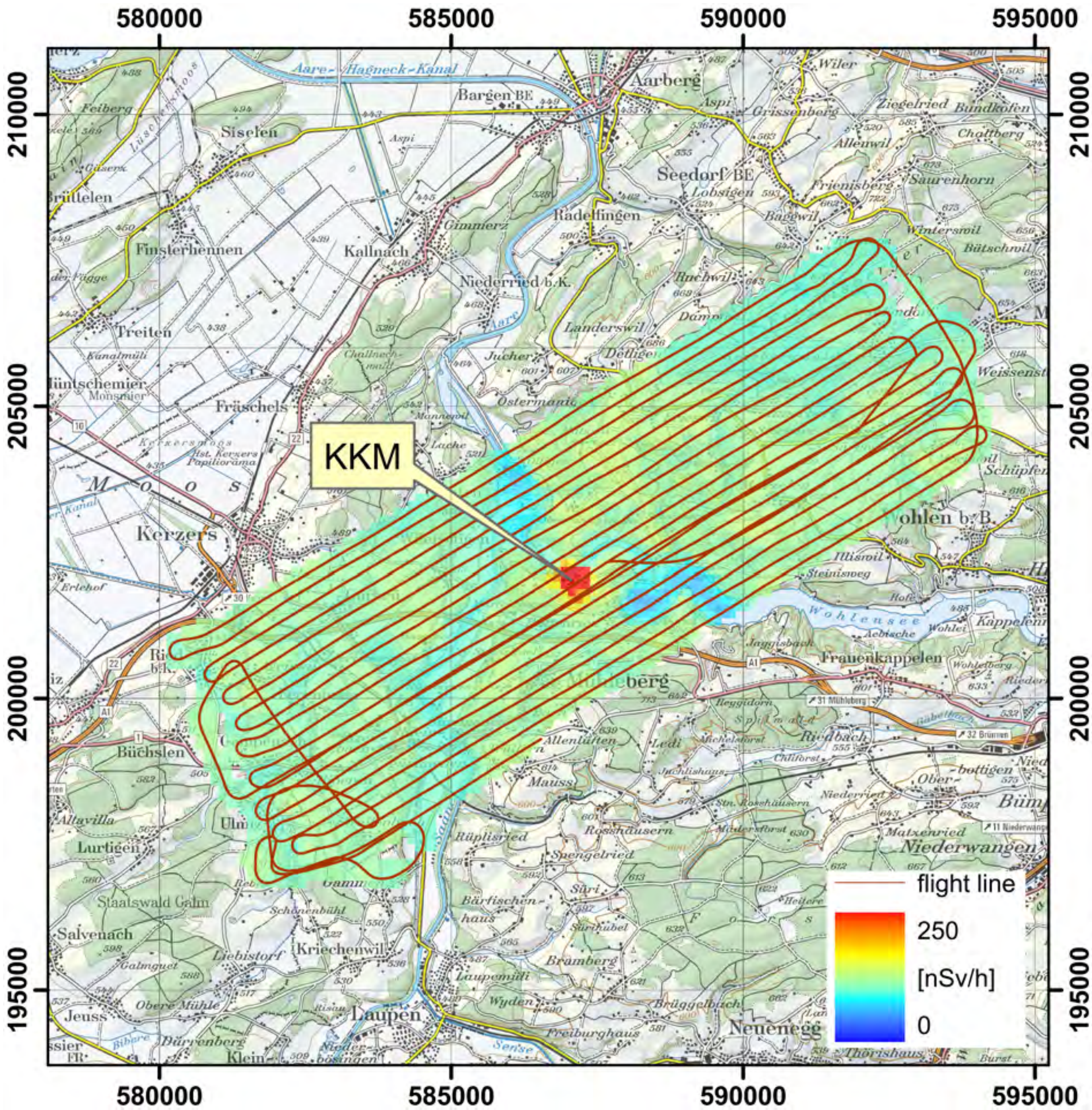

Figure 11: Dose rate in the vicinity of KKM. PK100 ©2015 swisstopo (JD100042).

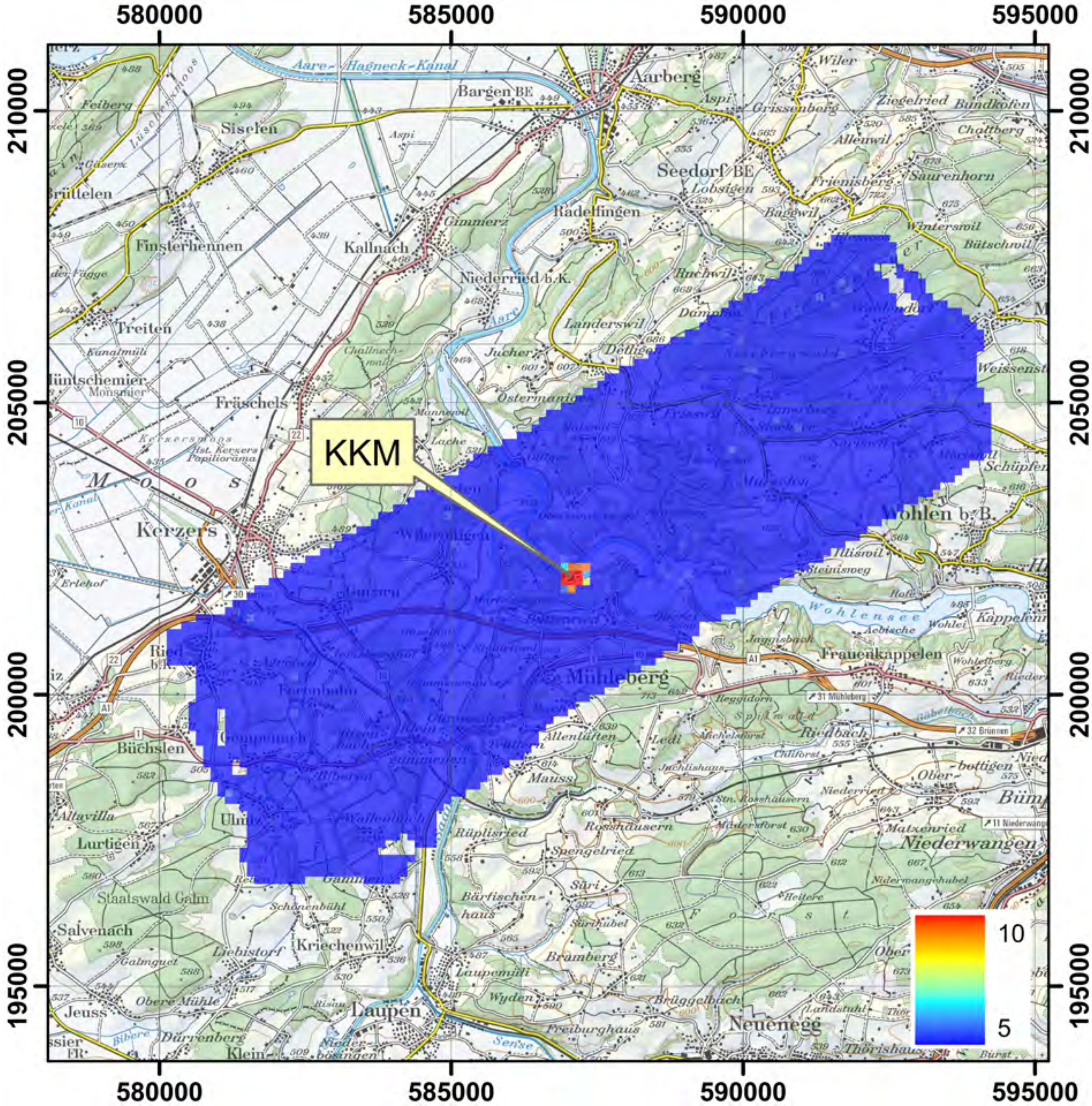

Figure 12: MMGC-ratio in the vicinity of KKM. PK100 ©2015 swisstopo (JD100042).

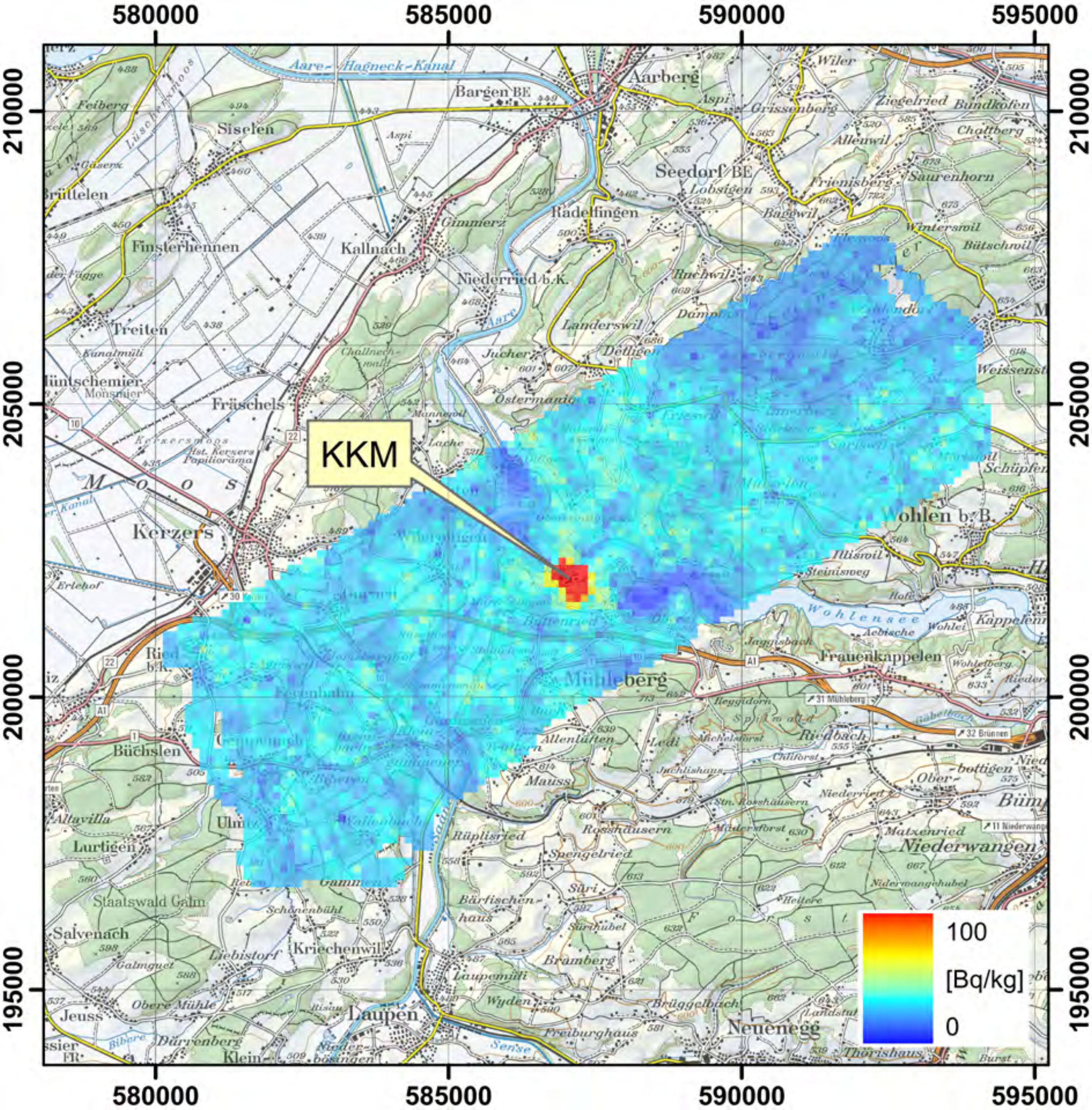

Figure 13: ^{232}Th activity concentration in the vicinity of KKM. PK100 ©2015 swisstopo (JD100042).

2.4 Urseren Valley

On request of the University of Basel, the area of the Urseren Valley was surveyed. The map of the dose rate (Figure 14) shows higher values due to the altitudes of this alpine region. The total dose rate consists of a cosmic component and a terrestric component depicted in Figure 15. The maps of the terrestric component of the dose rate (Figure 15) and the activity concentrations of the natural radionuclides ^{232}Th (Figure 16) and ^{40}K (Figure 17) show elevated readings over debris cones and alluvial fans abounding in the valley (Figure 19) referred in the according legend (Figure 20) as the different types of “Schuttkegel” . The spatial distribution of the artificial radionuclide ^{137}Cs (Figure 18) differs from the natural radionuclides and can be mainly attributed to the fall-out pattern of the Chernobyl accident.

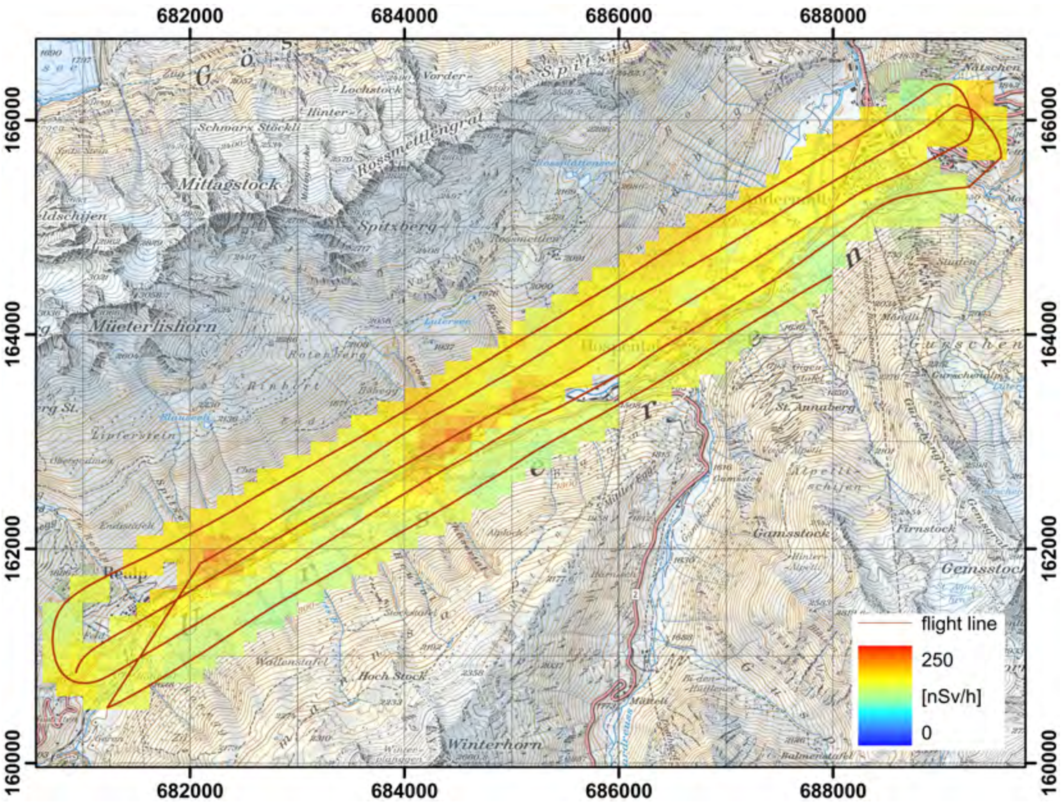

Figure 14: Dose rate in the Urseren valley. PK50 ©2015 swisstopo (JD100042).

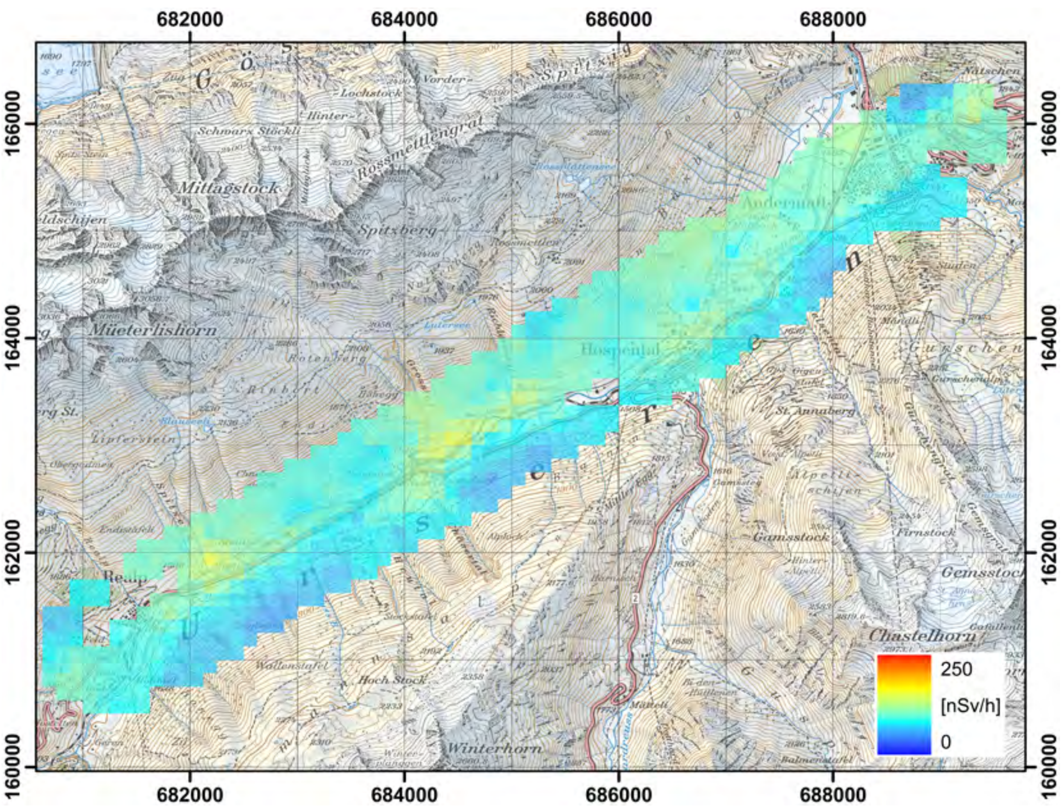

Figure 15: Terrestric component of the dose rate in the Urseren valley. PK50 ©2015 swisstopo (JD100042).

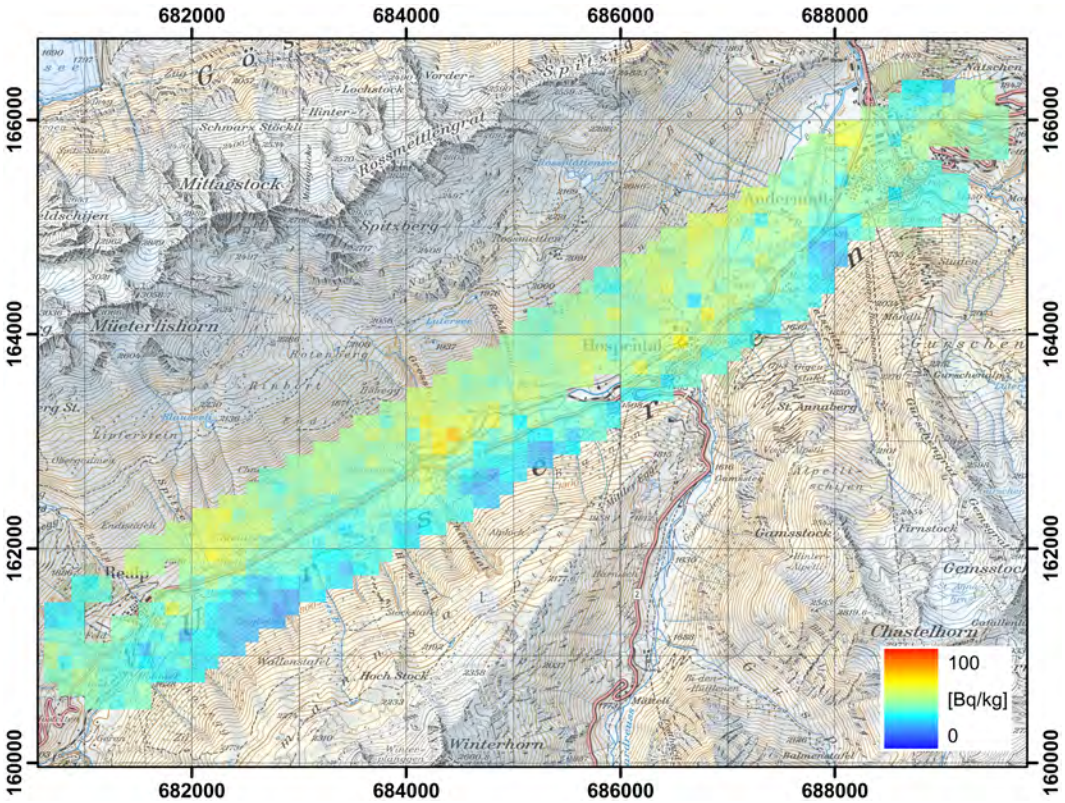

Figure 16: ^{232}Th activity concentration in the Urseren valley. PK50 ©2015 swisstopo (JD100042).

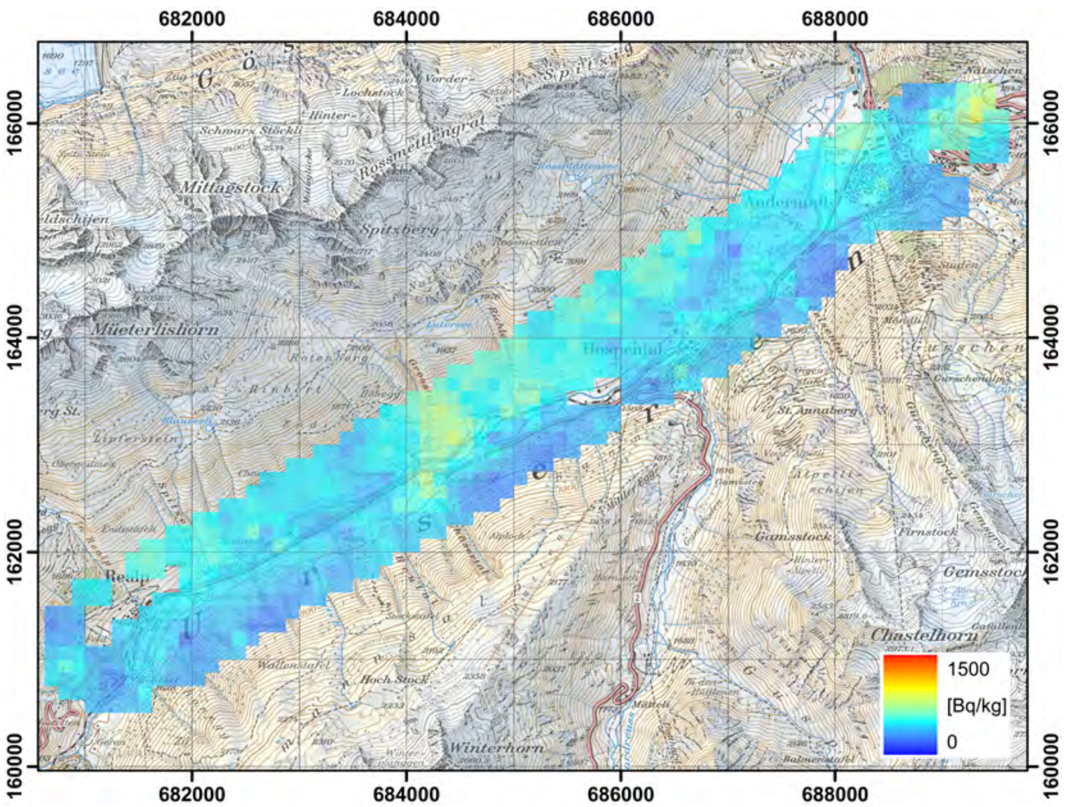

Figure 17: ^{40}K activity concentration in the Urseren valley. PK50 ©2015 swisstopo (JD100042).

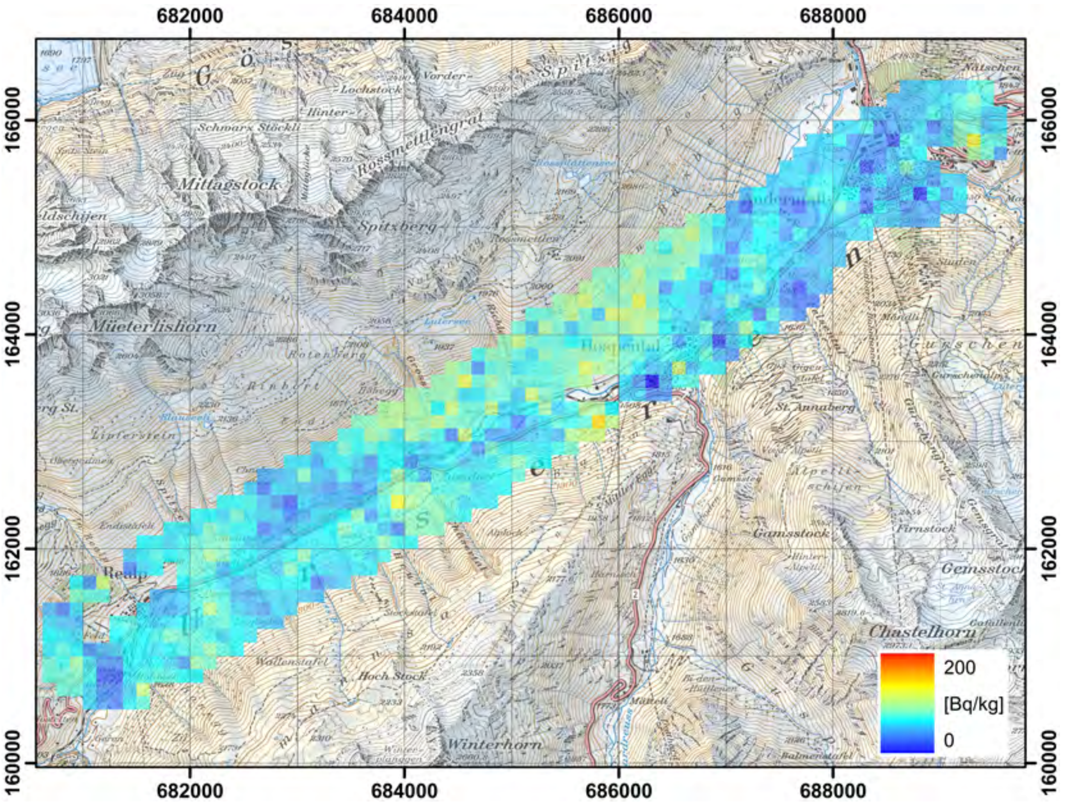

Figure 18: ^{137}Cs activity concentration in the Urseren valley. PK50 ©2015 swisstopo (JD100042).

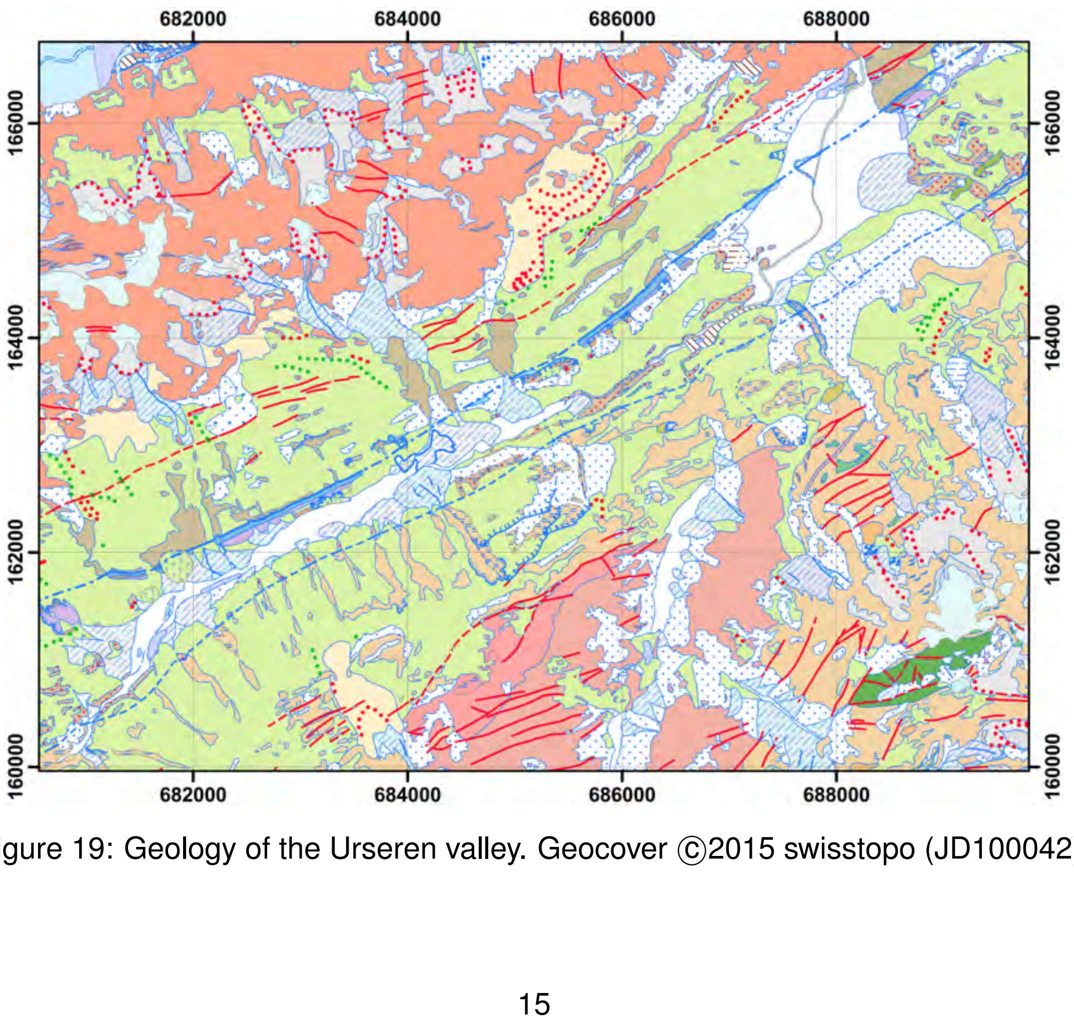

Figure 19: Geology of the Urseren valley. Geocover ©2015 swisstopo (JD100042).

Figure 20: Legend part 1 for the geological map of the Urseren valley (in German). Geocover ©2015 swisstopo (JD100042).

Figure 21: Legend part 2 for the geological map of the Urseren valley (in German). Geocover ©2015 swisstopo (JD100042).

2.5 Piora Valley

The area of the Piora valley was also surveyed for the University of Basel project. As observed in the Urseren valley, the map of the total dose rate (Figure 22) shows clearly the influence of the elevation when compared to its terrestric component (Figure 23). The elevated terrestric dose rate (Figure 23) and activity concentration of ^{232}Th (Figure 24) depicted over the Lago di Dentro (coordinate 699531, 156326) are an artefact due to the interpolation of measured points into grid values. The grid values over the lake are interpolated from point values measured on a flight line (Figure 22) over the lakeshore where increased amounts of natural radionuclides are detected. These and other elevated values of natural radionuclides (Figures 24 and 25) are correlated to detritus deposits (referred as the different types of "Schuttkegel" in Figure 28) as was observed similarly in the Urseren valley. The map of the activity concentration of ^{137}Cs (Figure 26) shows slightly elevated concentrations typical for southern Switzerland, which suffered significant rain-out of radioactive aerosol particles from the Chernobyl accident.

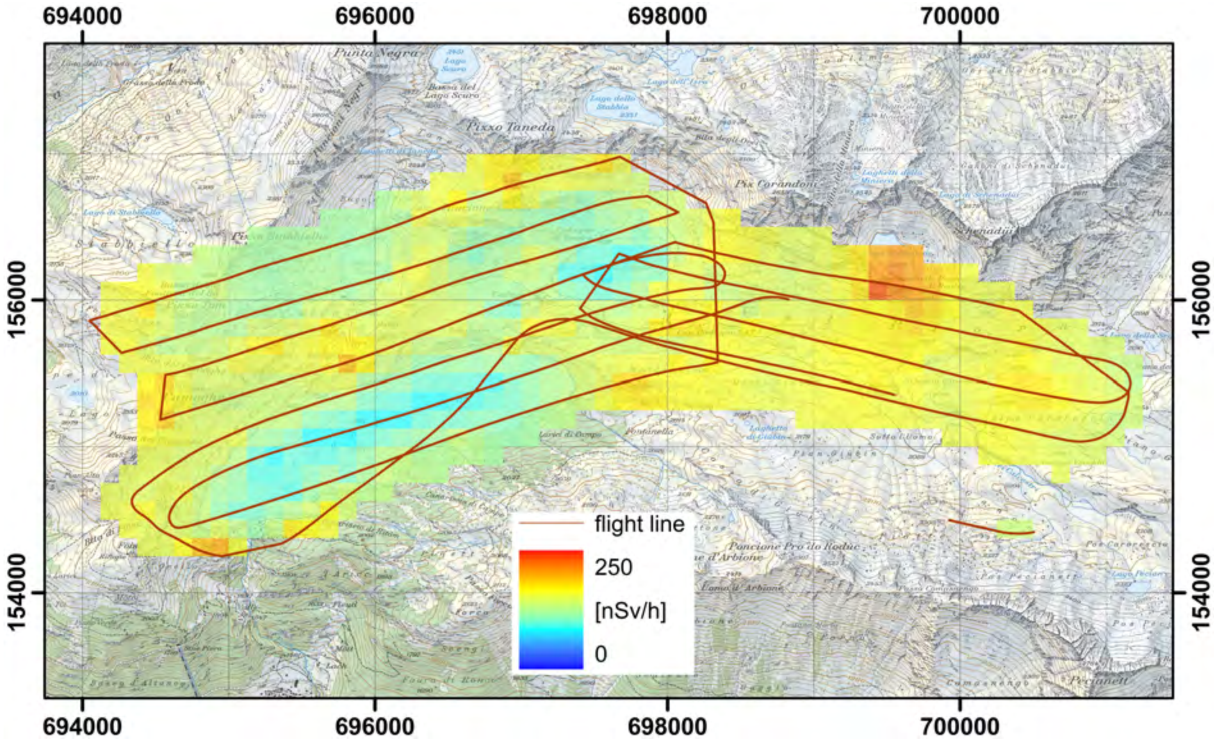

Figure 22: Dose rate in the Piora valley. PK50 ©2015 swisstopo (JD100042).

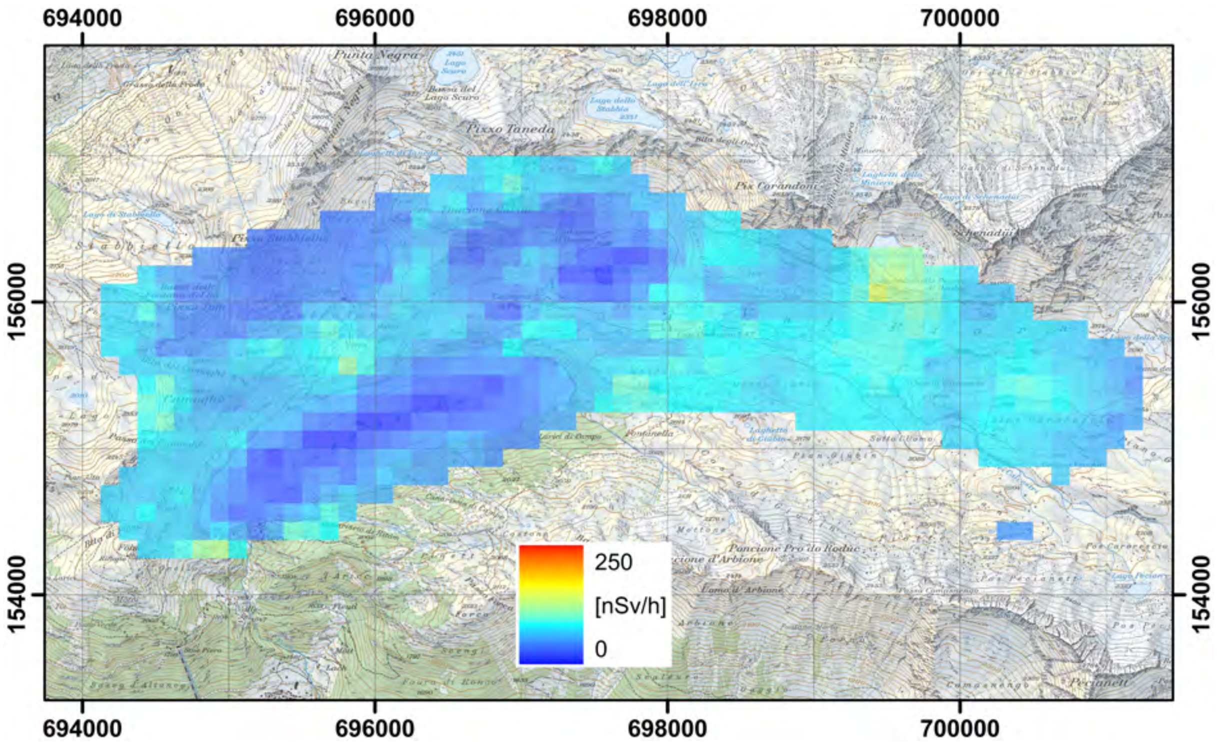

Figure 23: Terrestric component of the dose rate in the Piora valley. PK50 ©2015 swisstopo (JD100042).

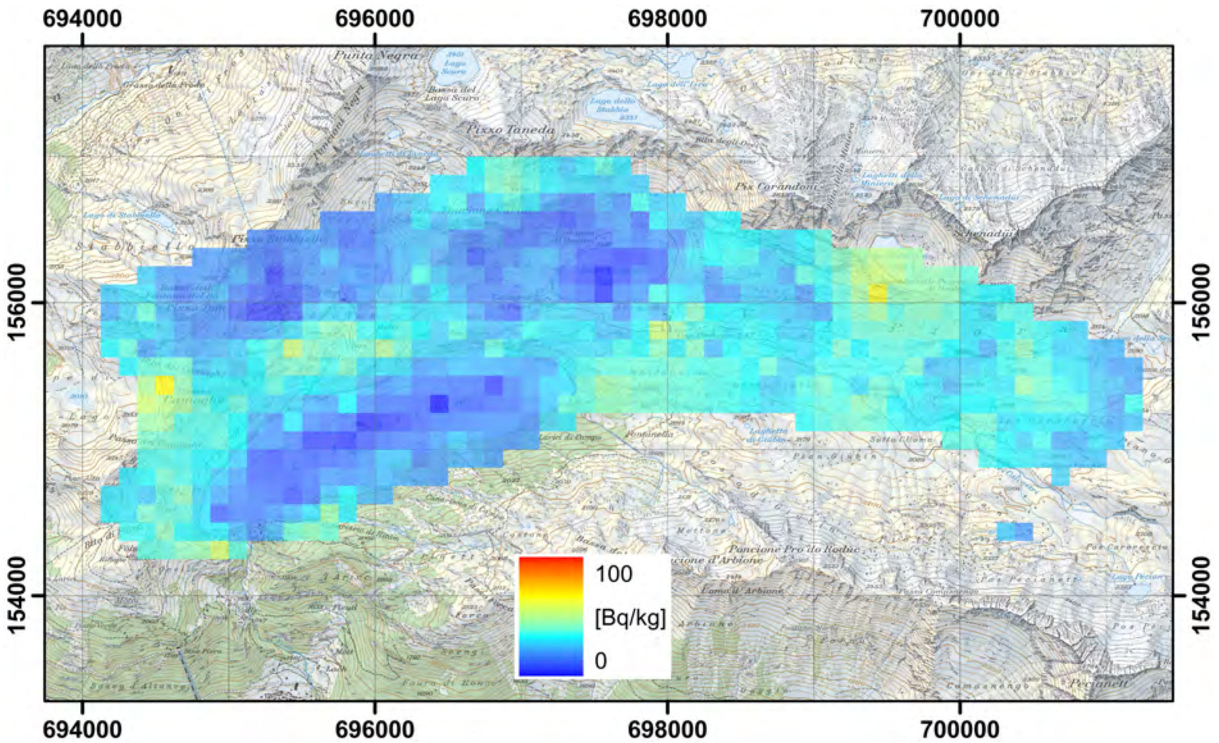

Figure 24: ^{232}Th activity concentration in the Piora valley. PK50 ©2015 swisstopo (JD100042).

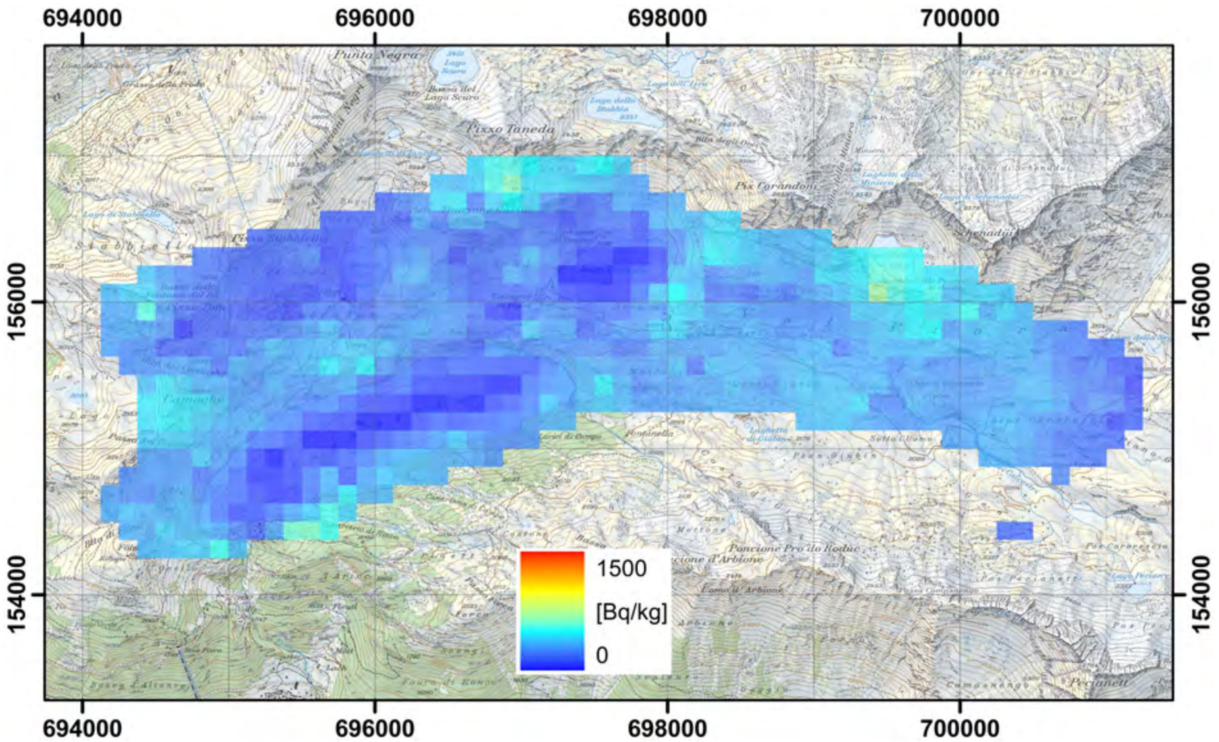

Figure 25: ^{40}K activity concentration in the Piora valley. PK50 ©2015 swisstopo (JD100042).

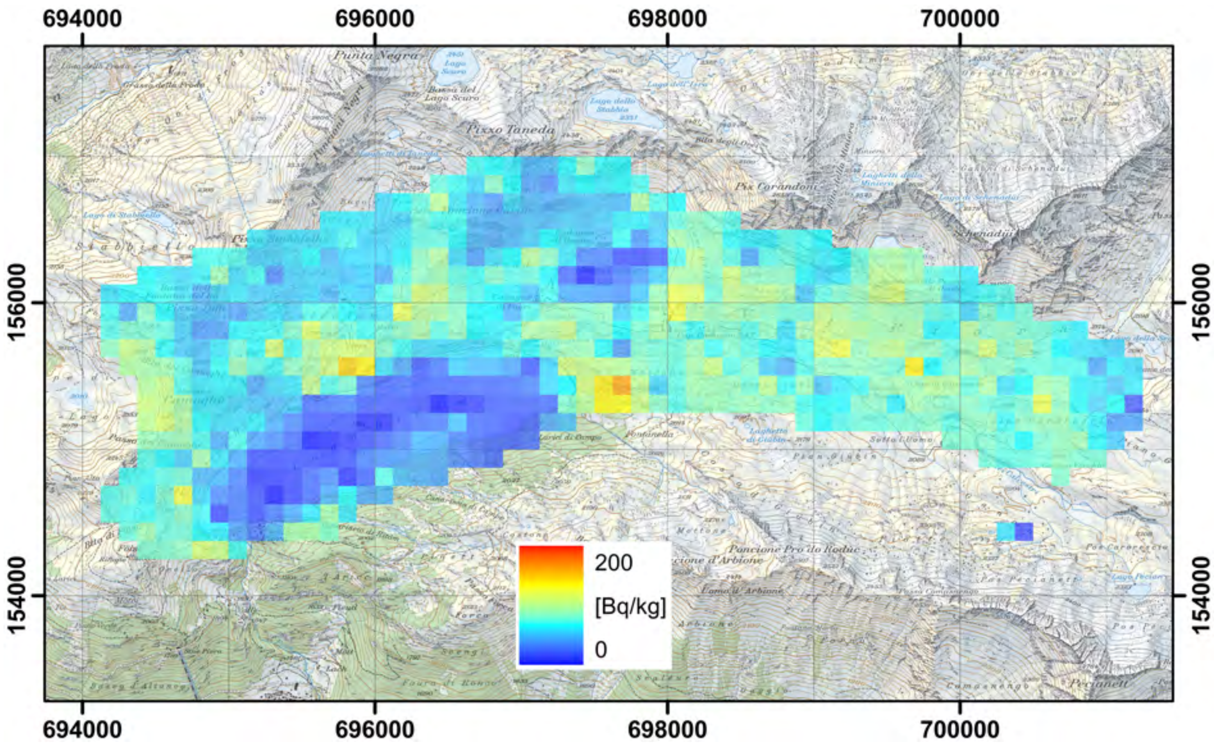

Figure 26: ^{137}Cs activity concentration in the Piora valley. PK50 ©2015 swisstopo (JD100042).

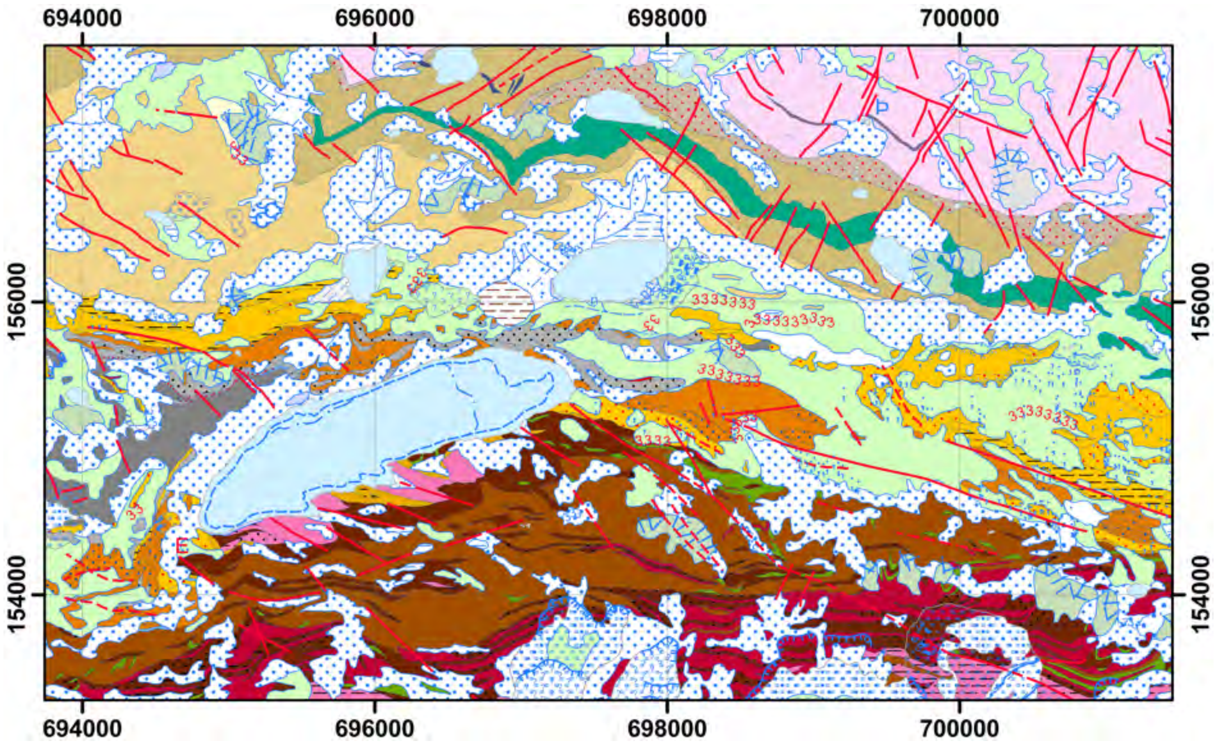

Figure 27: Geology of the Piora valley. Geocover ©2015 swisstopo (JD100042).

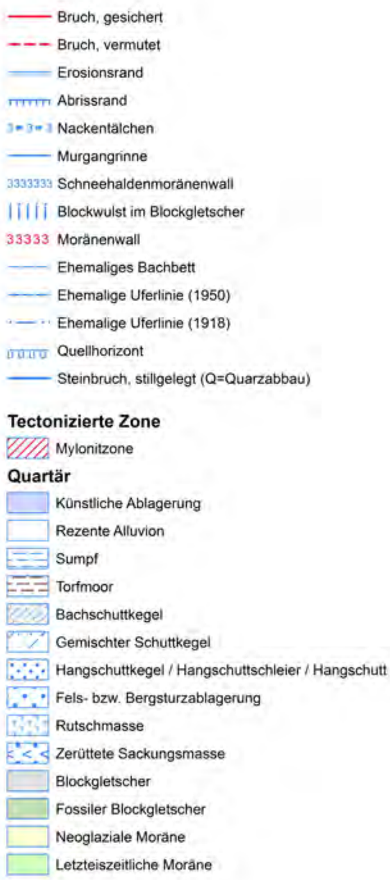

Figure 28: Legend part 1 for the geological map of the Piora valley (in German). Geocover ©2015 swisstopo (JD100042).

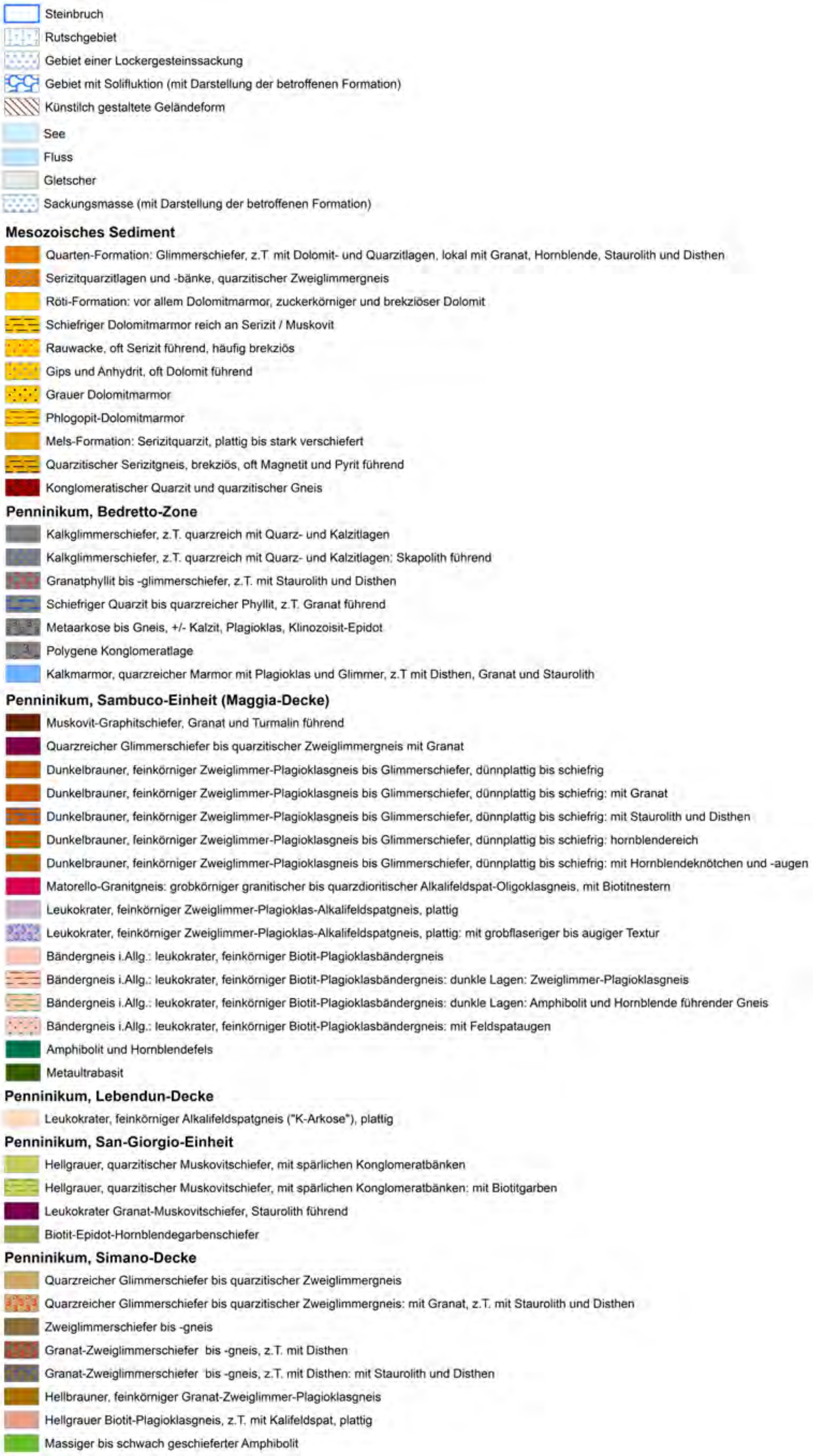

Figure 29: Legend part 2 for the geological map of the Piora valley (in German). Geocover ©2015 swisstopo (JD100042).

Figure 30: Legend part 3 for the geological map of the Piora valley (in German). Geocover ©2015 swisstopo (JD100042).

2.6 Intercomparison of detectors

The NBC-EOD Centre of Competence (KompZen) is in the process to purchase new airborne gammaspectroscopy systems (RLL), which are planned to replace also the old systems (ARM) employed by the National Emergency Operations Centre (NEOC). The ARM system could prove during the last twenty years its merits in multiple intercomparisons with ground measurements and foreign airborne gammaspectrometry systems, thus providing a reference for the assessment of the RLL system. During the purchase process, field tests are performed which lead to further improvements by the RLL manufacturer. The last intercomparison flights between the ARM and RLL systems were performed over the vicinity of the Paul Scherrer Institute (PSI) on March 18th after an upgrade of the RLL evaluation software by the manufacturer. The results were documented in a PSI technical report (TM 96-15-08) on April 17th. Several photon sources were located in the test area. The proton accelerator and an associated spallation source are located on the western part of PSI. The accelerator was in maintenance shut-down during the intercomparison flights. The accelerator facility on the western part of PSI and storage buildings on the eastern part of PSI are easily detectable with airborne measurements. Additionally, two radioactive point sources were placed on the PSI premises by radiation protection staff of PSI. A well-known anomaly of the radionuclide ^{232}Th located at the nearby Rotbergegg facilitated a comparison of results over elevated natural radioactivity. Table 4 shows an overview of the different photon sources.
The presented results will be used to further improve the RLL airborne gammaspectrometry system.

Photon source	Coordinate		Nuclide	Activity or Activity Concentration
	x	y		
Accelerator	659051	265364	^{60}Co, ^{58}Co	unknown
Strorage building	659567	265814	^{60}Co, ^{137}Cs	unknown
Rotbergegg	657664	266180	^{232}Th	93 Bq/kg
Rotbergegg	657664	266180	^{40}K	270 Bq/kg
^{137}Cs-source	659121	265173	^{137}Cs	3.5 GBq
^{60}Co-source	659083	265790	^{60}Co	286 MBq

Table 4: Photon sources in the test area.

2.6.1 Data evaluation

The data evaluation bases on Ascii-files in the “European Radiometric and Spectrometry” (ERS)-format. The ERS-files were imported into a Microsoft Excel workbook and further evaluated. In a first step, the coordinates PE, PN und PZ in WGS84-Format were transformed into Swiss National Grid coordinates using the following approximate formulae (source: Swisstopo).

$$\varphi' = \frac{PN \cdot 3600 - 169028.66}{10000}$$

$$\lambda' = \frac{PE \cdot 3600 - 26782.5}{10000}$$

$$x\,[m] = 600072.37 + 211455.93 \cdot \lambda' - 10938.51 \cdot \lambda' \cdot \varphi' - 0.36 \cdot \lambda' \cdot \varphi'^2 - 44.54 \cdot \lambda'^3$$

$$y\,[m] = 200147.07 + 308807.95 \cdot \varphi' + 3745.25 \cdot \lambda'^2 + 76.63 \cdot \varphi'^2 - 194.56 \cdot \lambda'^2 \cdot \varphi' + 119.79 \cdot \varphi'^3$$
$$z\,[m] = PZ - 49.55 + 2.73 \cdot \lambda' + 6.94 \cdot \varphi'$$

Compared to the original formulae provided by swisstopo, x and y directions are swapped, so that x is in west-east and y in south-north direction for more convenient reading of the coordinates. The flights consisted of two line patterns oriented in south-north and west-east directions. Additionally, the flights with the RLL system were performed in “standard” mode with five seconds averaged spectra and “raw” mode with one second spectra. These line patterns and modes were evaluated separately. The raw data provided by the RLL system were additionally evaluated with the ARM evaluation software using the parameter-file of detector D as a substitute for a compatible parameter file of the RLL system. Thus, a direct point-to-point comparison could be achieved, eliminating the influence of the slightly different flight lines. For mapping, the xy-point data were imported via a text file into the ArcMap geographical information system and converted there into raster data with a cell size of 20 m, rendering typically one raster cell per point datum.

2.6.2 Ambient dose rate dH*(10)/dt, identifier DHSR

The ambient dose rate dH*(10)/dt in one meter above ground showed a very similar spatial pattern independent on the measuring system, measuring mode, flight direction and data evaluation procedure. Thus, a direct quantitative comparison was performed. The DHSR of RLL data points evaluated with the RLL algorithms for both directions and both measuring modes were associated with the ARM evaluated DHSR measured with the ARM system by the distance of the measured coordinates of the data points. Figure 31 shows the resulting scatter diagram of the associated data points. Both data sets are correlated as should be expected. The green solid line depicts identical values of the dose rates determined with the RLL and ARM systems. The dashed green lines represent an offset of 20% of full scale from identity.

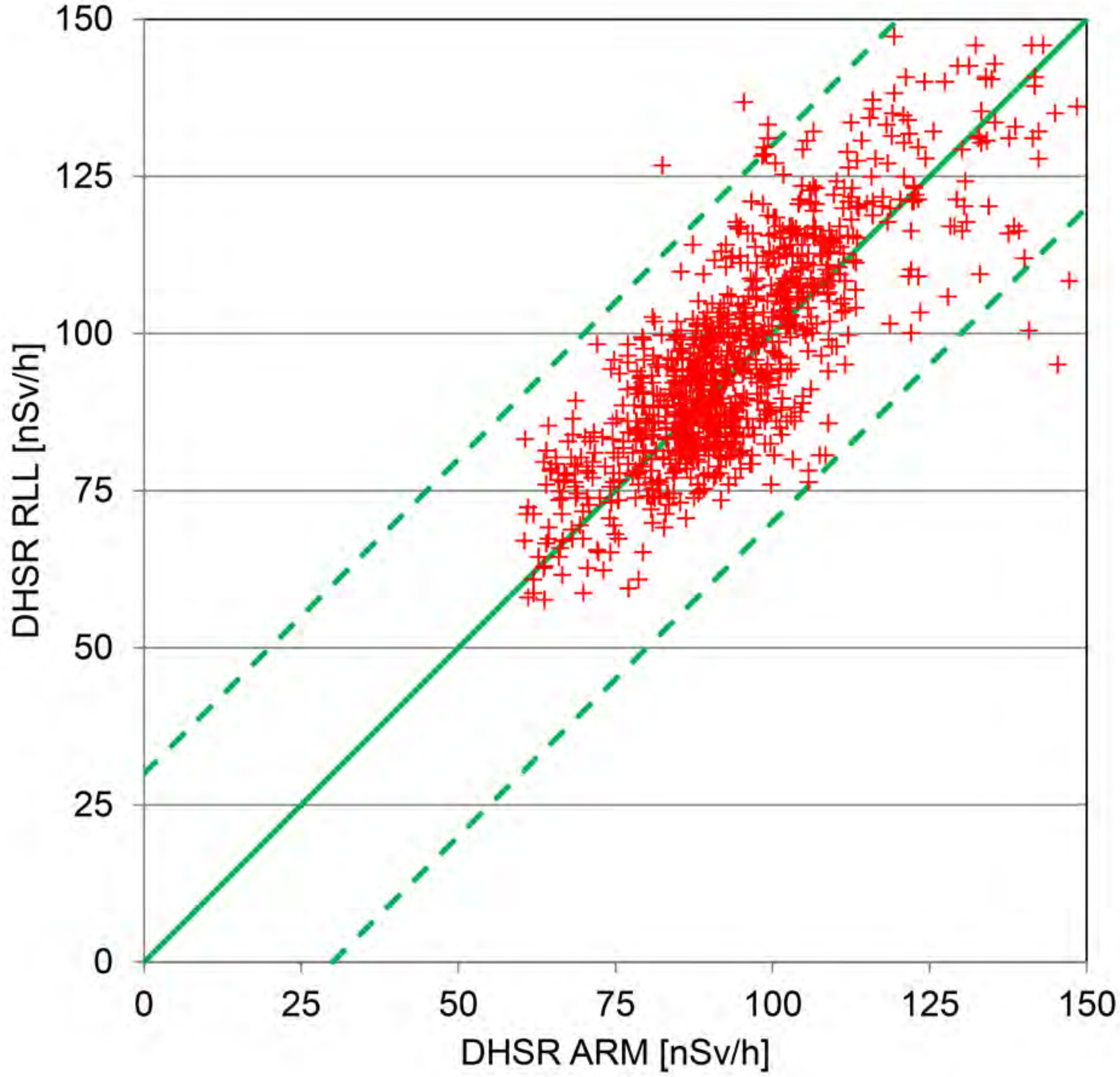

Figure 31: Comparison of evaluated values of DHSR for coordinates with distances less than 10 m. The solid green line represents exact rapport; the dashed green lines have an offset of 20% (of full scale).

2.6.3 Man-Made Gross Count (MMGC)-Ratio, identifier &MMGC

The MMGC-ratio is the ratio of the spectrum count sum between energies of 400 keV and 1400 keV to the count sum between energies of 1400 keV and 3000 keV. This ratio is a valuable tool to identify areas with suspected presence of artificial radionuclides during the flight. When this ratio was defined, the unit was set to per cent to render an integer data value, targeting at minimizing storage space. As the MMGC-ratio has typically values above 450% and storage limitations are less stringent today, this choice may be reconsidered. Figure 32 shows the advantages of the MMGC-ratio. The potential locations of artificial radionuclides on the premises of PSI are clearly indicated, whereas the ^{232}Th-anomaly with elevated dose rates at Rotbergegg is depicted as background. Analyzing the results of the MMGC-ratio evaluated from all flights with the RLL system with the RLL evaluation software showed a clear discrepancy to the values obtained with the ARM system. Whereas the ARM system renders over the measuring area MMGC-ratios between 345% and 3624% with an average of 472%, the values of the RLL system derived from the evaluated data in ERS-format range between 11% and 105% with an average of 21%, or about a factor of 23 less. The map of the MMGC-ratio measured with the RLL system shows a similar pattern to the map derived from the ARM data if the color scale is adjusted accordingly (Figure 33). The differences over the accelerator building were caused by the removal of shielding blocks over the proton channel for maintenance during the time between the measuring flights.

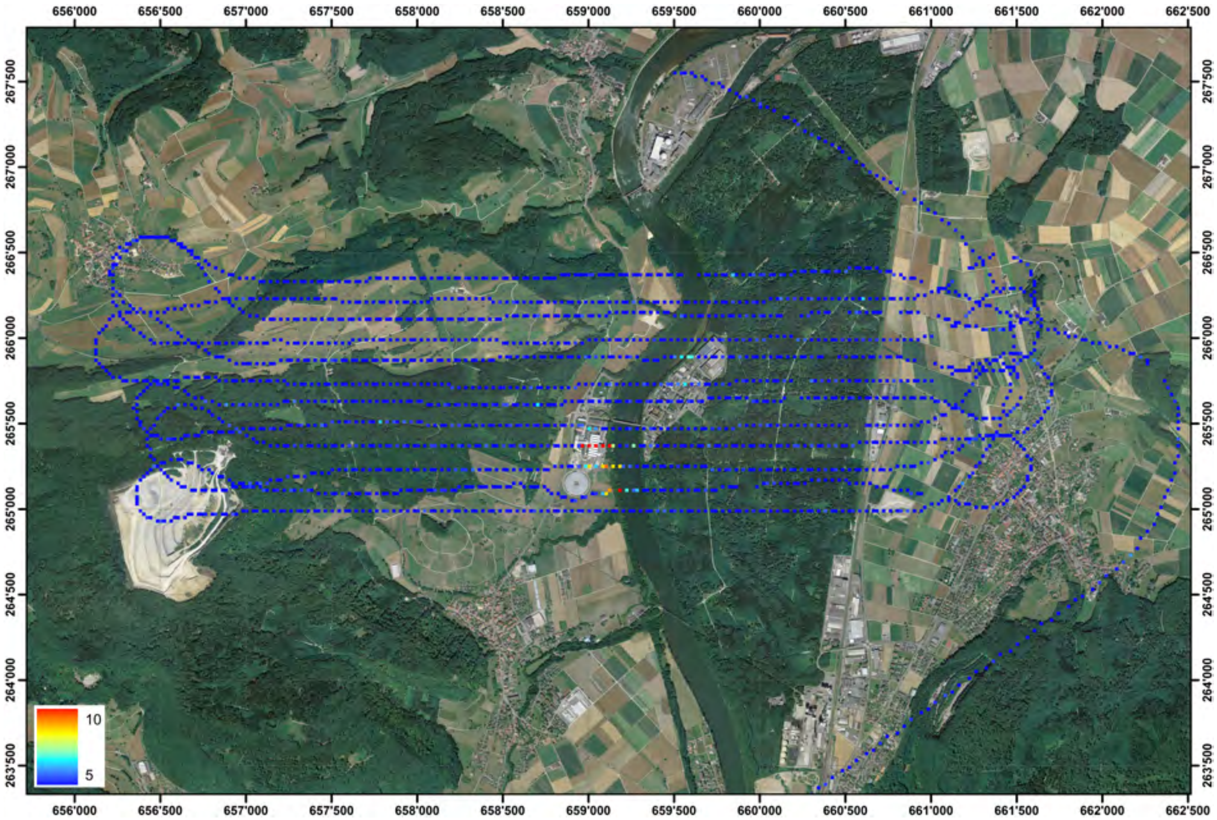

Figure 32: MMGC-ratio. Measuring system ARM, data evaluation ARM.
swissimage ©2015 swisstopo (JD100042).

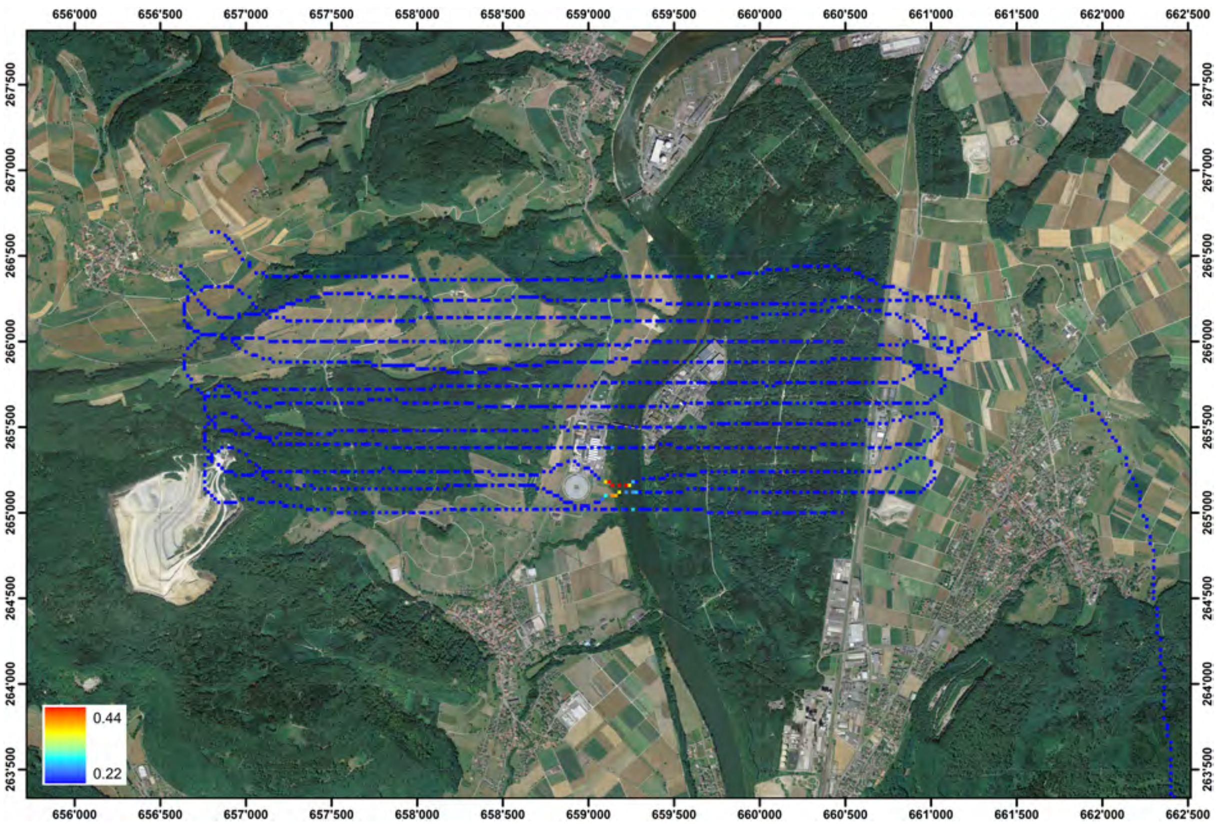

Figure 33: MMGC-ratio. Measuring system RLL, 5 s average spectra, data evaluation RLL.
swissimage ©2015 swisstopo (JD100042).

2.6.4 ^{137}Cs point source activity, identifier AP_Cs-137

The evaluated data of identifier AP_Cs-137 in ERS-format was selected according to the location of the different photon sources (Table 4) using the highest value near the position of the source. The source was clearly located and identified by all systems and the source activity was determined reasonably well with both systems (Table 5). Over the accelerator building, ^{137}Cs activity of few GBq is reported by the ARM system, whereas all RLL evaluations render a value of zero (Table 6). The reported ^{137}Cs activity of the ARM system may be caused by a misinterpretation of scattered photons emitted by the radionuclide ^{58}Co (Figure 34). Similar results are obtained over the storage building, where the ARM system detects ^{137}Cs activity in the region of the detection limit, whereas the results of the RLL system yield values of zero (Table 7. The spectrum shows only a slight indication of photons emitted from ^{137}Cs (Figure 35).

System, mode direction	Coordinate of maximum [m]		Activity [GBq]
	x	y	
ARM, NS	659177	265104	3.1
ARM, WE	659159	265192	5.6
RLL, standard, NS	659146	265168	3.2
RLL, raw, NS	659159	265187	3.3
RLL, standard, WE	659185	265168	3.4
RLL, raw, WE	659120	265225	2.2

Table 5: Results of the ^{137}Cs point source activity near the location of the placed source with an activity of 3.5 GBq at (659121, 265173).

System, mode direction	Coordinate of maximum [m]		Activity [GBq]
	x	y	
ARM, NS	659045	265363	2.6
ARM, WE	659047	265389	3.2
RLL, standard, NS	659067	265396	0
RLL, raw, NS	659054	265396	0
RLL, standard, WE	659028	265377	0
RLL, raw, WE	659041	265377	0

Table 6: Results of the ^{137}Cs point source activity near the location of the accelerator at (659051, 265364).

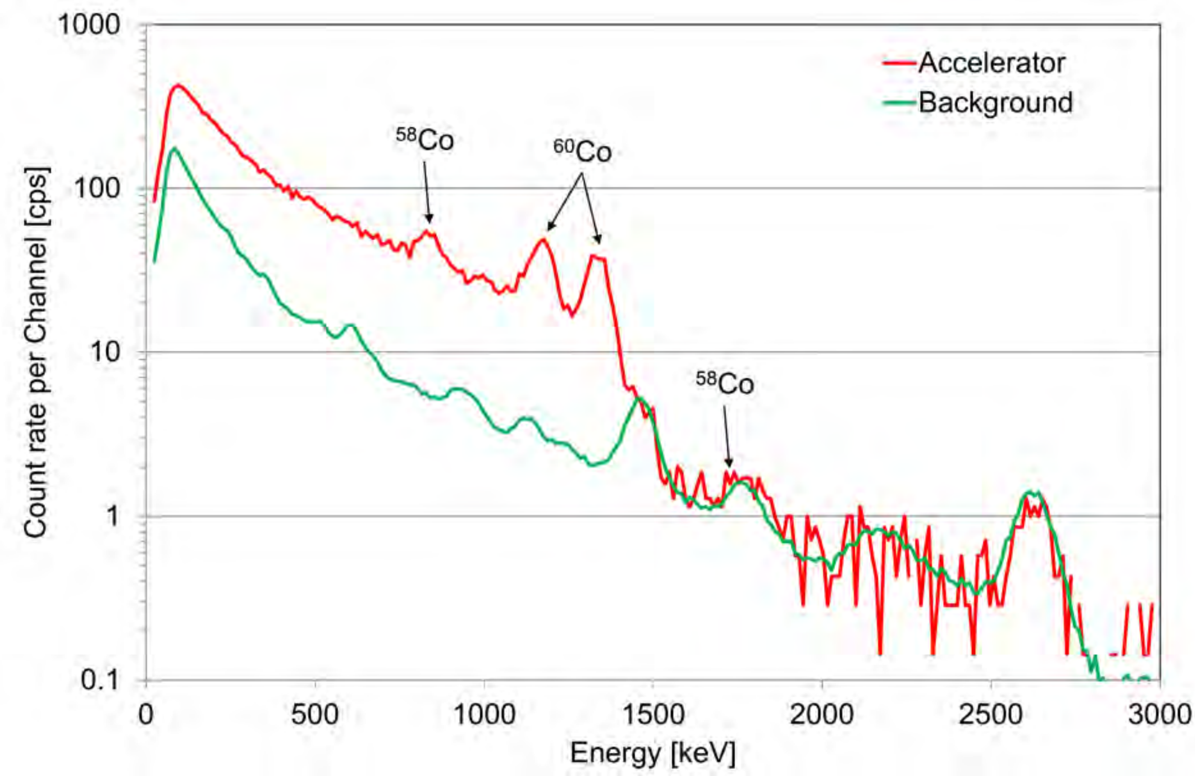

Figure 34: Photon spectrum over the accelerator building compared to the background measured with the ARM system.

System, mode direction	Coordinate of maximum [m]		Activity [GBq]
	x	y	
ARM, NS	659612	265883	0.3
ARM, WE	659569	265805	0.7
RLL, standard, NS	659554	265821	0
RLL, raw, NS	659566	265821	0
RLL, standard, WE	659567	265764	0
RLL, raw, WE	659558	265821	0

Table 7: Results of the ^{137}Cs point source activity near the location of the storage building at (659567, 265814).

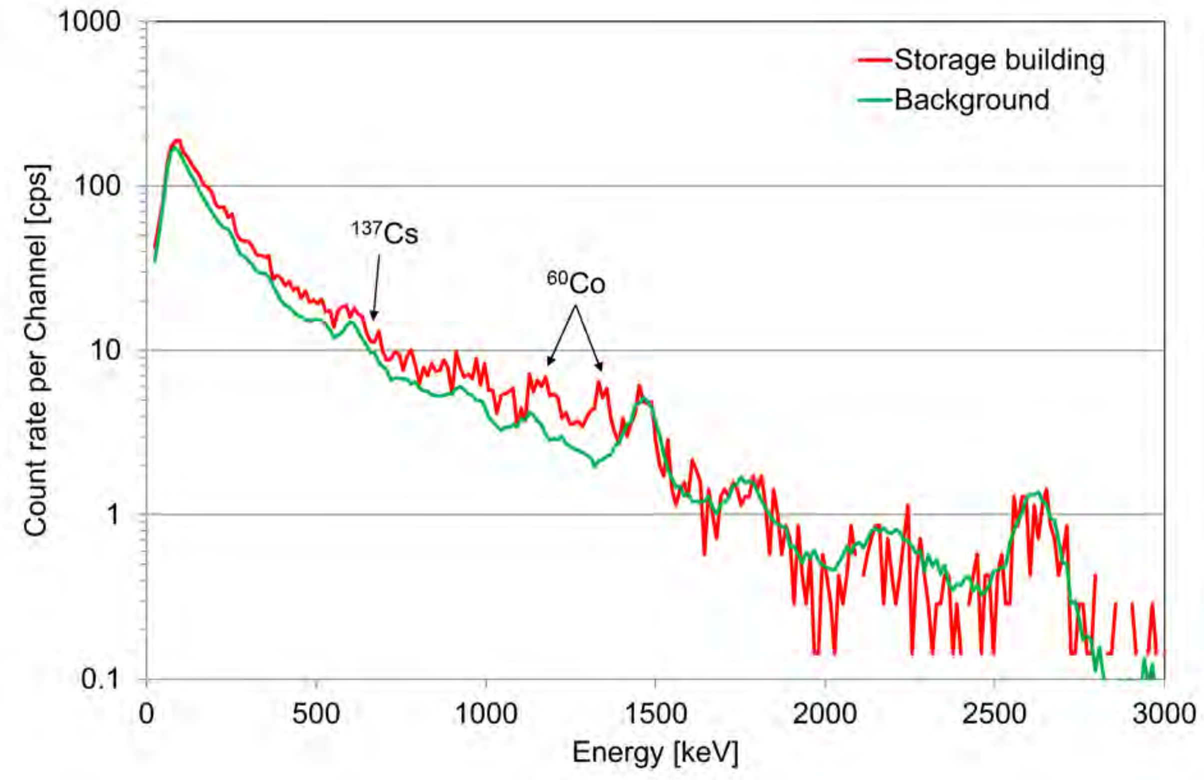

Figure 35: Photon spectrum over the storage building compared to the background measured with the ARM system.

2.6.5 ^{60}Co point source activity, identifier AP_Co-60

The evaluated data of identifier AP_Co-60 in ERS-format was selected according to the location of the different photon sources (Table 4) using the highest value near the position of the source. The activity values determined with the ARM system near the source are about half of the specified activity (Table 8), whereas all values determined with the RLL system read zero. The spectrum of the RLL system (raw mode) in the vicinity of the ^{60}Co-source (condensed to 256 channels) shows a clear indication of photons emitted by ^{60}Co (Figure 36). In the case of ^{60}Co point source activity at the location of the accelerator, all systems report values between 0.5 GBq and 2.5 GBq (Table 9). This could be expected, as a clear signal is visible in the photon spectrum (Figure 34).The activity values determined with the RLL system are lower than those determined with the ARM system. The activities derived from the RLL standard mode are slightly lower than those obtained from the raw mode data since in standard mode the spectrum is averaged over five seconds and temporal peaks in the count rate are smoothed out. As the activity of the source is unknown, the comparison is more of a qualitative nature.
The signal of photons emitted by ^{60}Co is noticeably weaker over the storage building (Figure 35) which is reflected in lower reported activities of the ARM system (Table 10). The signal seems to be near the lower threshold of the RLL systems, as the reported values are partly set to zero.

System, mode direction	Coordinate of maximum [m]		Activity [MBq]
	x	y	
ARM, NS	659134	265725	141
ARM, WE	659056	265788	184
RLL, standard, NS	659076	265797	0
RLL, raw, NS	659063	265778	0
RLL, standard, WE	659102	265759	0
RLL, raw, WE	659102	265740	0

Table 8: Results of the ^{60}Co point source activity near the location of the placed source with an activity of 286 MBq at (659083, 265790).

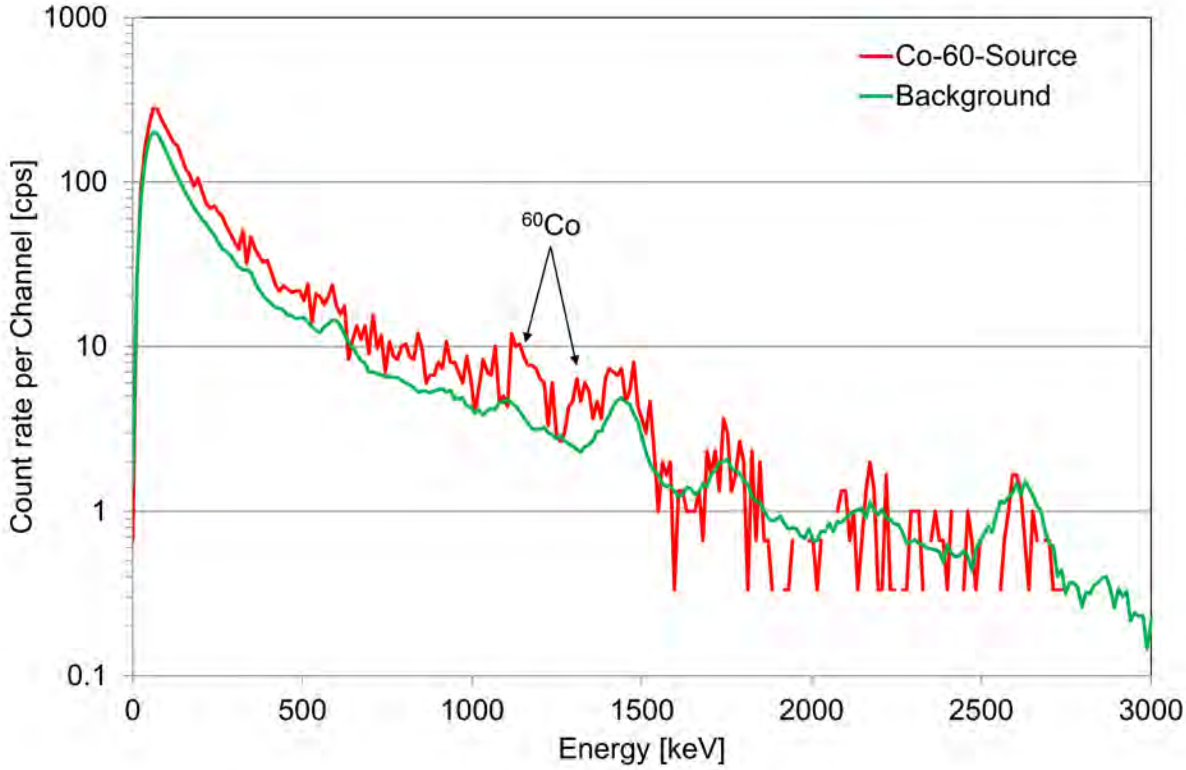

Figure 36: Photon spectrum over the ^{60}Co-source compared to the background measured with the RLL system.

System, mode direction	Coordinate of maximum [m]		Activity [GBq]
	x	y	
ARM, NS	659045	265363	1.7
ARM, WE	659047	265389	2.5
RLL, standard, NS	659067	265396	0.5
RLL, raw, NS	659054	265396	0.8
RLL, standard, WE	659028	265377	1.2
RLL, raw, WE	659041	265377	1.5

Table 9: ^{60}Co point source activity near the location of the accelerator at (659051, 265364).

System, mode direction	Coordinate of maximum [m]		Activity [MBq]
	x	y	
ARM, NS	659612	265883	94
ARM, WE	659569	265805	345
RLL, standard, NS	659554	265821	144
RLL, raw, NS	659566	265821	0
RLL, standard, WE	659567	265764	0
RLL, raw, WE	659558	265821	144

Table 10: ^{60}Co point source activity near the location of the storage building at (659567, 265814).

2.6.6 ^{232}Th activity concentration, identifier AD_Th-232

The test area includes a well-known ^{232}Th-anomaly over Rotbergegg with activity concentrations of 93 Bq/kg measured with in-situ gammaspectrometry. The area of the anomaly was not covered by the RLL flights with north-south flight direction. The comparison was therefore restricted to the west-eastern flight direction for both systems. The maps of the ^{232}Th-activity concentration over the anomaly derived from the ARM system (Figure 37) and the RLL system in standard mode (Figure 38) are alike. The main difference is the reporting of elevated ^{232}Th activity concentrations over the accelerator building (lower right corner of the map) by the RLL system. The according photon spectrum (Figure 34) shows background values for the ^{208}Tl-photon peak at 2615 keV over the accelerator. The maps of the ^{232}Th activity concentration derived from the measurement in RLL raw mode shows visibly lower concentrations over the complete test area (Figure 39). The artefact over the accelerator building of the standard mode is not reproduced. Both observations indicate a different evaluation algorithm for standard and raw mode of the RLL system. For quantitative analysis, a rectangle between coordinates (657545, 266292) and (657945, 265953) was closer inspected (Table 11). As was already visible from the maps (Figures 37 to 39), the ^{232}Th activity concentrations derived by the ARM system and the RLL system in standard mode agree very well. The maximum reported activity concentration matches results of the in-situ measurement. In contrast, the results obtained from the RLL measurement in raw mode yields only about 70% of the activity concentration as suspected from the comparison of the respective maps.

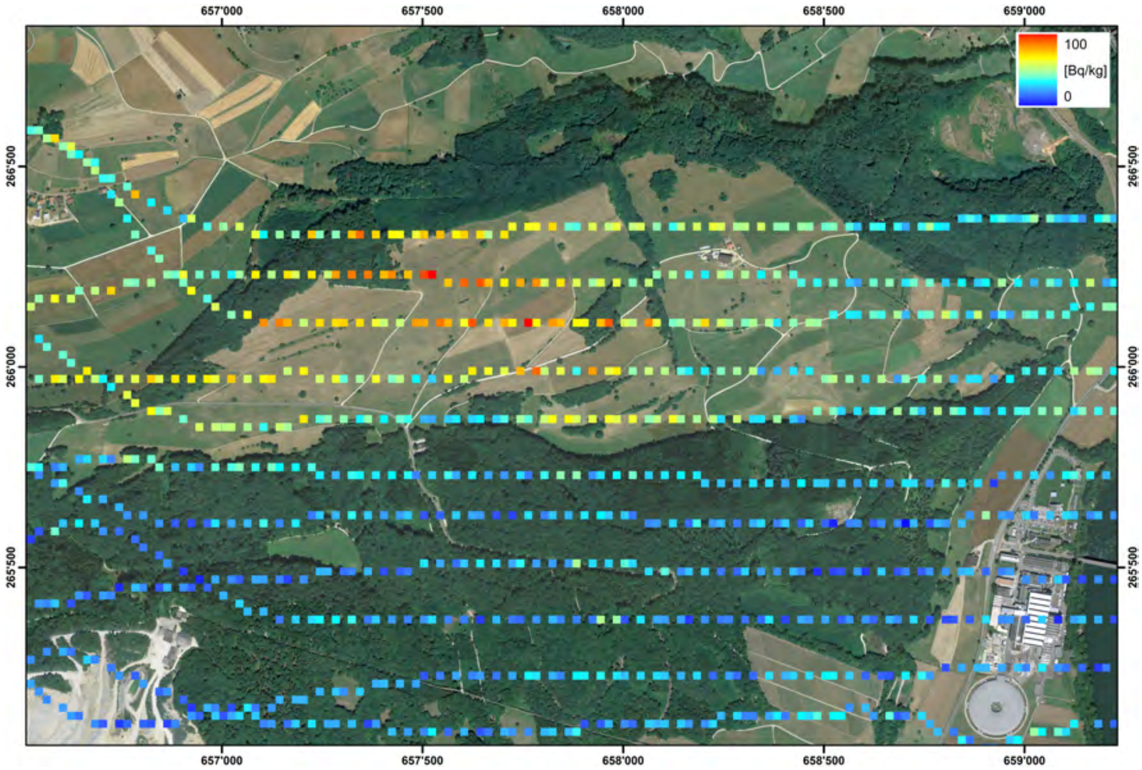

Figure 37: ^{232}Th activity concentration in the vicinity of the anomaly at Rotbergegg. Measuring system ARM, data evaluation ARM. swissimage ©2015 swisstopo (JD100042).

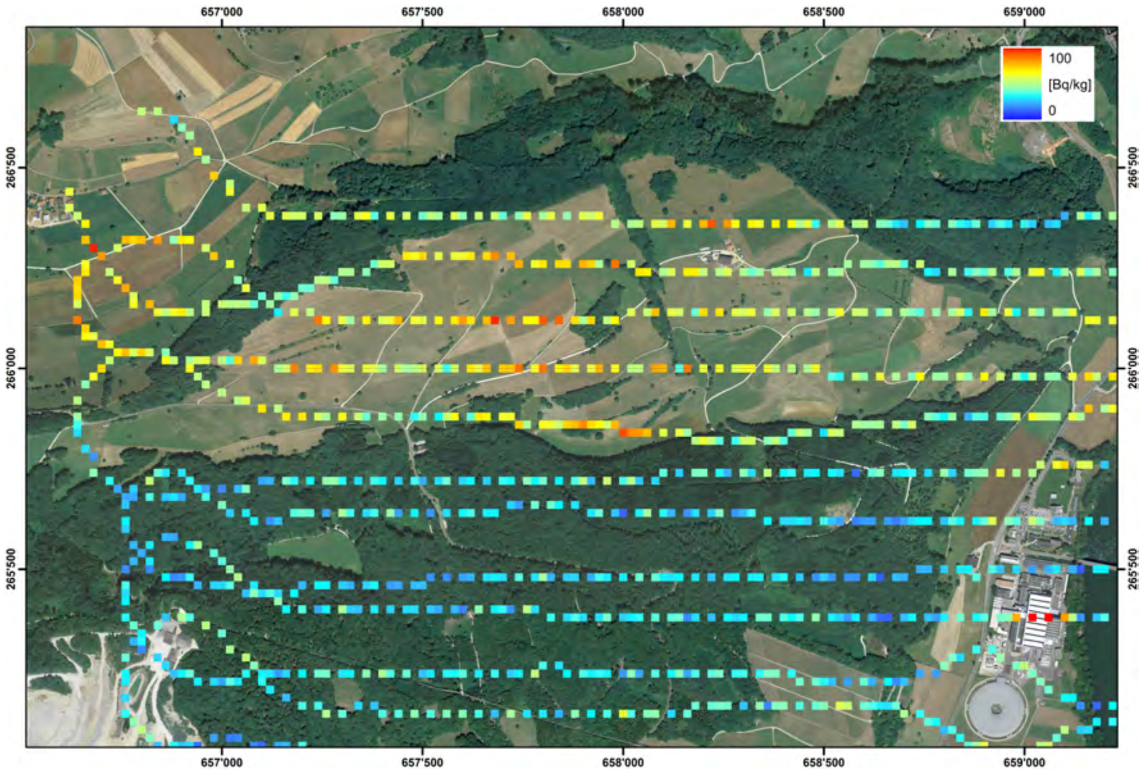

Figure 38: ^{232}Th activity concentration in the vicinity of the anomaly at Rotbergegg. Measuring system RLL, 5 s average spectra, data evaluation RLL. swissimage ©2015 swisstopo (JD100042).

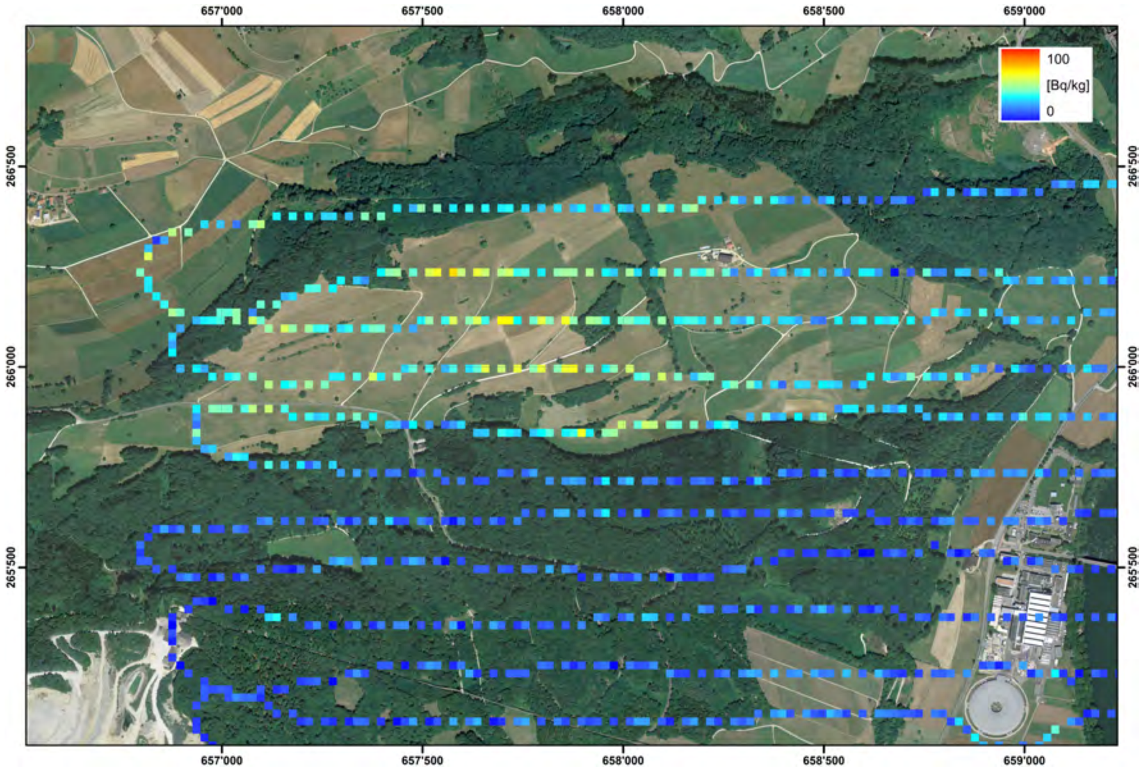

Figure 39: ^{232}Th activity concentration in the vicinity of the anomaly at Rotbergegg. Measuring system RLL, 1 s raw spectra, data evaluation RLL. swissimage ©2015 swisstopo (JD100042).

Parameter	ARM	RLL	
		standard	raw
Number of datapoints in rectangle	35	40	42
Average [^{232}Th activity concentration [Bq/kg]	71	72	49
Standard deviation of ^{232}Th activity concentration [Bq/kg]	14	12	12
Maximum of ^{232}Th activity concentration [Bq/kg]	103	98	72
Minimum of ^{232}Th activity concentration [Bq/kg]	36	35	24

Table 11: Comparison of ^{232}Th activity concentrations over the anomaly at Rotbergegg.

2.6.7 ^{40}K activity concentration, identifier AD_K-40

For convenience, the derived activity concentration of ^{40}K was analysed in the identical rectangle used in the previous section. The results are listed in Table 12. In-situ measurements rendered a ^{40}K activity concentration of 270 Bq/kg.

Parameter	ARM	RLL	
		standard	raw
Number of datapoints in rectangle	35	40	42
Average [^{40}K activity concentration [Bq/kg]	213	123	161
Standard deviation of ^{40}K activity concentration [Bq/kg]	95	52	53
Maximum of ^{40}K activity concentration [Bq/kg]	415	246	278
Minimum of ^{40}K activity concentration [Bq/kg]	30	29	52

Table 12: Comparison of ^{40}K activity concentrations over the anomaly at Rotbergegg.

2.6.8 Conclusions

A direct comparison of ambient dose rate determined by both systems shows reasonable agreement between both systems. As two different linear interpretations show similar correlation coefficients, further experience is necessary for a fine tuning of the calibration parameters.
From the ^{137}Cs and ^{60}Co point source activities reported by the RLL system, it can be assumed, that the RLL data evaluation software uses a lower threshold (for example the decision limit) below which at least the values stored in the ERS-files are set to zero. For the single data point, this proceeding can be justified as values below the decision limit are meaningless. On the other hand, the statistical distribution of measured values is changed due to the cut-off and averaging or combination of the information from adjacent data points is prohibited. It is recommended to keep the statistical distribution intact and store all results, even in the case of physical meaningless values (for example negative activity). Thus, averaging would be still possible. Objectionable values can always be discriminated later on in the data presentation, for example with a reasonable color scale.
Whereas the ^{232}Th activity concentrations determined with the RLL system in standard mode agree well with results from the ARM system and ground measurements, the results determined by the RLL system in raw mode yield values which are about 30% lower, indicating a difference of evaluation algorithms used in the respective modes. An elevated ^{232}Th activity concentration reported by the RLL system in standard mode over the accelerator building could be identified as evaluation artefact and the responsible algorithm should be inspected.
The ^{40}K activity concentrations derived by the RLL system are at about 60% of the values measured by the ARM system. Nevertheless, for a potential adjustment of calibration factors a comparison with further ground measurements is indispensable.

2.7 International Aero-Gammaspectrometry Campaign AGC15

An international intercomparison was organised by the German Bundesamt für Strahlenschutz (BfS) and the German Federal Police in the vicinity of Chemnitz. Five teams from Germany (BfS, 2 teams), France (Institut de radioprotection et de sûreté nucléaire , IRSN), Czech republic (Státní ústav radiační ochrany, SURO) and Switzerland (Nationale Alarmzentrale, NAZ) participated in the intercomparison exercise. The exercise consisted of four tasks:

1. Reference area
   The reference area is surveyed by all participating teams to obtain a direct intercomparison of results.

2. Composite mapping
   A large area is surveyed by all measuring teams in team work with each team mapping a different sub-area. The results from the individual teams are reported to the organiser, who compiles composite maps from the data.

3. Source search
   Radioactive sources are placed in a test area. The task of the teams is the location of the sources, identification of the radionuclides and determination of the source activity.

4. Joint mapping
   Two teams survey a given area. The task of the teams is the development of an appropriate flight plan, measurement and compilation of composite radiological maps.

The results of the intercomparison exercise will be published and presented in a scientific symposium in 2016 by BfS.

2.7.1 Unusual intrinsic background

At the beginning of the exercise, the measuring teams had the opportunity to perform background mesaurements over a lake near Borna. Measurements over a lake can be used for background determination as the photons emitted from radionuclides in the ground are attenuated by the water layer. The main interest of this measurement for the Swiss team was a check on airborne activity of radon progeny as the intercomparison area is well-known for past uranium mining. The spectrum over the lake showed no indication of unusual radon activity concentrations in the air (red curve in Figure 40). Nevertheless, the peak of the photon emission of ^{40}K at 1460 keV was surprisingly large. Fortunately, the measurement in the Piora valley performed few days before the intercomparison exercise include measurements over the Ritom lake and the spectrum of these measurements (green curve in Figure 40) could be used for a further investigation. Due to the altitude of the alpine Piora valley, the spectrum shows generally larger count rates, but the ^{40}K peak was significantly lower during the measurement. This indicates that the intrinsic background of the helicopter changed during the days between the measurements in Switzerland and the start of the intercomparison campaign. A special battery carried in the helicopter only for missions abroad was suspected as culprit causing the background increase. This could be confirmed with a second measurement over the lake near Borna after the battery was unloaded. The spectrum (blue curve in Figure 40) shows a ^{40}K peak reduced back to normal levels. Due to the tight schedule of the intercomparison exercise, measuring tasks 1-3 were already completed during the time needed for identifying and resolving the background problem. The increased background during some of the measuring flights was compensated with new background correction values. Prior to the exercise, a software modification was performed to take into account different formats of terrain model files used for topographic correction, leading to a change in the detector definition file. Thus a total of three different detector definition files was used in this year. “DefinitionFile_DetD_ch.txt” is the normal definition file matched to the software modification, “DefinitionFile_DetD_de_oBat.txt” is the definition file used in German territory and “DefinitionFile_DetD_de_BackNeu.txt” is the definition file used in German territory adjusted for the increased background. The parameters in these definition files are listed at the end of the report for documentation purposes.

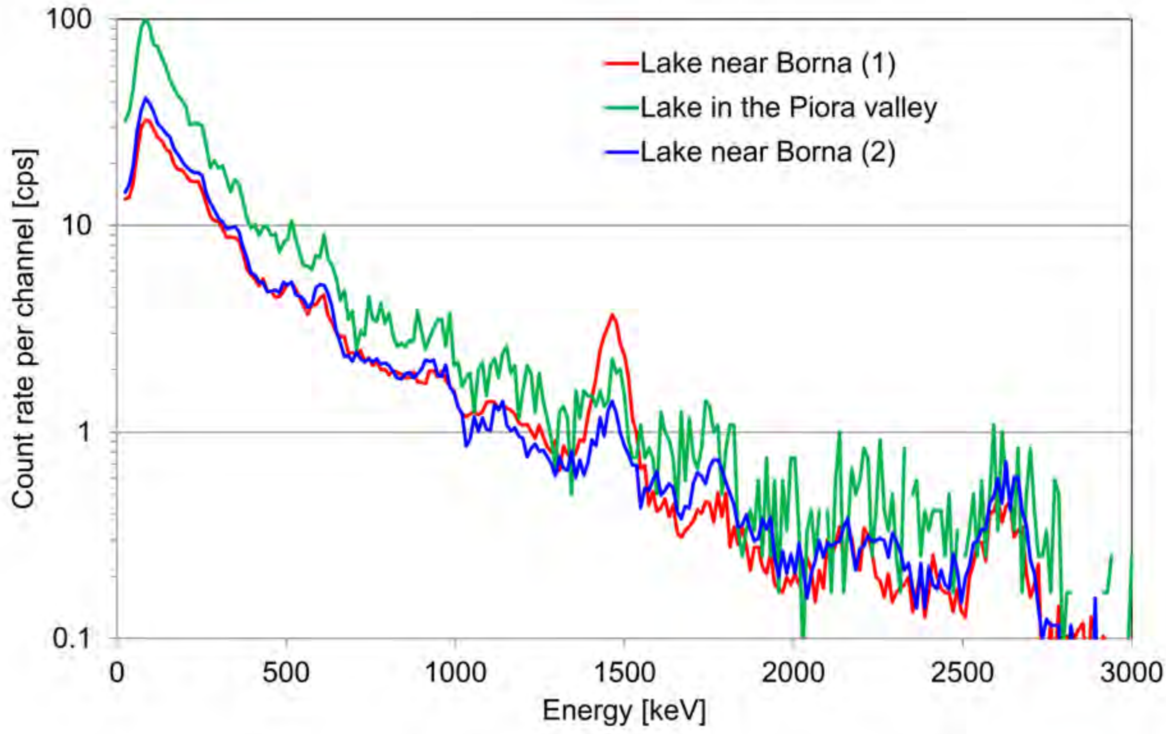

Figure 40: Photon spectra measured over lakes.

2.7.2 Reference area

The reference area is located near Seelingstädt. Prominent in the reference area are two settling ponds, now dry, used formerly in a uranium extraction facility. Both are clearly distinguishable in the dose rate map (Figure 42) with dose rates up to 550 nSv/h. A re-scaled dose rate map (Figure 43) shows the highest dose rates south of the southern settling pond. The spectra over the settling ponds (Figure 41) show clearly increased peaks of the photon emission of the ^{238}U decay product ^{214}Bi. An additional increase of the ^{232}Th decay product ^{208}Tl can be observed over the southern settling pond. The map of ^{238}U activity concentration (Figure 44) depicts elevated readings up to 740 Bq/kg over the settling ponds. As in the dose rate map, a re-scaled map of the^{238}U activity concentration (Figure 45) shows larger values at the southern settling pond.

The ^{238}U map bases on measurements of the 1765 keV photon emission of the decay product ^{214}Bi. This radionuclide is also present in the air above the soil, as a precursor (^{222}Rn) is a noble gas and can be exhaled from soil into the atmosphere. The amout of airborne ^{214}Bi

compared to ^{214}Bi in the soil varies with weather conditions. As airborne ^{214}Bi can be nearer to the detector in the helicopter than ^{214}Bi in soil, an overestimation of the ^{238}U soil activity concentration may result. The map of the ^{232}Th activity concentration (Figure 46) shows slightly elevated concentrations over the southern settling pond as already indicated from the respective spectrum (Figure 41). Looking into the geological map of the area (Figure 49 shows the northern area with elevated uranium concentration correlated to the artificial aggradation referred as “Künstliche Aufschüttung” in Figure 50). In contrast, the southern area with elevated uranium concentration does not accord to the respective artificial aggradation but is located to the south of it in an area with crumbled slate referred as “Sand- bis Schluffstein (Salzton), Kalk- und Dolomitstein (Leinedolomit), Anhydrit / Gips, Steinsalz / Lösungsrückstände” in Figure 50. Paleozoic rocks (schists, phyllites) are predominant. Their natural activities are highly overshadowed by radiation from the settling ponds.
The map of ^{137}Cs activity concentration (Figure 48) shows low values throughout the reference area. The elevated uranium concentration yields the opportunity to check on the quality of the stripping correction matrix (Table 1). In the case of misaligned correction values, the pattern of the elevated values of ^{238}U activity concentration would be reproduced in the derived activity concentrations of the natural radionuclide ^{40}K and the artificial radionuclide ^{137}Cs (Figures 47 and 48). As this is not the case, the values listed in Table 1 are affirmed.

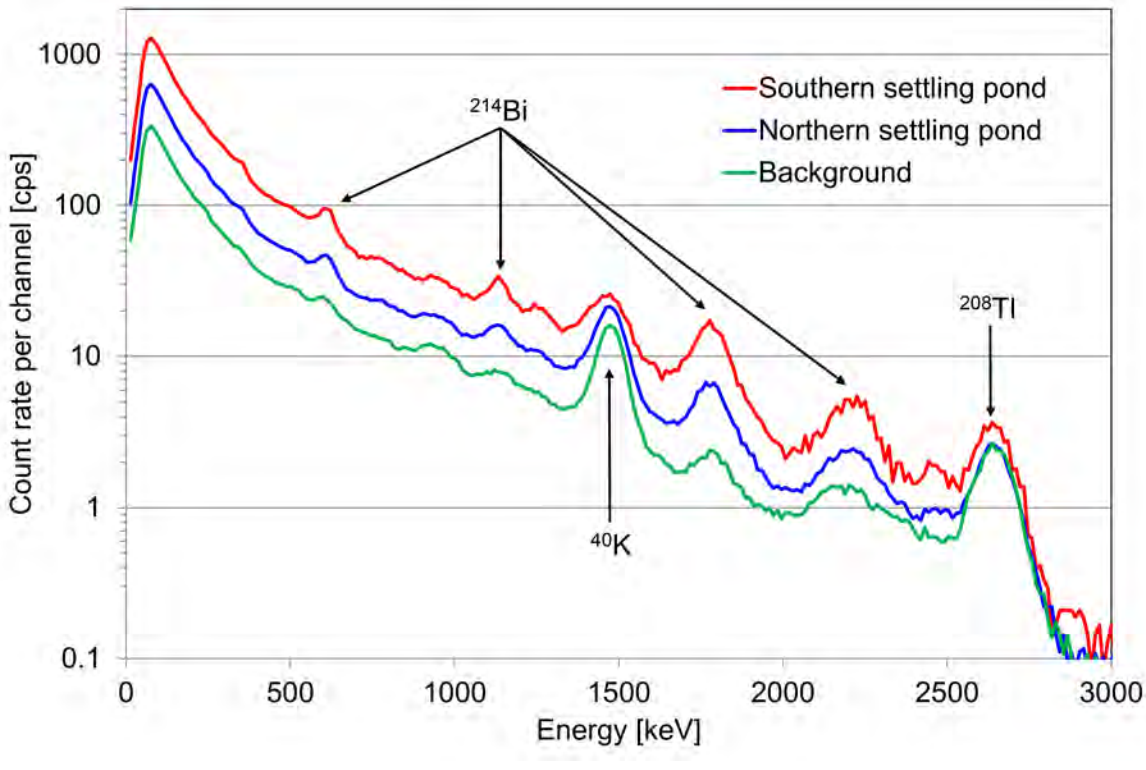

Figure 41: Photon spectra measured over the settling ponds.

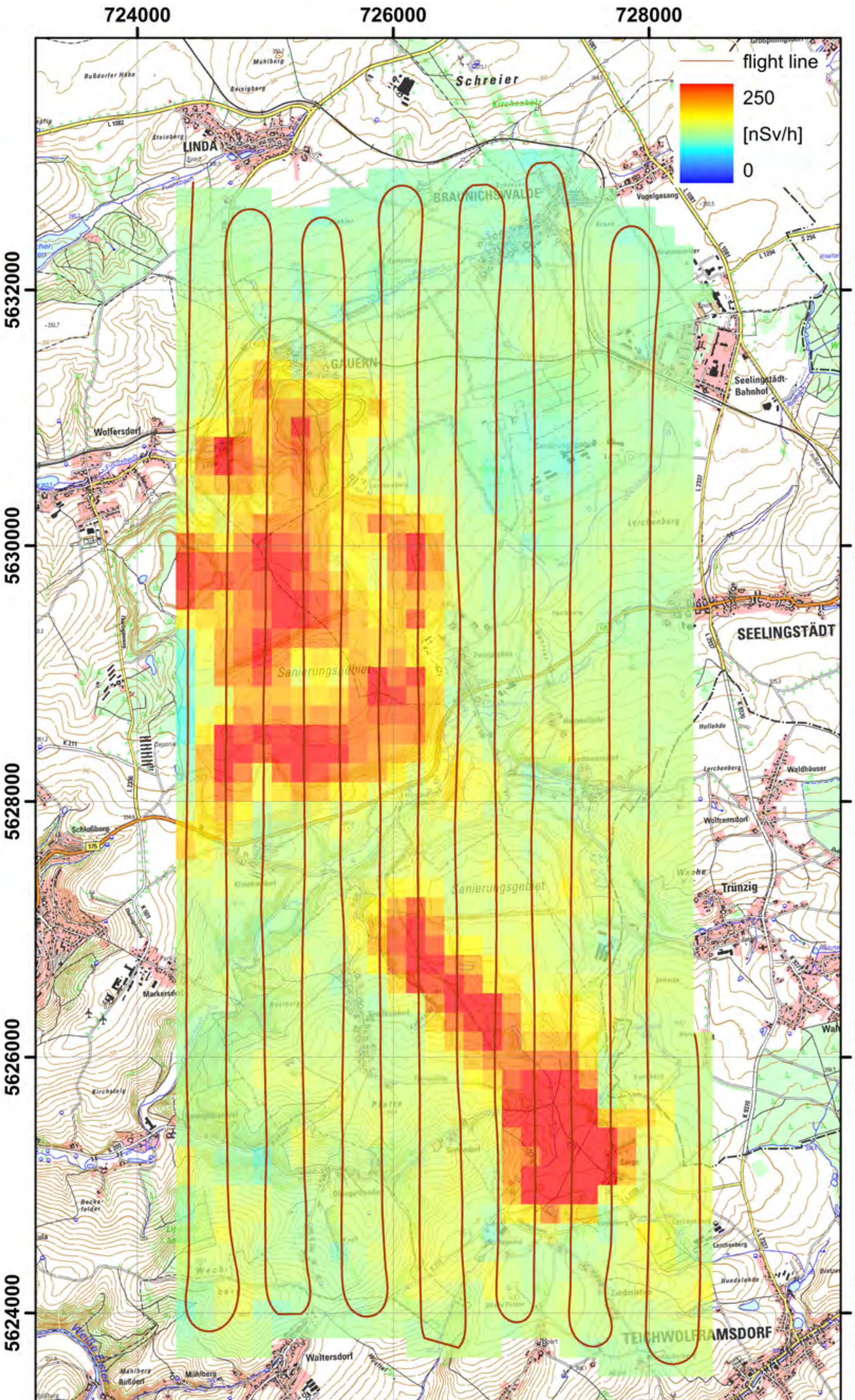

Figure 42: Dose rate over the reference area near Seelingstädt. DTK25 ©Bundesamt für Kartographie und Geodäsie, Frankfurt a. M.

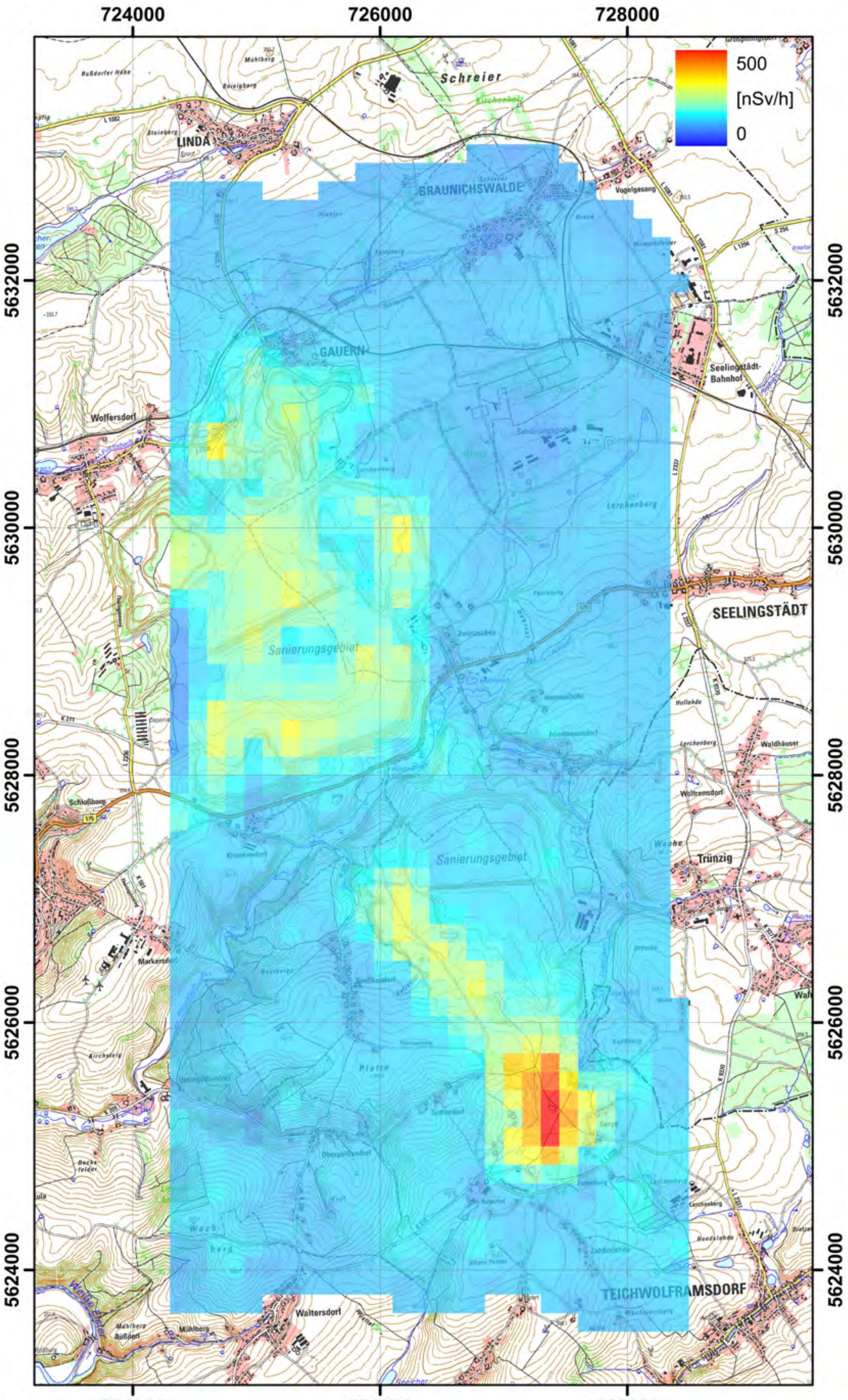

Figure 43: Dose rate over the reference area near Seelingstädt (re-scaled). DTK25 ©Bundesamt für Kartographie und Geodäsie, Frankfurt a. M.

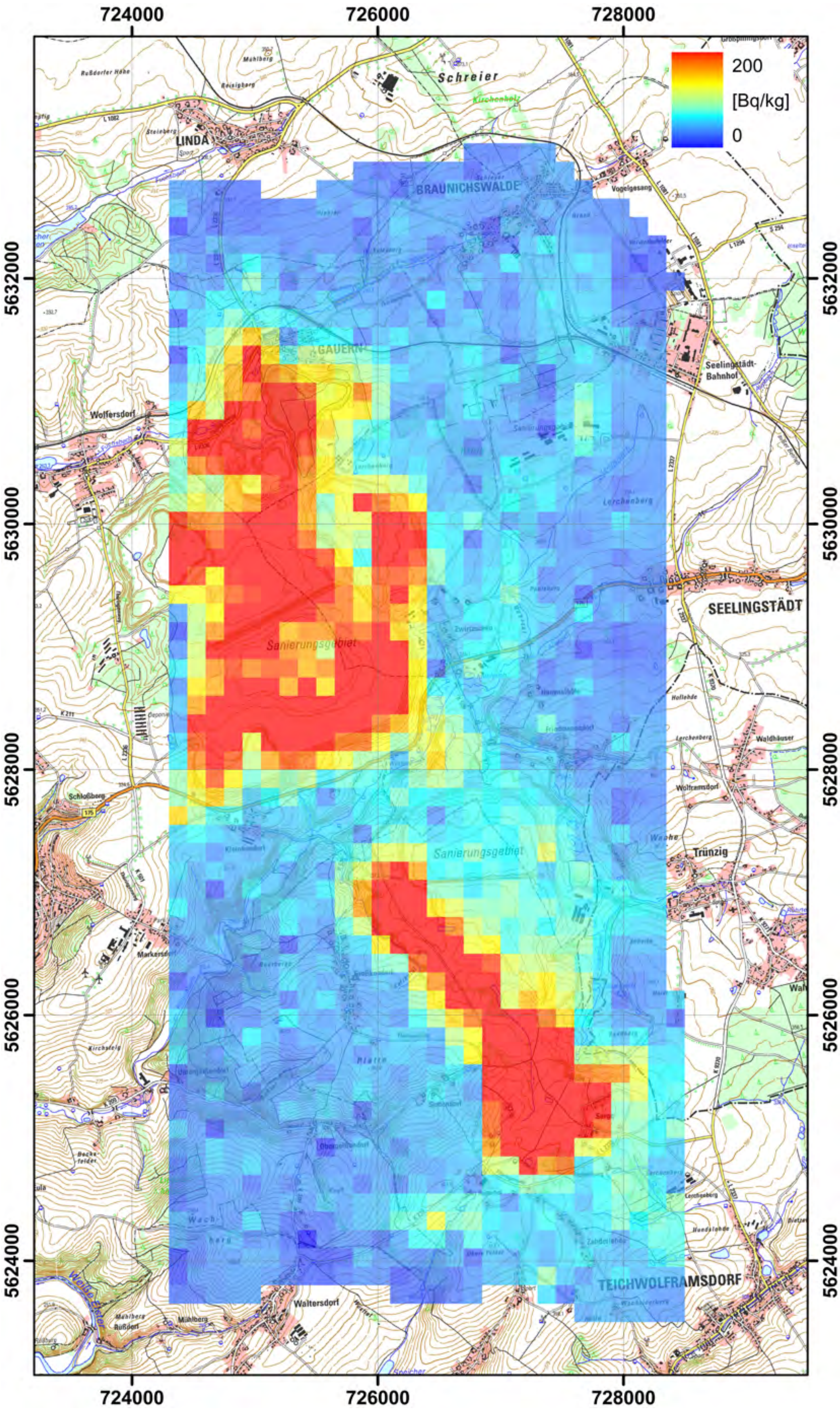

Figure 44: ^{238}U activity concentration of the reference area near Seelingstädt. DTK25 ⓒBundesamt für Kartographie und Geodäsie, Frankfurt a. M.

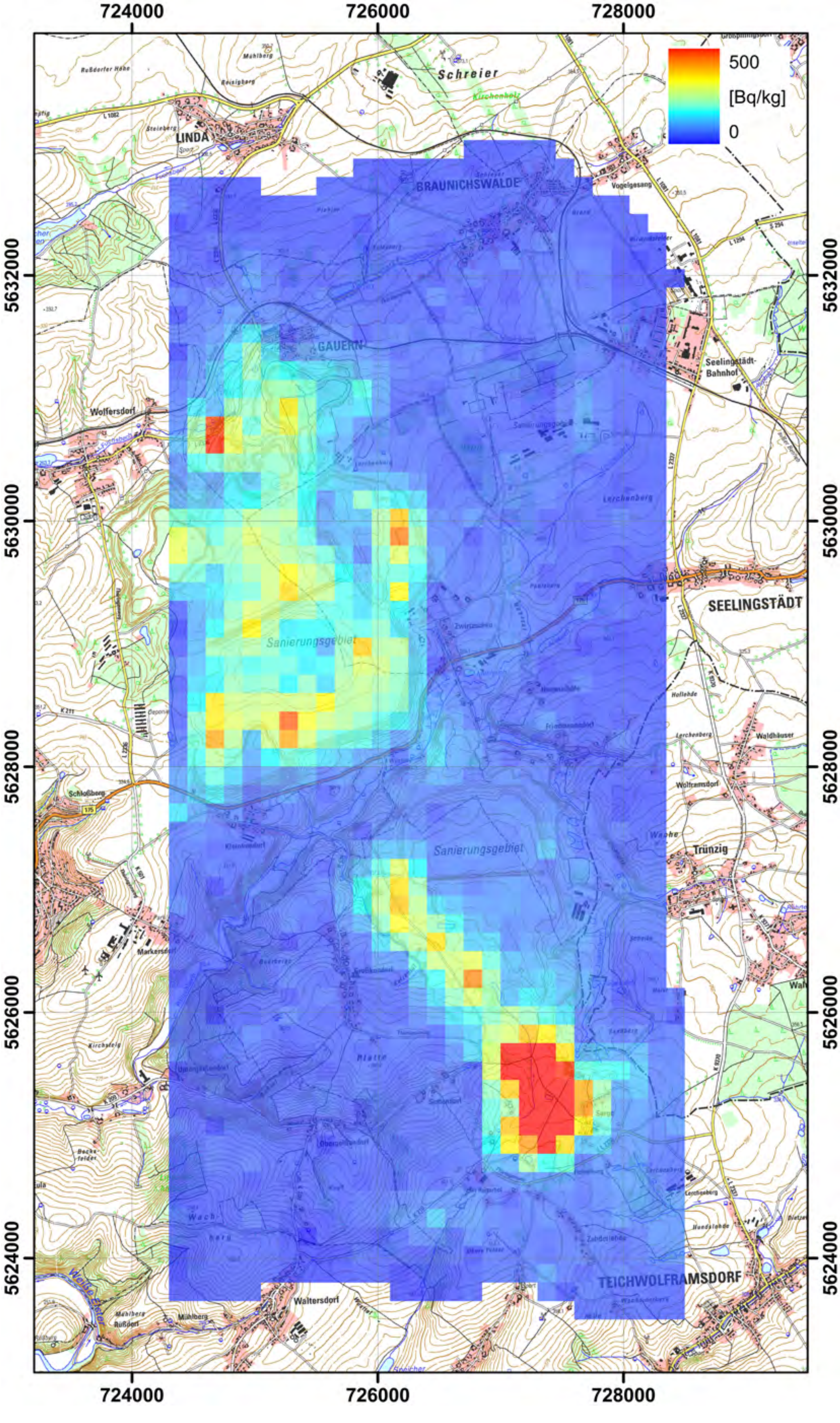

Figure 45: ^{238}U activity concentration of the reference area near Seelingstädt (re-scaled). DTK25 ⓒBundesamt für Kartographie und Geodäsie, Frankfurt a. M.

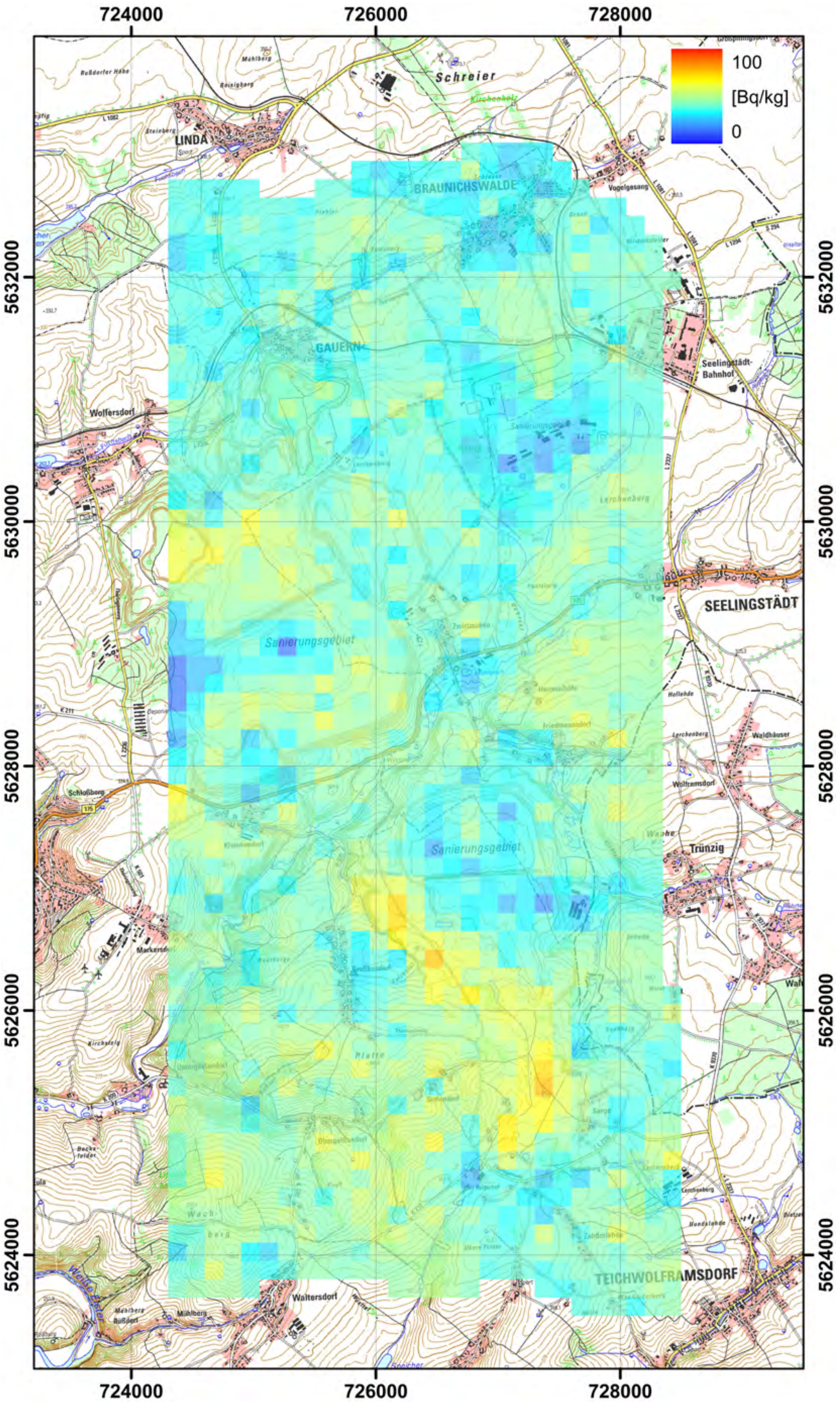

Figure 46: ^{232}Th activity concentration of the reference area near Seelingstädt. DTK25 ©Bundesamt für Kartographie und Geodäsie, Frankfurt a. M.

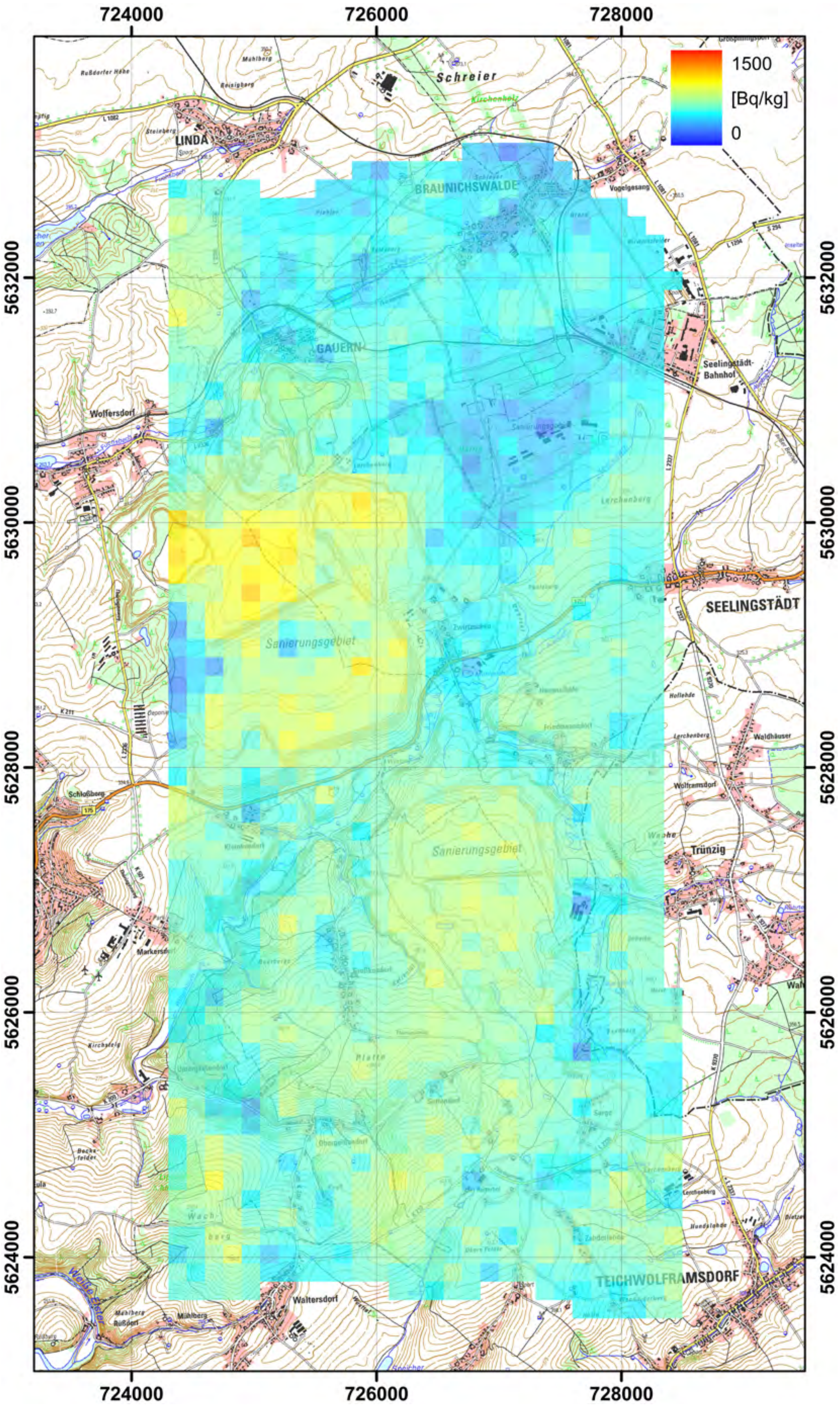

Figure 47: ^{40}K activity concentration of the reference area near Seelingstädt. DTK25 ⓒBundesamt für Kartographie und Geodäsie, Frankfurt a. M.

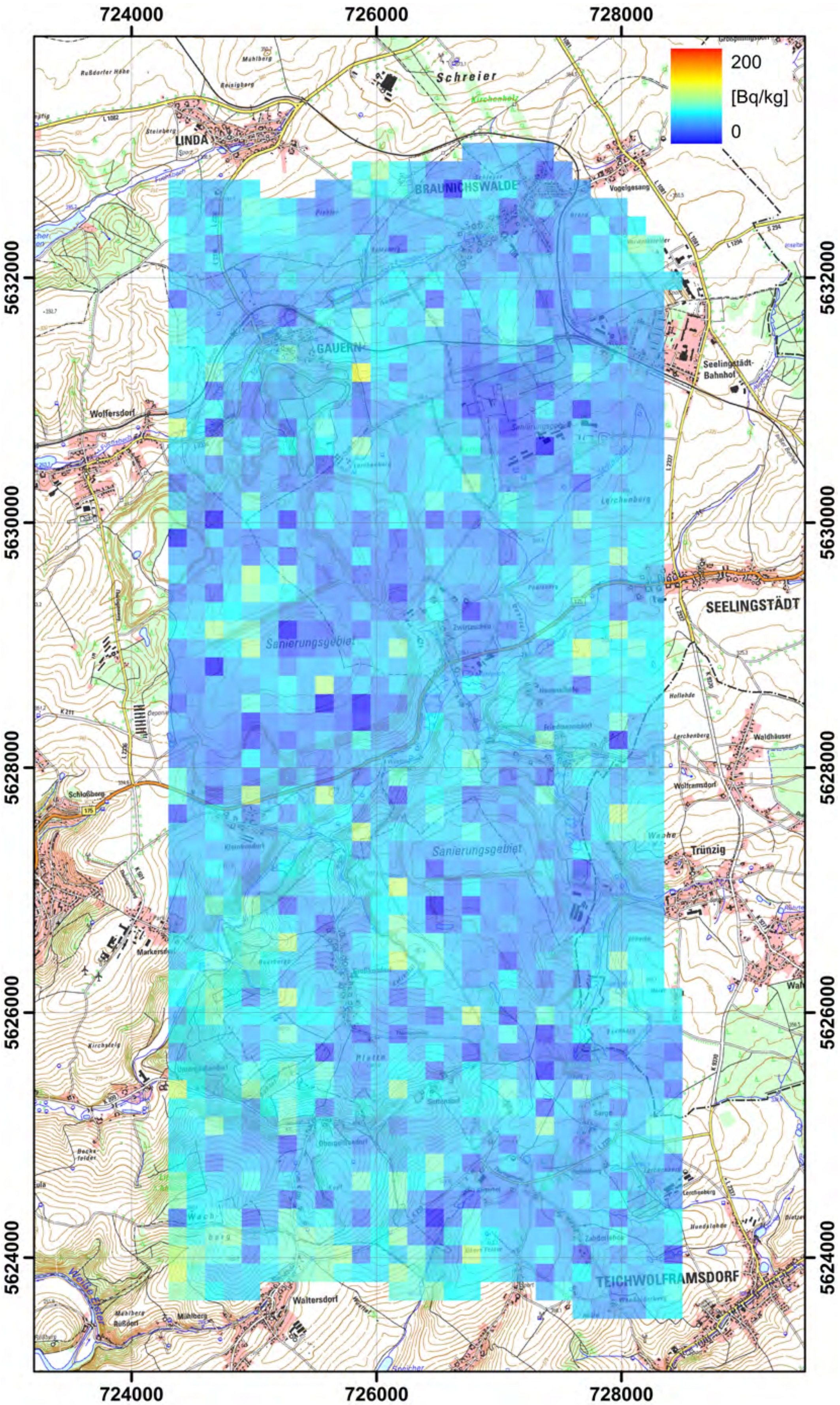

Figure 48: ^{137}Cs activity concentration of the reference area near Seelingstädt. DTK25 ⓒBundesamt für Kartographie und Geodäsie, Frankfurt a. M.

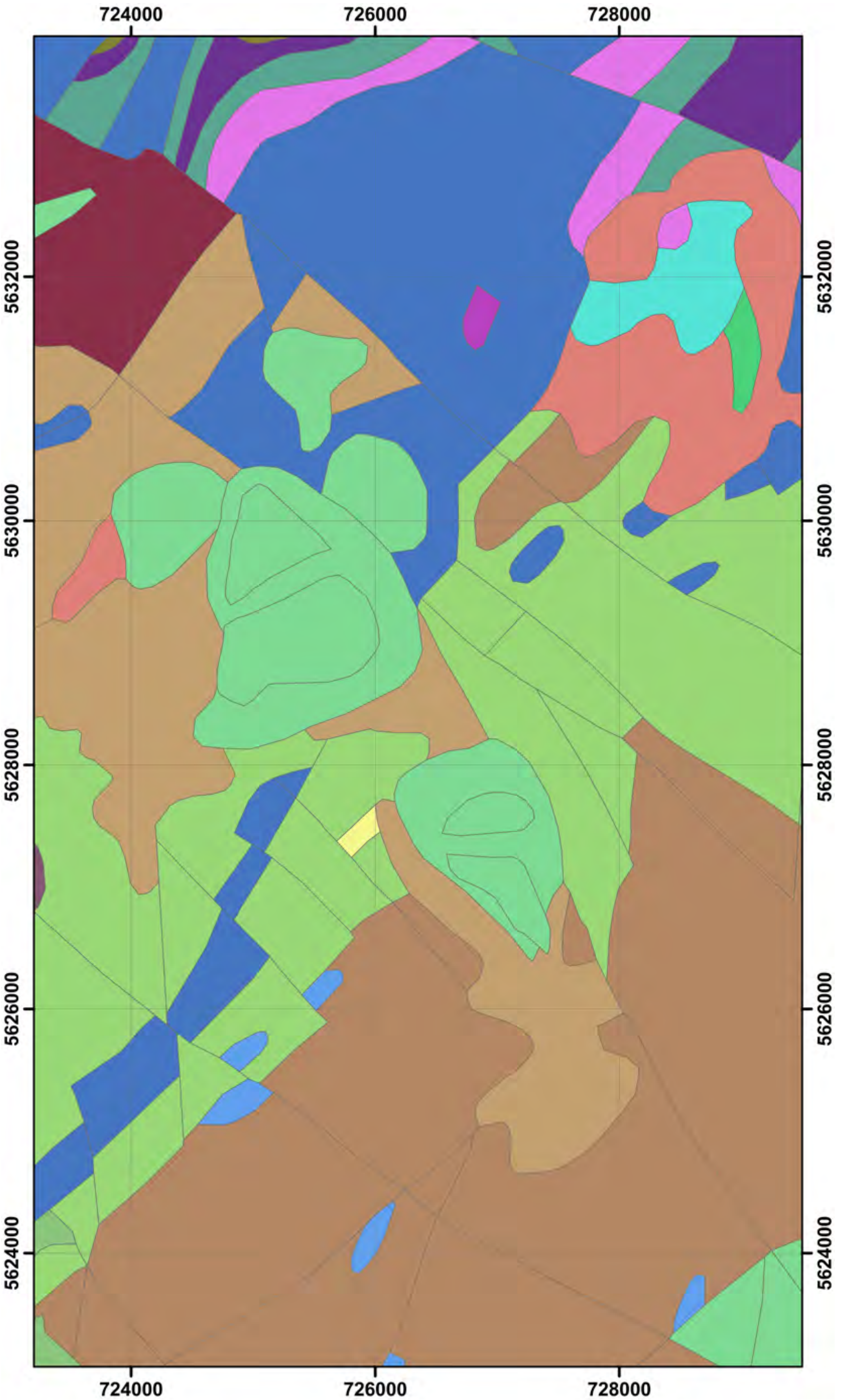

Figure 49: Geology of the reference area near Seelingstädt. GÜK200 ©Bundesamt für Kartographie und Geodäsie, Frankfurt a. M..

Figure 50: Legend for the geological map of the reference area near Seelingstädt (in German). GÜK200 ©Bundesamt für Kartographie und Geodäsie, Frankfurt a. M..

2.7.3 Composite mapping

A total area of 2000 square kilometers was measured by the five teams with a line spacing of 1 km. Each measuring team was assigned a square of 20 km times 20 km. The area assigned to the Swiss team named B1 was located near Reichenbach in the north-west of the composite mapping area. The survey area includes two granitic bodies. A roughly circular granitic body (Kirchberger Granit) is well visible in the north-eastern part of Figure 57, comprising the localities Kirchberg and Lengenfeld. A smaller in northeast-southwest direction elongated granitic body (Bergauer Granit) is located in the south-western corner of Figure 57, comprising the locality Bergen. Both granite bodies were formed 300 Ma ago in the variscan orogeny.The generally elevated values of dose rate, ^{238}U, ^{232}Th, and ^{40}K activity concentrations reflect the granitic lithology. The dose rate map (Figure 51) shows an increased dose rate in the north-eastern part and a small area located in the south-west of the assigned area B1. The spectrum over the north-eastern subarea shows an elevated count rate in the peak associated with the ^{232}Th decay product ^{208}Tl compared to the background, whereas in the south-western subarea increased count rates of the high energy peaks of the ^{238}U decay product ^{214}Bi are observed (Figure 52). The map of the ^{238}U activity concentration (Figure 53) confirms the finding in the spectrum of the south-western subarea, but also indicates an increased value near the center of area B1. The spectrum (Figure 52) at this point, which is unremarkable in the dose rate map (Figure 51), shows indeed a nearly identical composition as the spectrum measured over the south-western corner of the measuring area. The geological map of area B1 (Figure 57) locates the center uranium anomaly close to an artificial aggradation referred as “Künstliche Aufschüttung” in Figure 58. The south western uranium anomaly is located over a metamorph intrusion body referred as “Metabasite” in Figure 58. Both ^{232}Th and ^{40}K activity concentrations show elevated values in the north-eastern part of area B1 (Figures 54 and 55), correlated to a granitic body (Figure 57) referred as “Granit, mittel- bis grobkörnig, porphyrisch” in Figure 58 which can be attributed to the often observed accumulation of natural radionuclides in granitic rock. The map of the activity concentration of the artificial radionuclide ^{137}Cs (Figure 56) shows slightly elevated values following the pattern of the ^{232}Th and ^{40}K activity concentrations (Figures 54 and 55) suggesting that the respective stripping and background correction should be inspected.

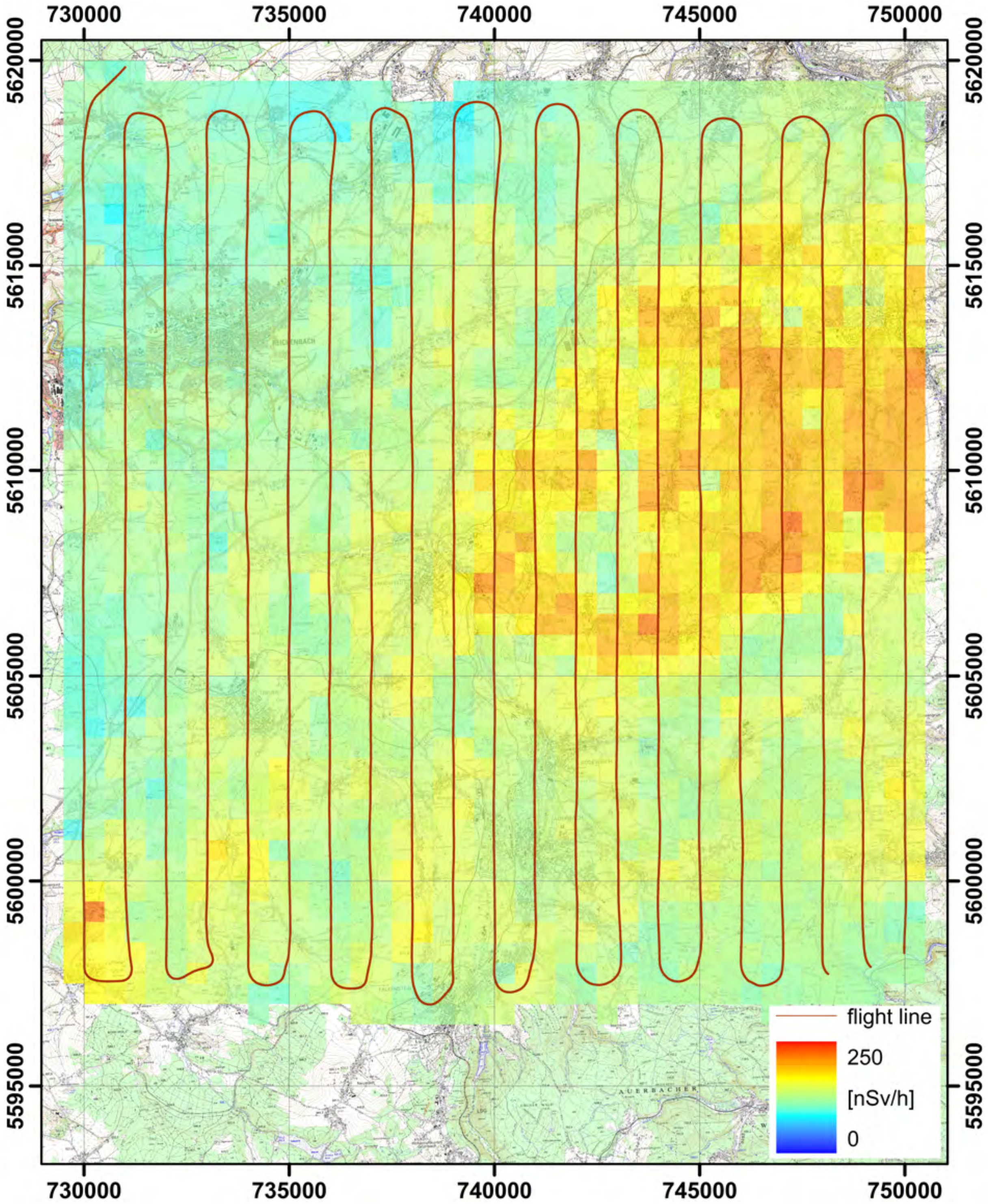

Figure 51: Dose rate over the composite mapping area B1. DTK25 ©Bundesamt für Kartographie und Geodäsie, Frankfurt a. M.

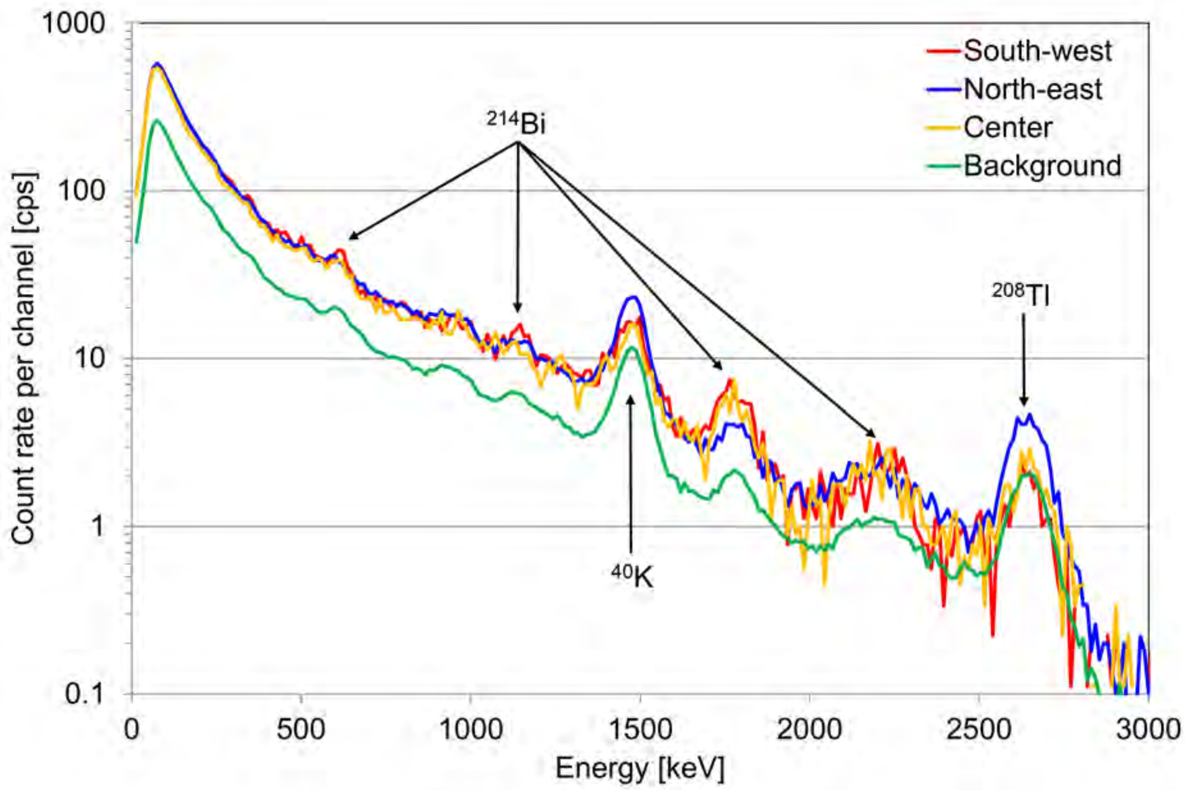

Figure 52: Photon spectra measured over area B1.

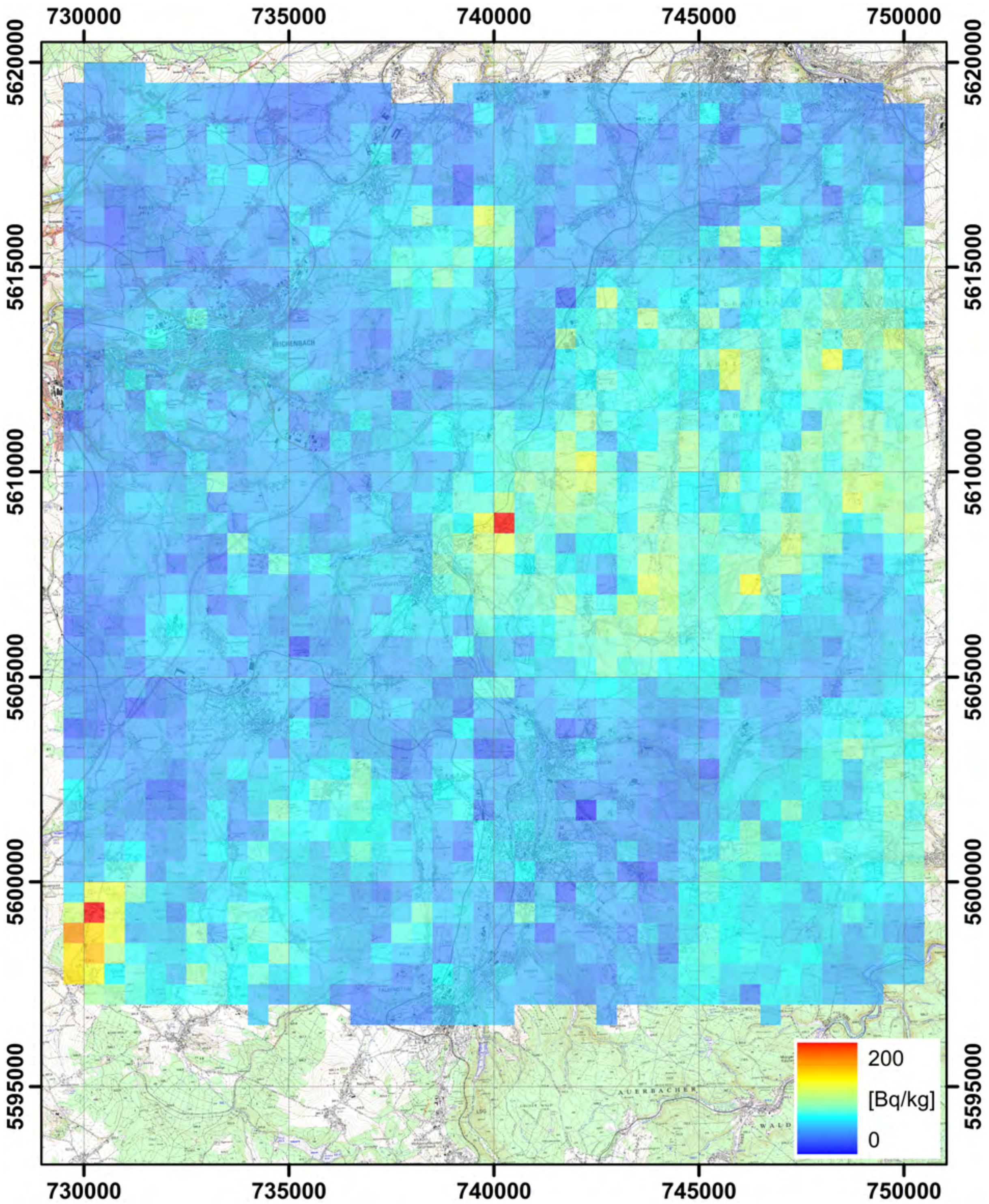

Figure 53: ^{238}U activity concentration of the composite mapping area B1. DTK25 ©Bundesamt für Kartographie und Geodäsie, Frankfurt a. M.

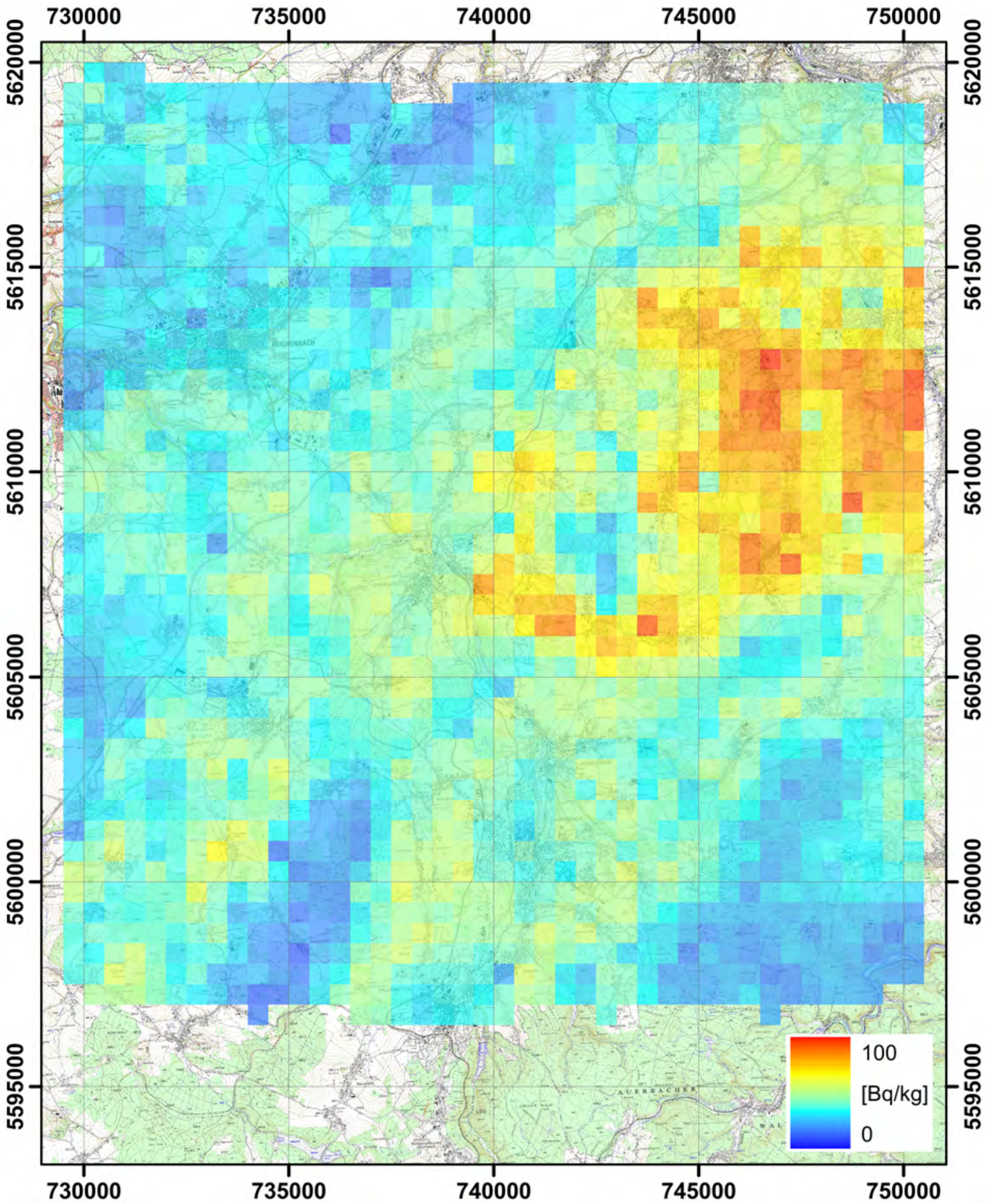

Figure 54: ^{232}Th activity concentration of the composite mapping area B1. DTK25 ©Bundesamt für Kartographie und Geodäsie, Frankfurt a. M.

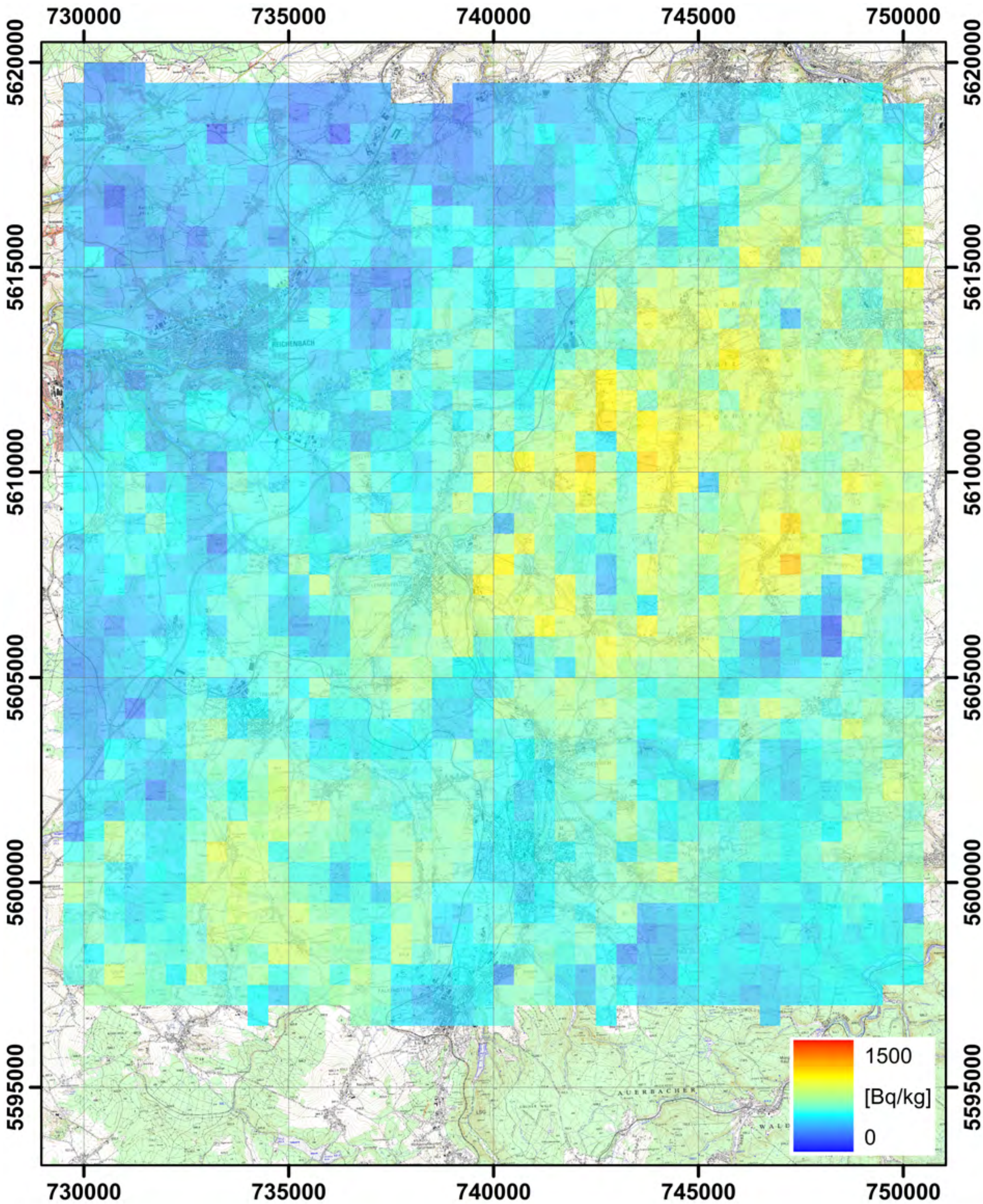

Figure 55: ^{40}K activity concentration of the composite mapping area B1. DTK25 ©Bundesamt für Kartographie und Geodäsie, Frankfurt a. M.

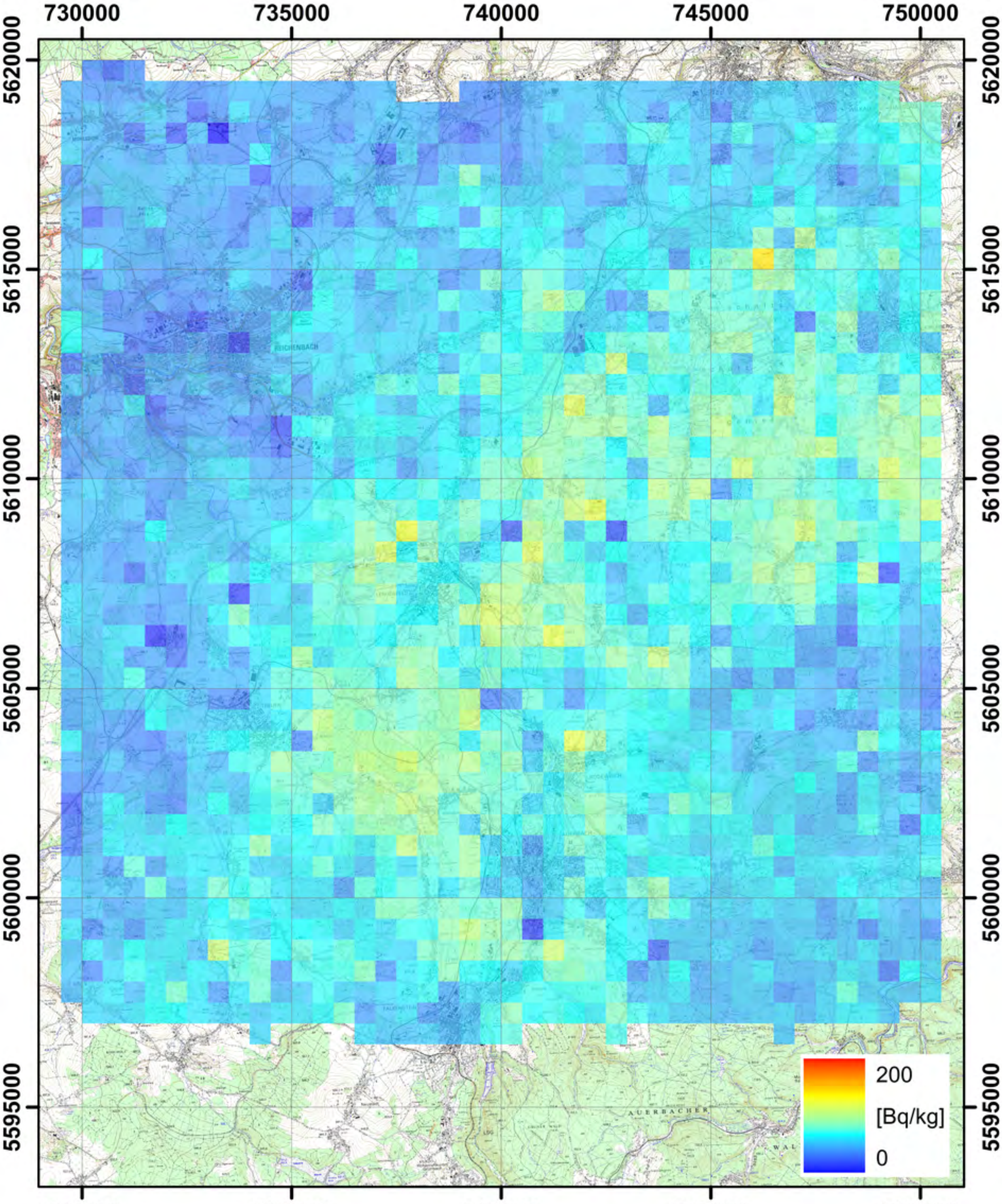

Figure 56: ^{137}Cs activity concentration of the composite mapping area B1. DTK25 ©Bundesamt für Kartographie und Geodäsie, Frankfurt a. M.

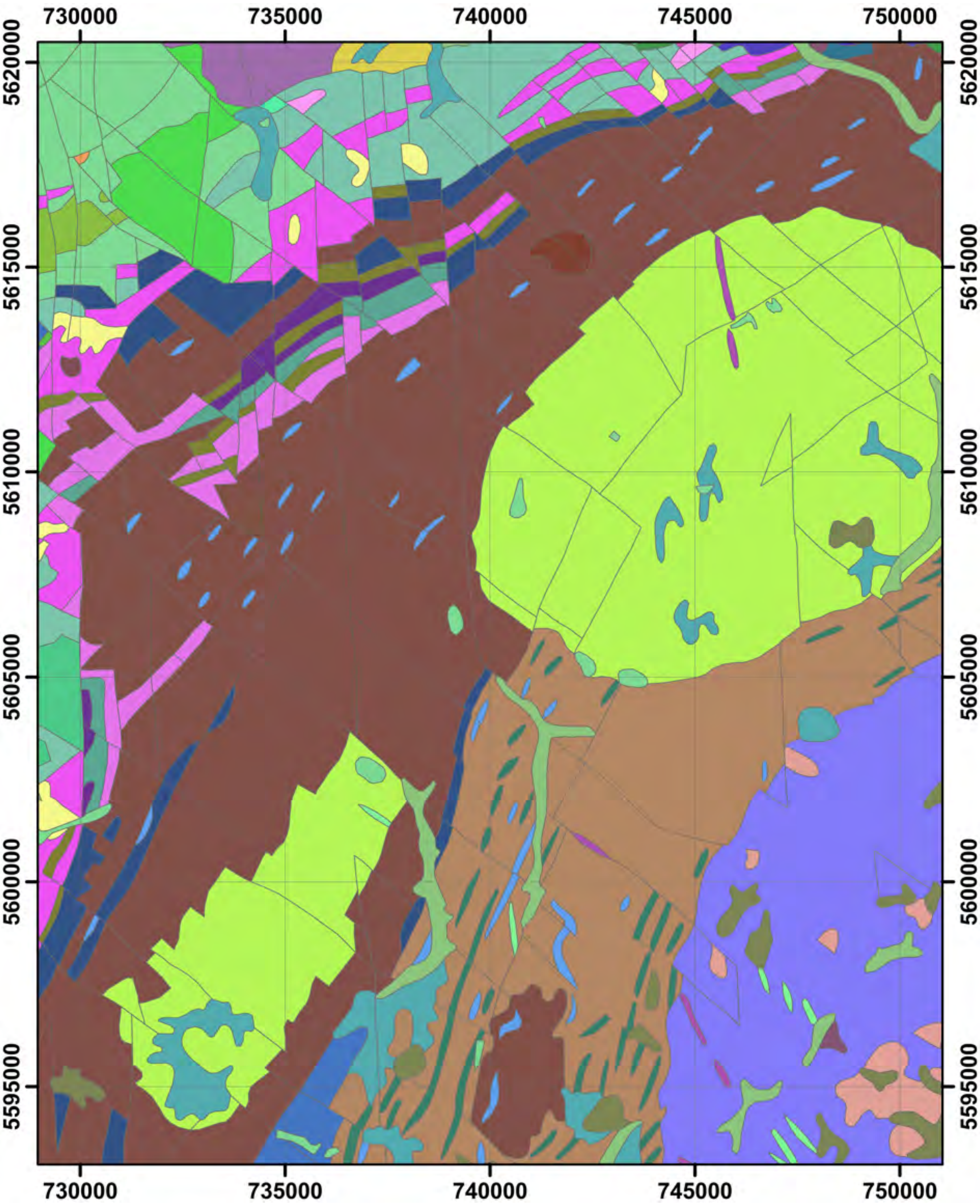

Figure 57: Geology of the composite mapping area B1. GÜK200 ©Bundesamt für Kartographie und Geodäsie, Frankfurt a. M..

Figure 58: Legend for the geological map of the reference area near Seelingstädt (in German). GÜK200 ©Bundesamt für Kartographie und Geodäsie, Frankfurt a. M..

2.7.4 Source search

Colleagues of the Helmholtz Zentrum Dresden Rossendorf (HZDR) placed radioactive sources on the premises of their institute to support the source search execise. Number of sources, radionuclides, activity and location were unknown to all participating teams.The Swiss search strategy spreads a dense net of flight lines over the search area, depending on the size of the area and the time available for the search flights. As the organiser provided ample flight time over the HZDR, addional flightlines could be introduced spontaneously by the measuring team (Figure 59). The dose rate map (Figure 60) over the source search area showed no clear increases. Thus, the placed sources had either rather low activities or contained radionuclides not detectable with airborne gammaspectrometry. The main parameter used for the identification of areas with suspected artificial radionuclides, the MMGC-ratio, showed only weak indications for the presence of artificial radionuclides in the standard color scale (Figure 61). Only the use of a more sensitive scale for the presentation of the MMGC-ratio, which is accompanied by a larger probability to produce false positive indications, pointed clearly to two possible source locations (Figure 62) at coordinates (847159,5668391) and (847188,5668085). The photon spectra measured over these two locations indicated the presence of ^{60}Co (Figure 63). A slight increase of the MMGC-ratio at coordinate (847475,5668123) was confirmed by the map of the Caesium net count rate (Figure 64) and by the photon spectrum over this point and suggested the presence of a ^{137}Cs source. Point source activities together with their uncertainties were estimated from the net count rates over the source locations (Table 13). All detected sources have activities near or below the detection limit of the measuring system at a ground clearance of 90 m (200 MBq for ^{60}Co and 500 MBq for ^{137}Cs). The disclosure of the parameters of the placed sources and the comparison with the reported values will be performed and published by the organisers.

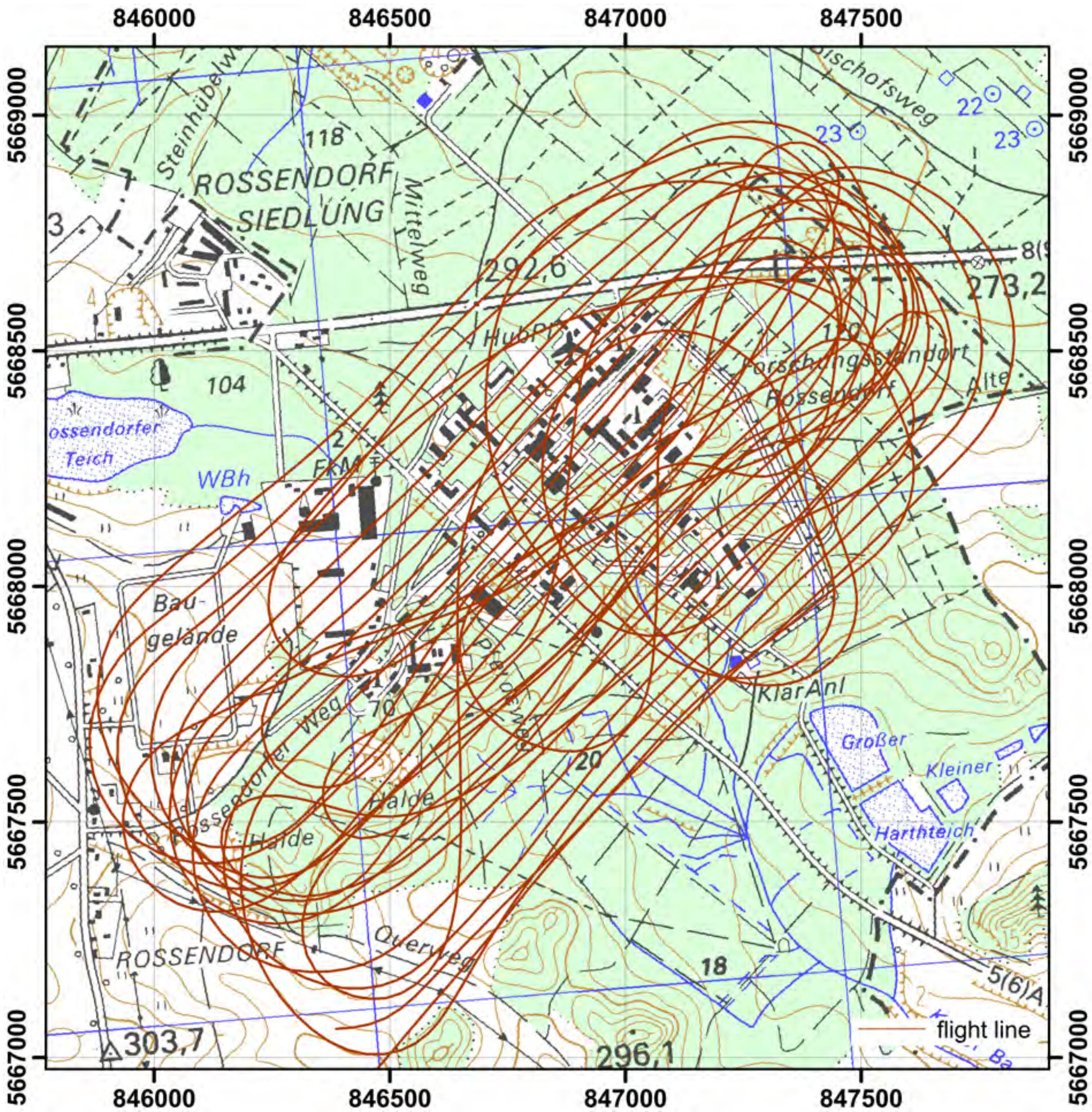

Figure 59: Flight line over the source search area. DTK25 ©Bundesamt für Kartographie und Geodäsie, Frankfurt a. M.

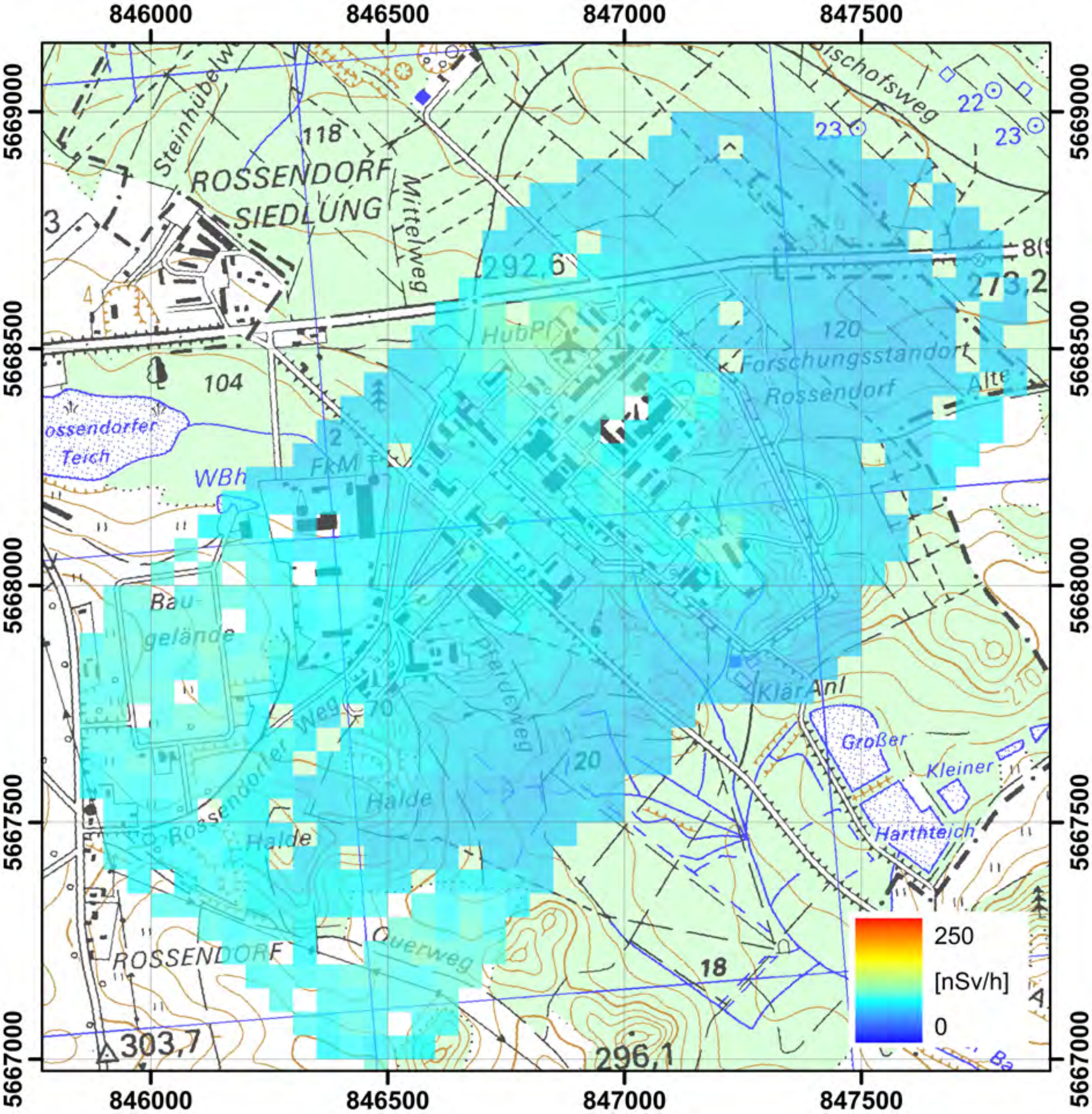

Figure 60: Dose rate over the source search area. DTK25 ©Bundesamt für Kartographie und Geodäsie, Frankfurt a. M.

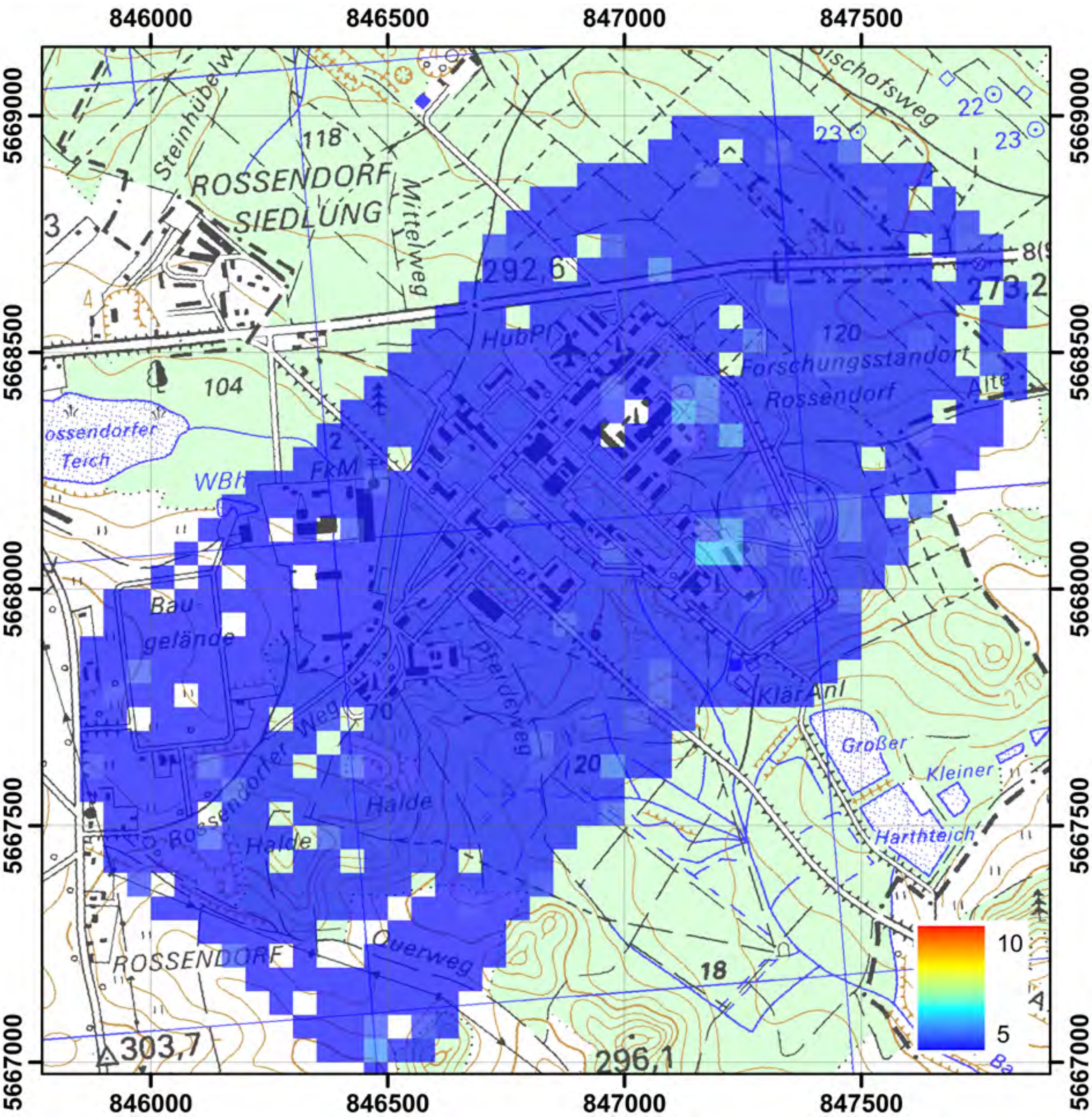

Figure 61: Man-made gross-count (MMGC) ratio over the source search area. DTK25 ©Bundesamt für Kartographie und Geodäsie, Frankfurt a. M.

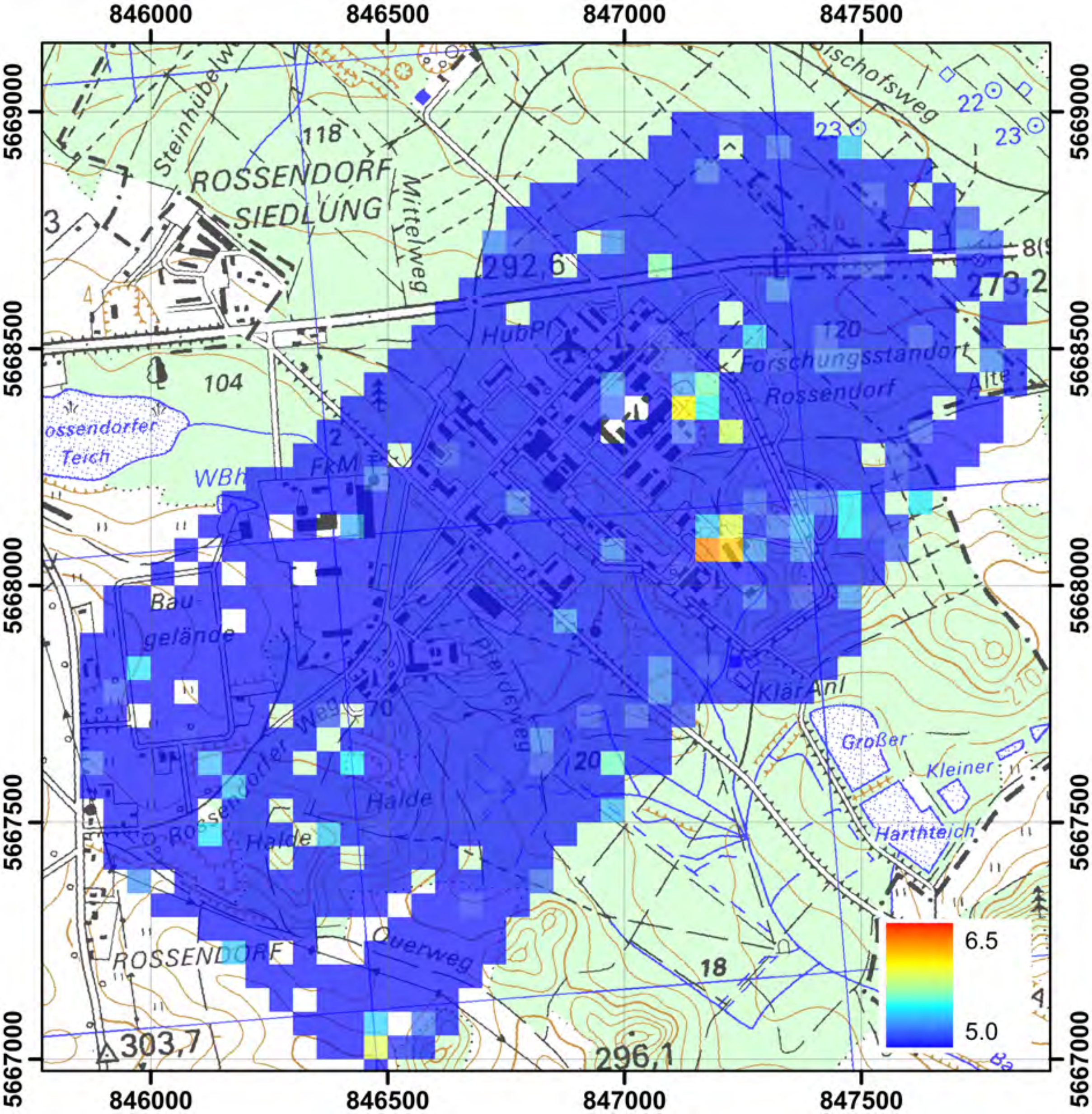

Figure 62: Man-made gross-count (MMGC) ratio over the source search area (re-scaled). DTK25 ©Bundesamt für Kartographie und Geodäsie, Frankfurt a. M.

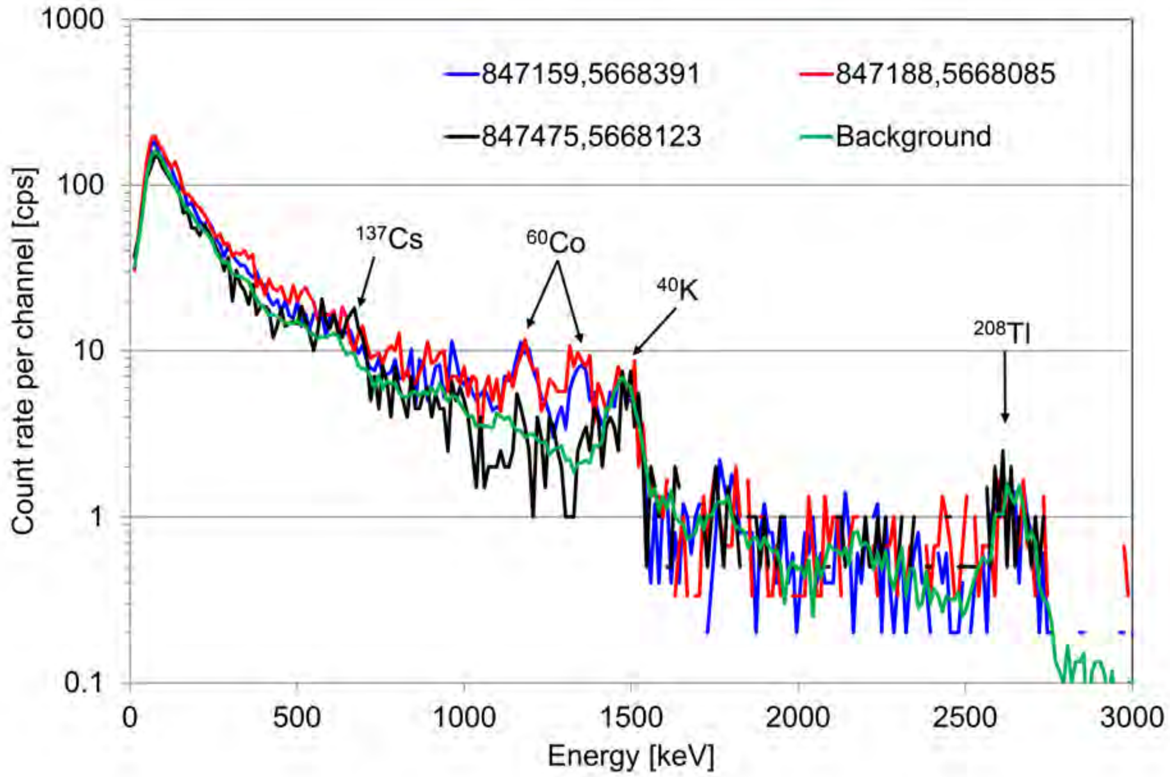

Figure 63: Photon spectra measured over the source search area.

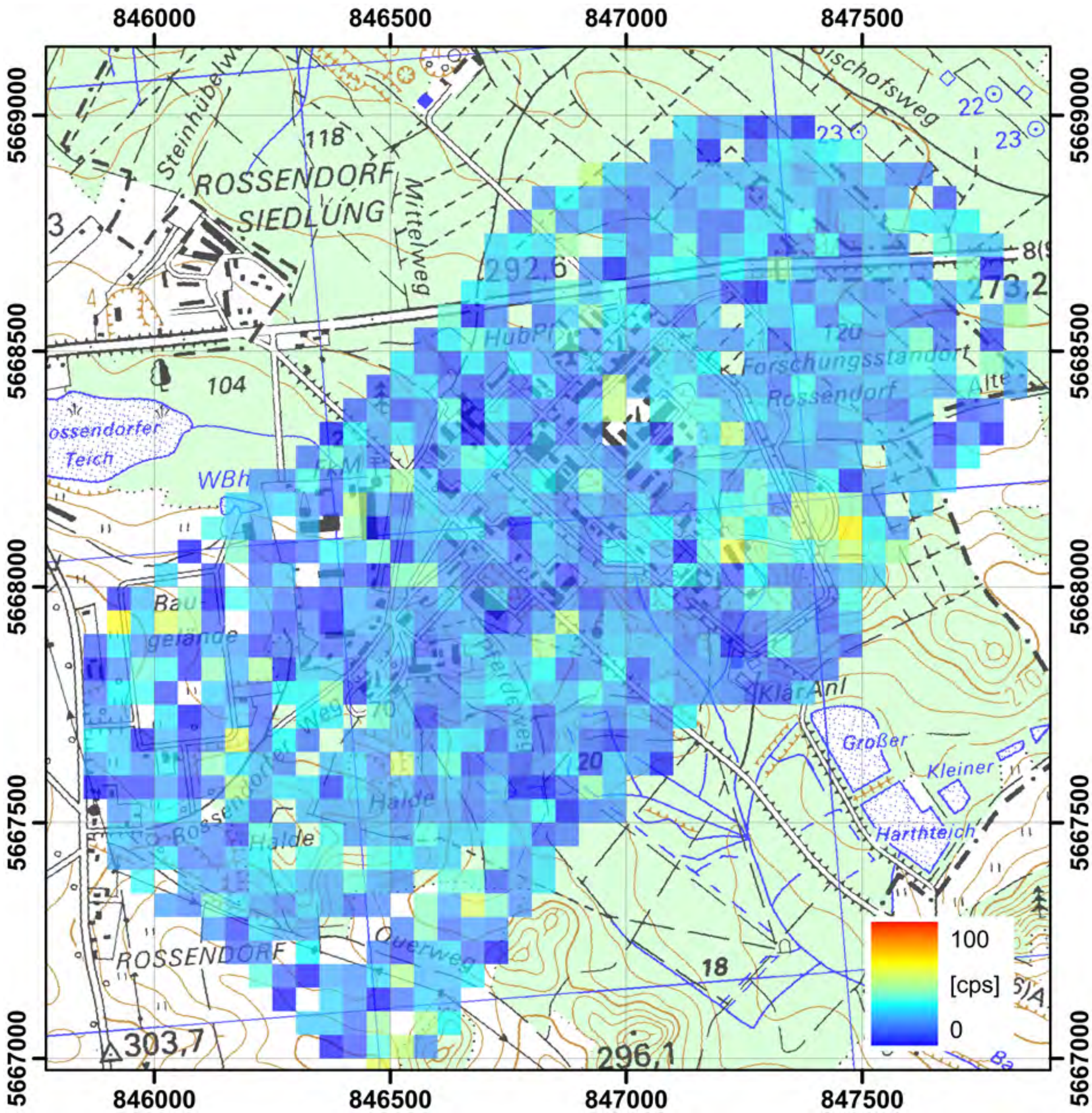

Figure 64: Net count rate in the ^{137}Cs energy window over the source search area. DTK25 ©Bundesamt für Kartographie und Geodäsie, Frankfurt a. M.

Nuclide	Coordinate		Activity
	x	y	[MBq]
^{60}Co	847188	5668085	400 ± 200
^{60}Co	847159	5668391	260 ± 130
^{137}Cs	847475	5668123	360 ± 200

Table 13: Estimated activities of the detected sources.

2.7.5 Joint mapping with team IRSN

The first joint mapping task was together with the French colleagues from IRSN in an area named E north of Zwickau. This was the first Swiss flight of the exercise with normal intrinsic background. As the organisers provided ample time for this task, the flight lines were planned with a rather large overlap to obtain a direct intercomparison between the results (Figure 65). The flight schedule of both teams was designed to enable simultaneous operation of both helicopters in area E. This report concentrates on the results of the Swiss team. The combined results of both teams will be analysed and published by the organisers of the intercomparison exercise. The dose rate map of the area (Figure 66) shows two clear areas with elevated dose rates which are associated with mining waste tips. The largest dose rates up to 900 nSv/h are measured over the south-western mining waste tip (Figure 67). The photon spectra show an increase of photons originating from the natural ^{238}U and ^{232}Th decay chains (Figure 68). The main component producing the elevated dose rate is ^{238}U with activity concentrations up to 1900 Bq/kg (Figures 69 and 70) with a small component of ^{232}Th at the north-eastern mining waste tip (Figure 71). The map of the ^{40}K activity concentration (Figure 72) shows elevated concentrations over the part of the south-western mining waste tip, which has a less high uranium signal. An interpretation of this pattern could be the ongoing recultivation of the waste tip. The area with elevated ^{40}K activity concentration and reduced ^{238}U activity concentration thus represents the area already covered with potassium rich topsoil. The absence of a spatial pattern similar to the spatial pattern of the natural radionuclides in the map of the ^{137}Cs activity concentration (Figure 73) indicates adequate stripping correction values.

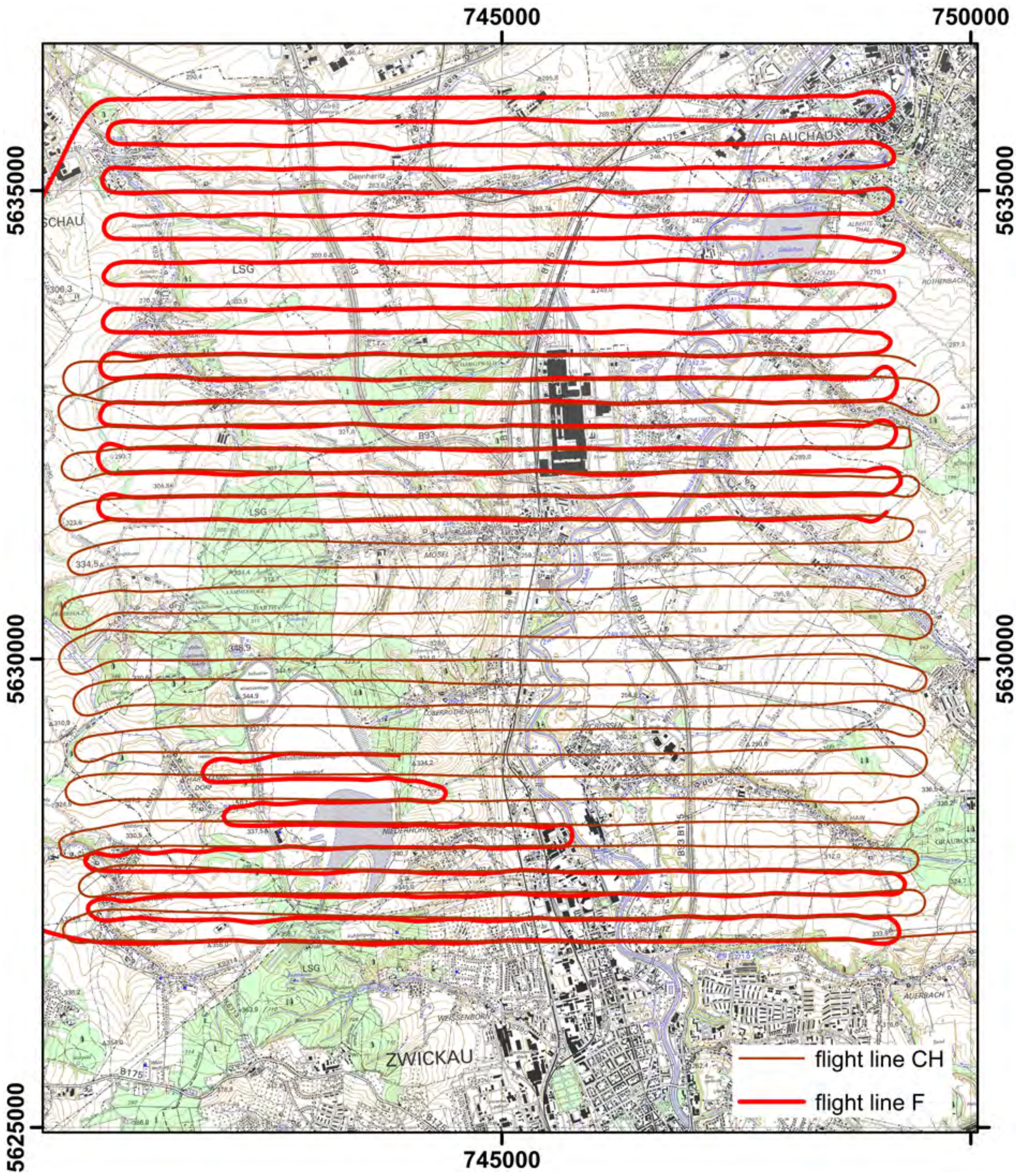

Figure 65: Flight lines over joint mapping area E. DTK25 ©Bundesamt für Kartographie und Geodäsie, Frankfurt a. M.

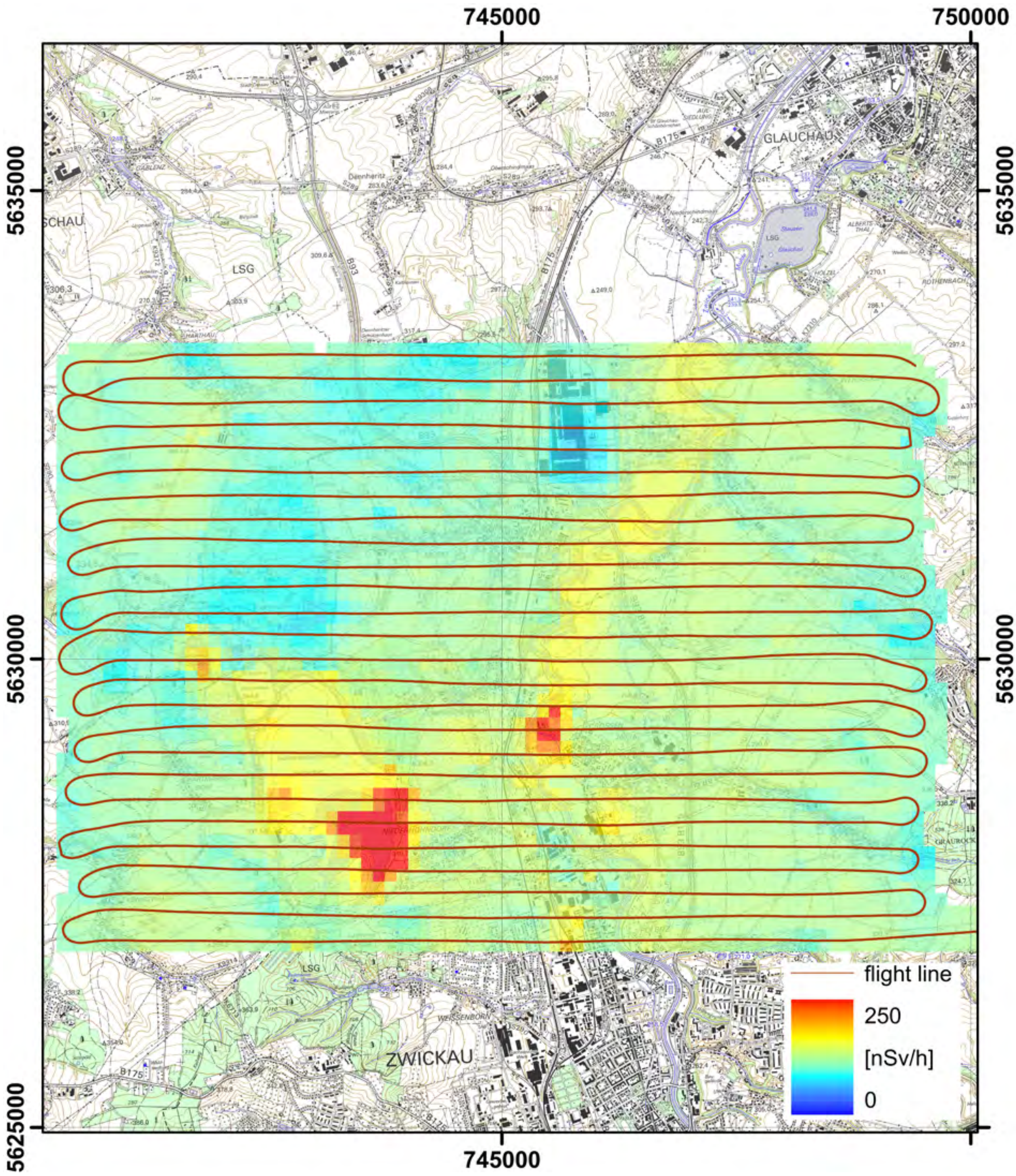

Figure 66: Dose rate over joint mapping area E. DTK25 ©Bundesamt für Kartographie und Geodäsie, Frankfurt a. M.

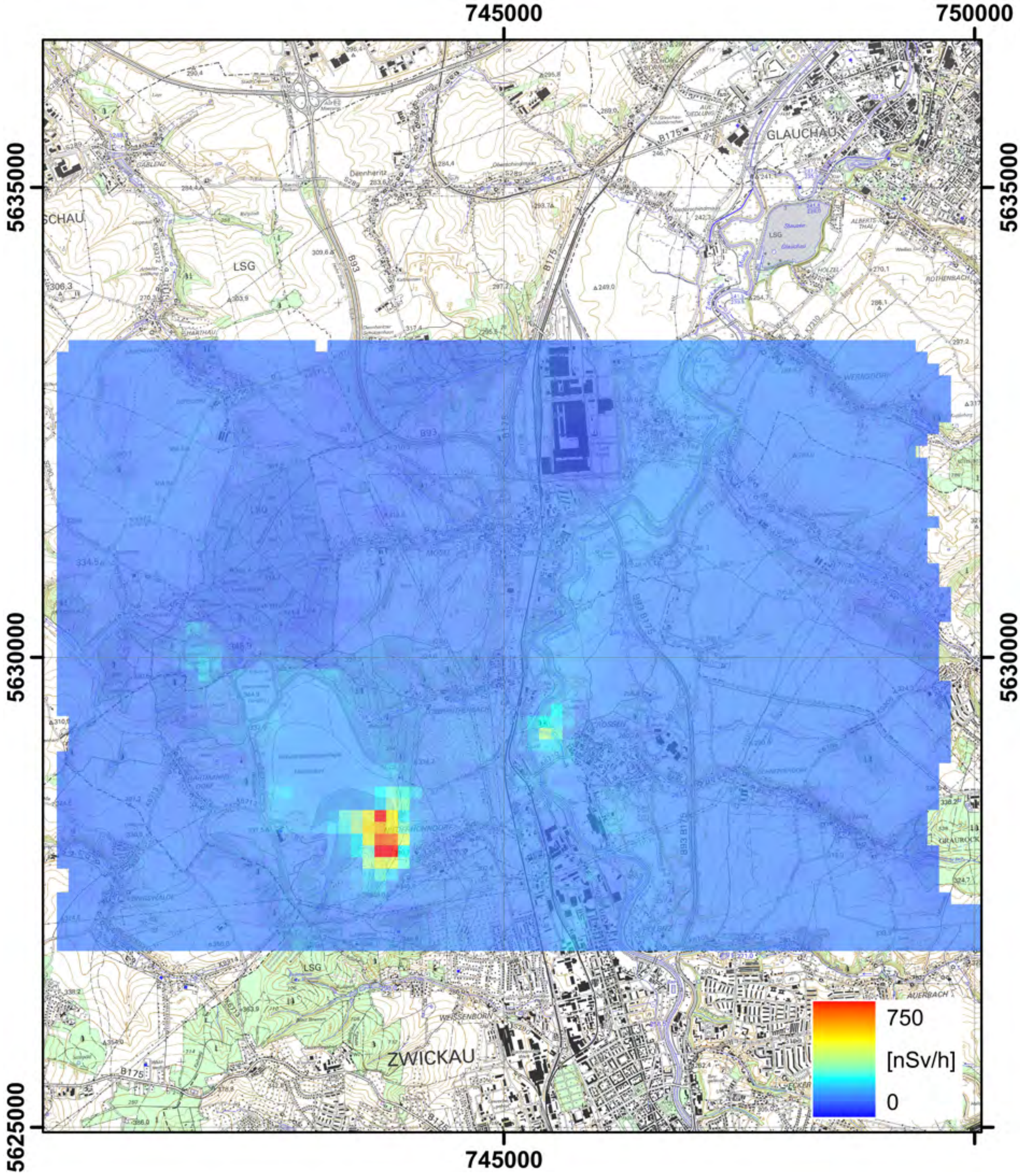

Figure 67: Dose rate over joint mapping area E (re-scaled). DTK25 ©Bundesamt für Kartographie und Geodäsie, Frankfurt a. M.

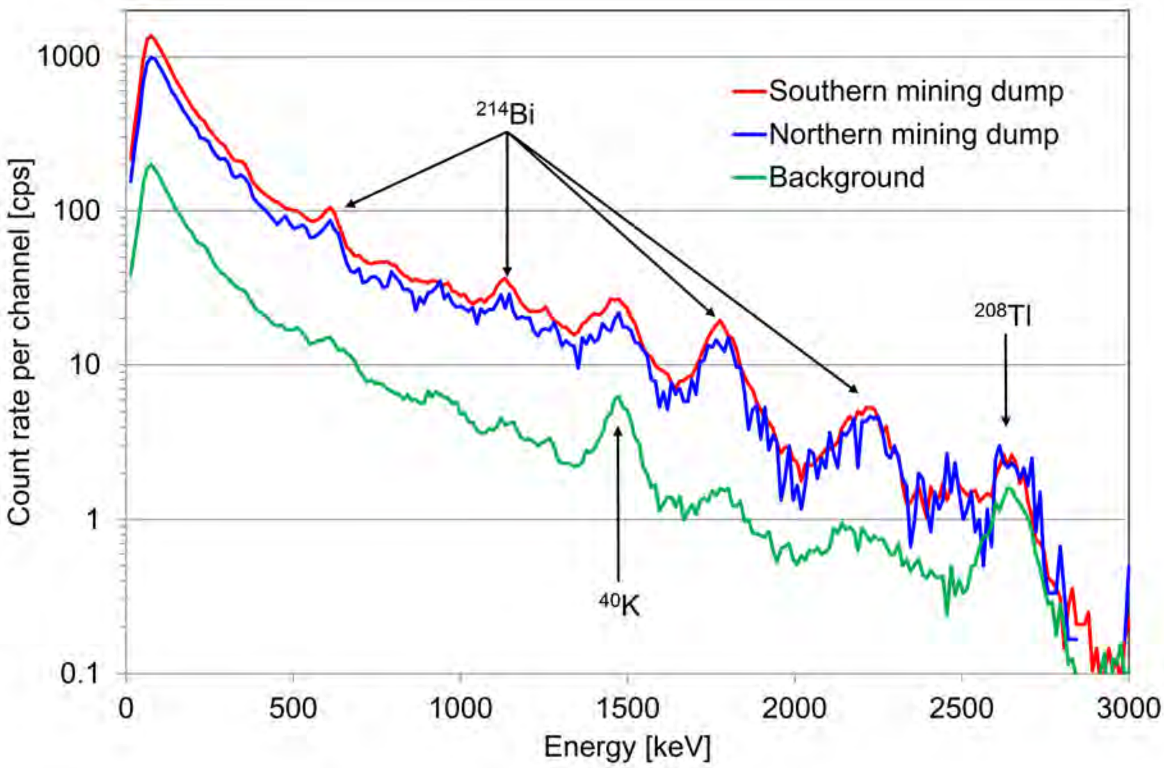

Figure 68: Photon spectra measured over joint mapping area E.

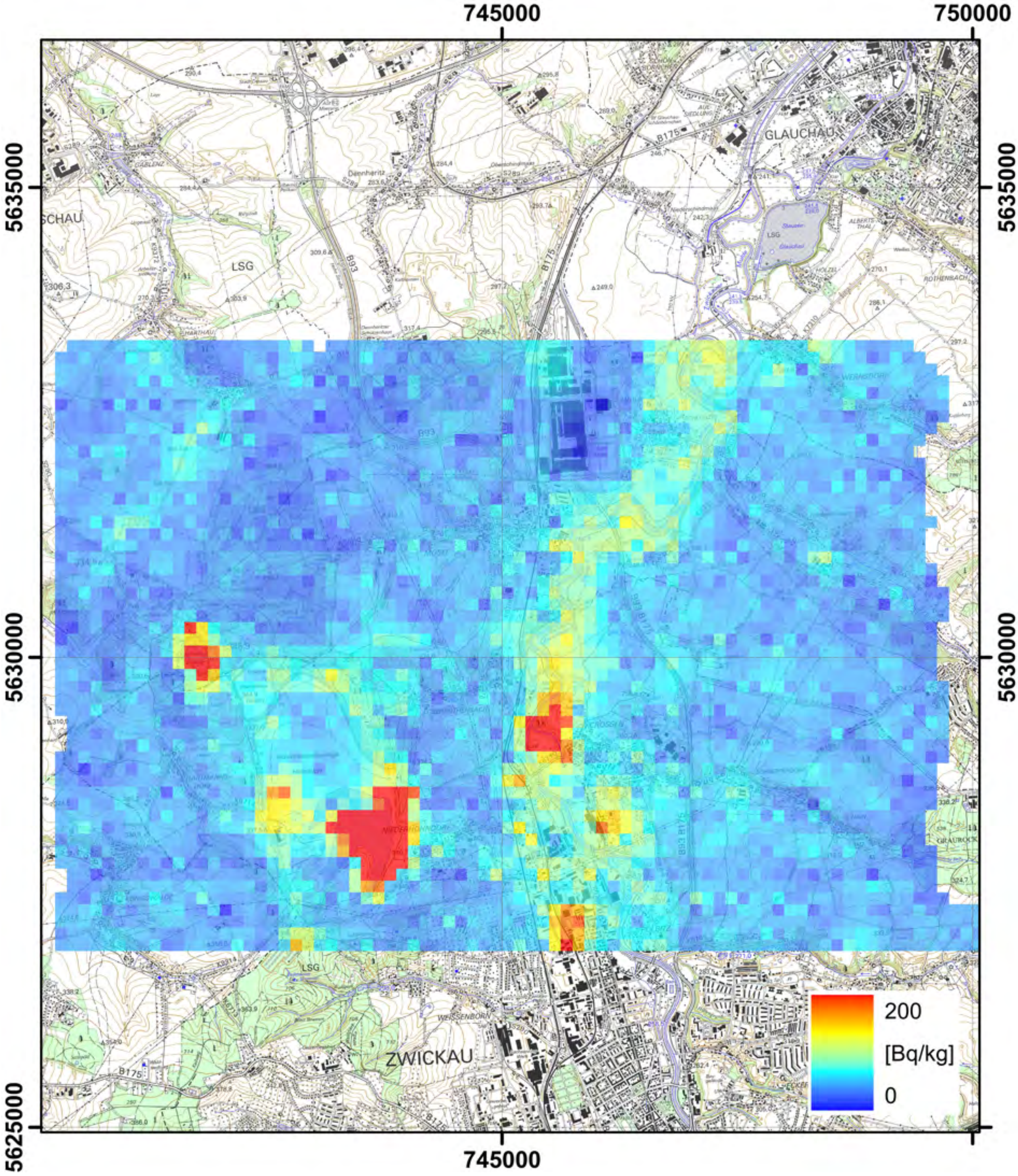

Figure 69: ^{238}U activity concentration of joint mapping area E. DTK25 ©Bundesamt für Kartographie und Geodäsie, Frankfurt a. M.

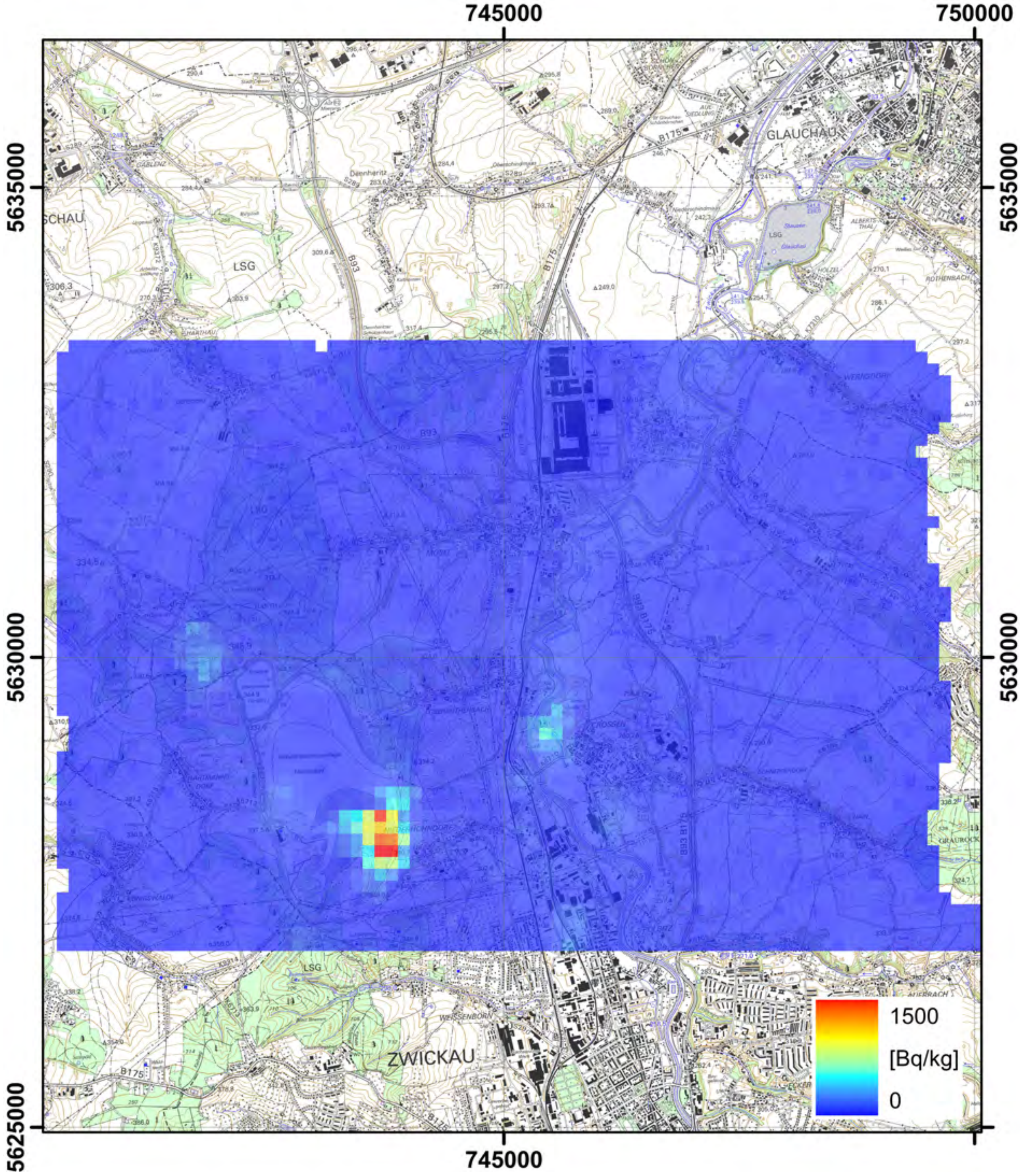

Figure 70: ^{238}U activity concentration of joint mapping area E (re-scaled). DTK25 ©Bundesamt für Kartographie und Geodäsie, Frankfurt a. M.

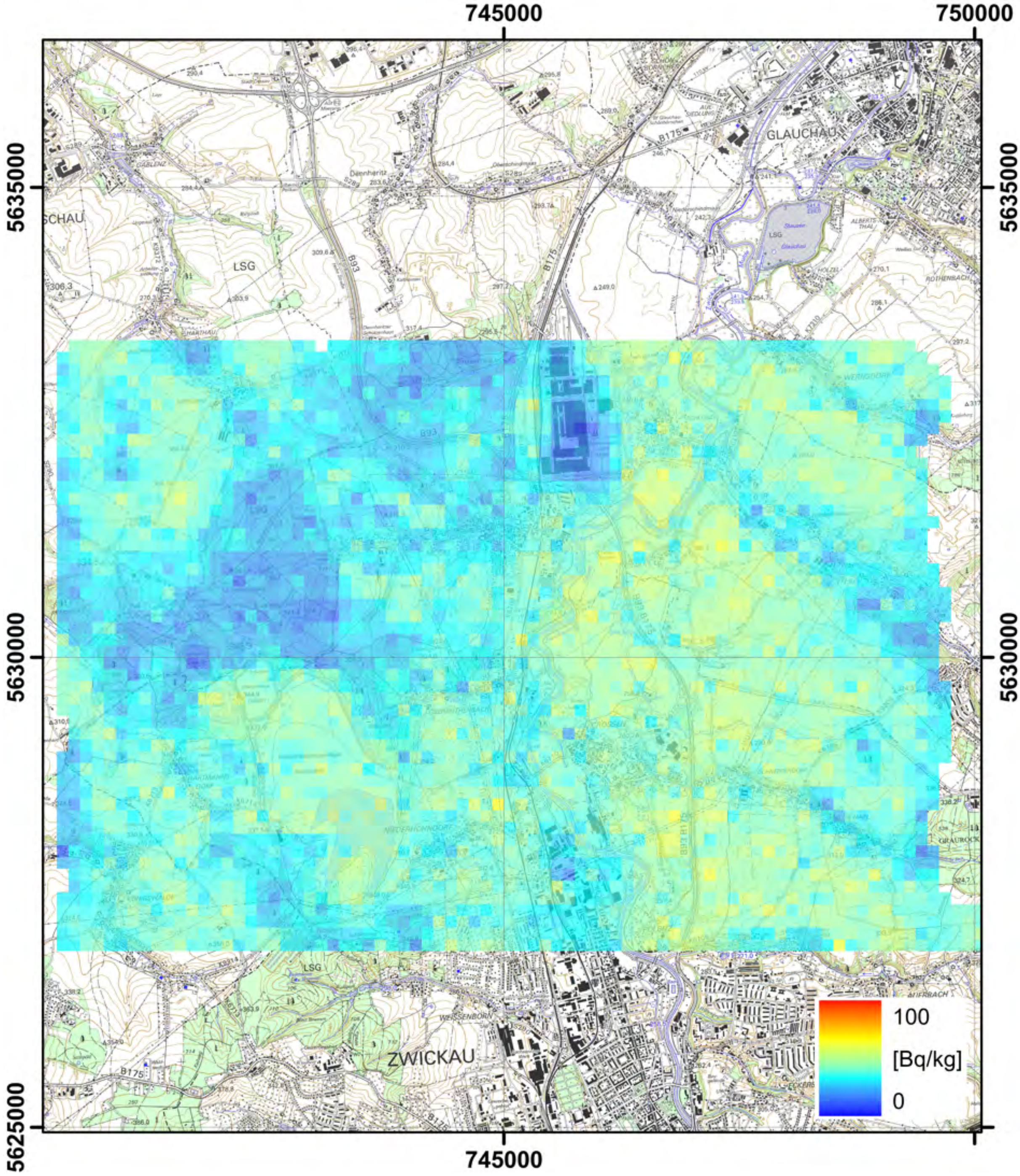

Figure 71: ^{232}Th activity concentration of joint mapping area E. DTK25 ©Bundesamt für Kartographie und Geodäsie, Frankfurt a. M.

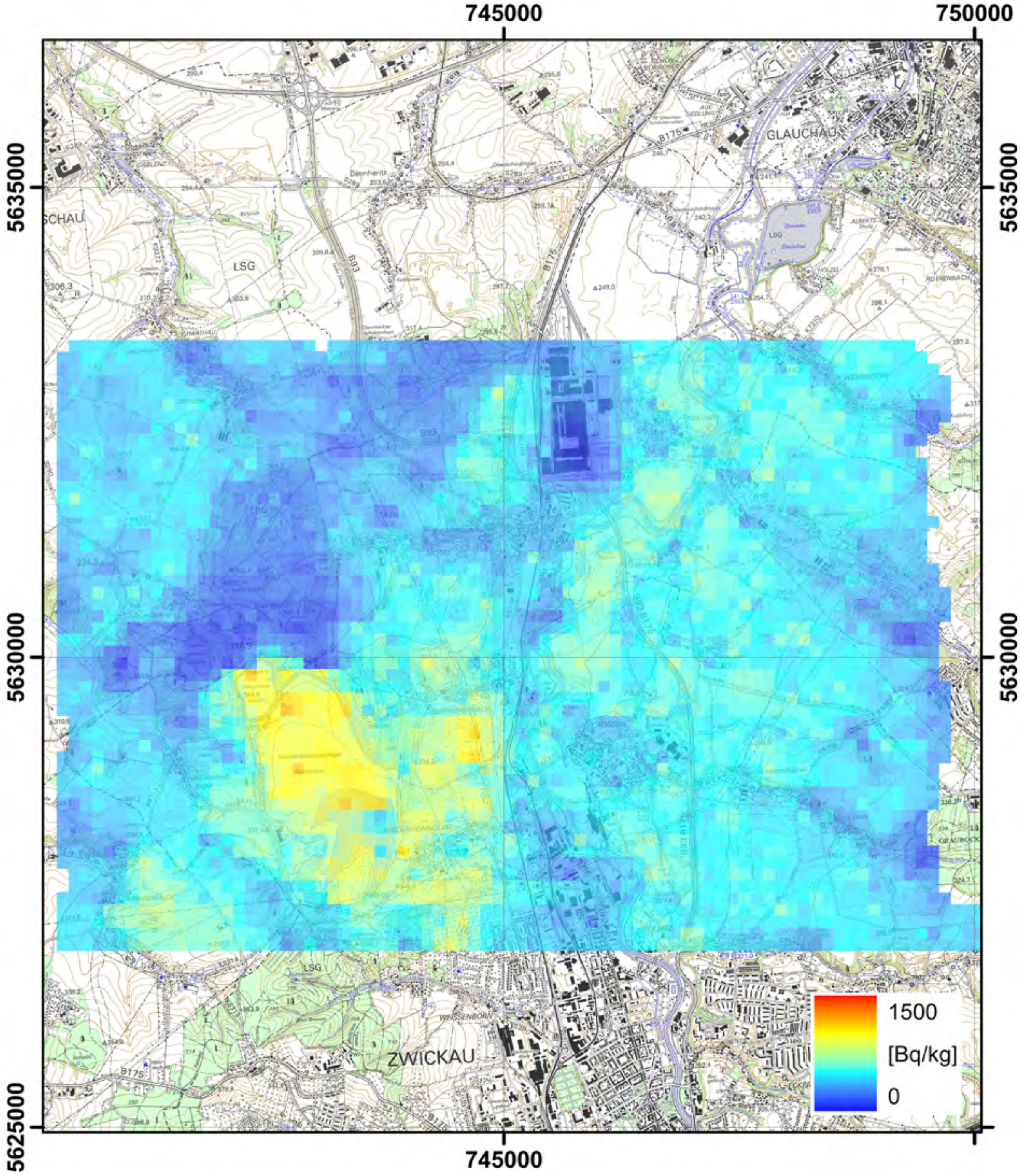

Figure 72: ^{40}K activity concentration of joint mapping area E. DTK25 ©Bundesamt für Kartographie und Geodäsie, Frankfurt a. M.

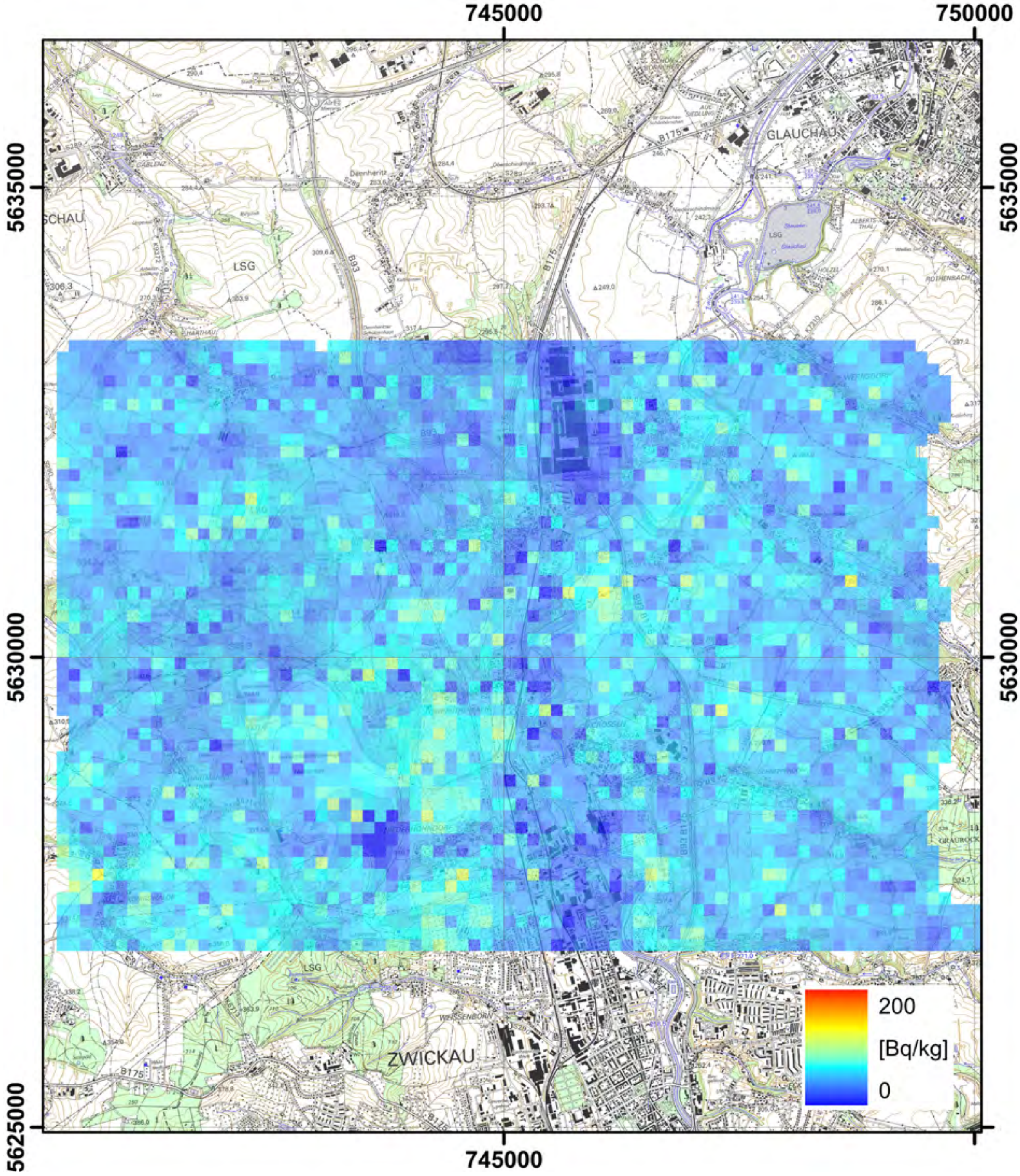

Figure 73: ^{137}Cs activity concentration of joint mapping area E. DTK25 ©Bundesamt für Kartographie und Geodäsie, Frankfurt a. M.

2.7.6 Joint mapping with team BfS2

The second joint mapping task was together with the German colleagues from BfS in an area named F east of Gera. Due to inclement weather, the available flight times were insecure and the flight lines were chosen to overlap over only one line for a direct comparison of values (Figure 74). The flight schedule of both teams was designed to enable simultaneous operation of both helicopters in area F. This report concentrates on the results of the Swiss team. The combined results of both teams will be analysed and published by the organisers of the intercomparison exercise. As in area E, the interesting structures of Area F are mining waste tips which were unfortunately located in the part of area F surveyed by the German colleagues. The map of the dose rate (Figure 75) in the part of area F surveyed by the Swiss team shows no evident anomalies.

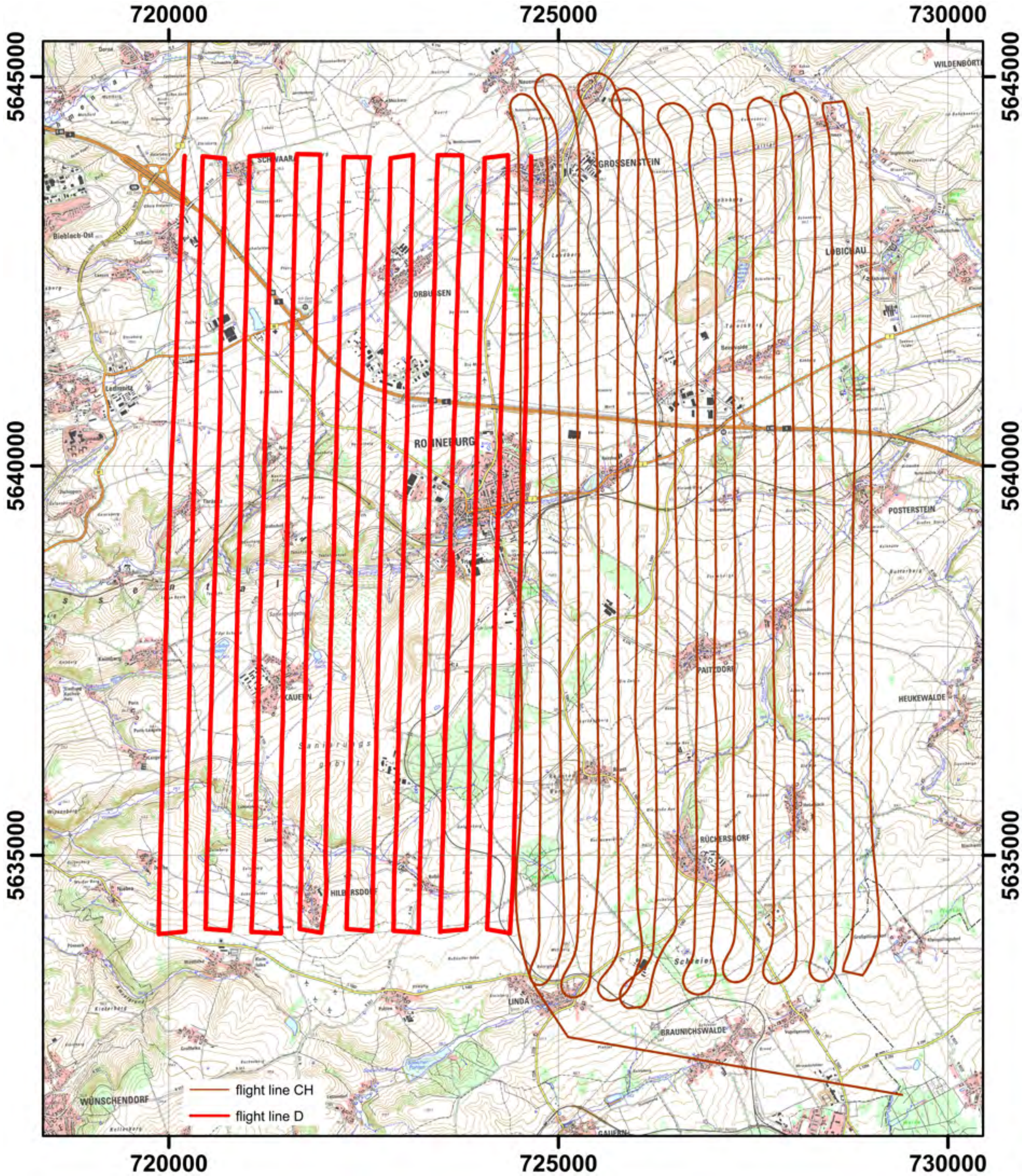

Figure 74: Flight lines over joint mapping area F. DTK25 ©Bundesamt für Kartographie und Geodäsie, Frankfurt a. M.

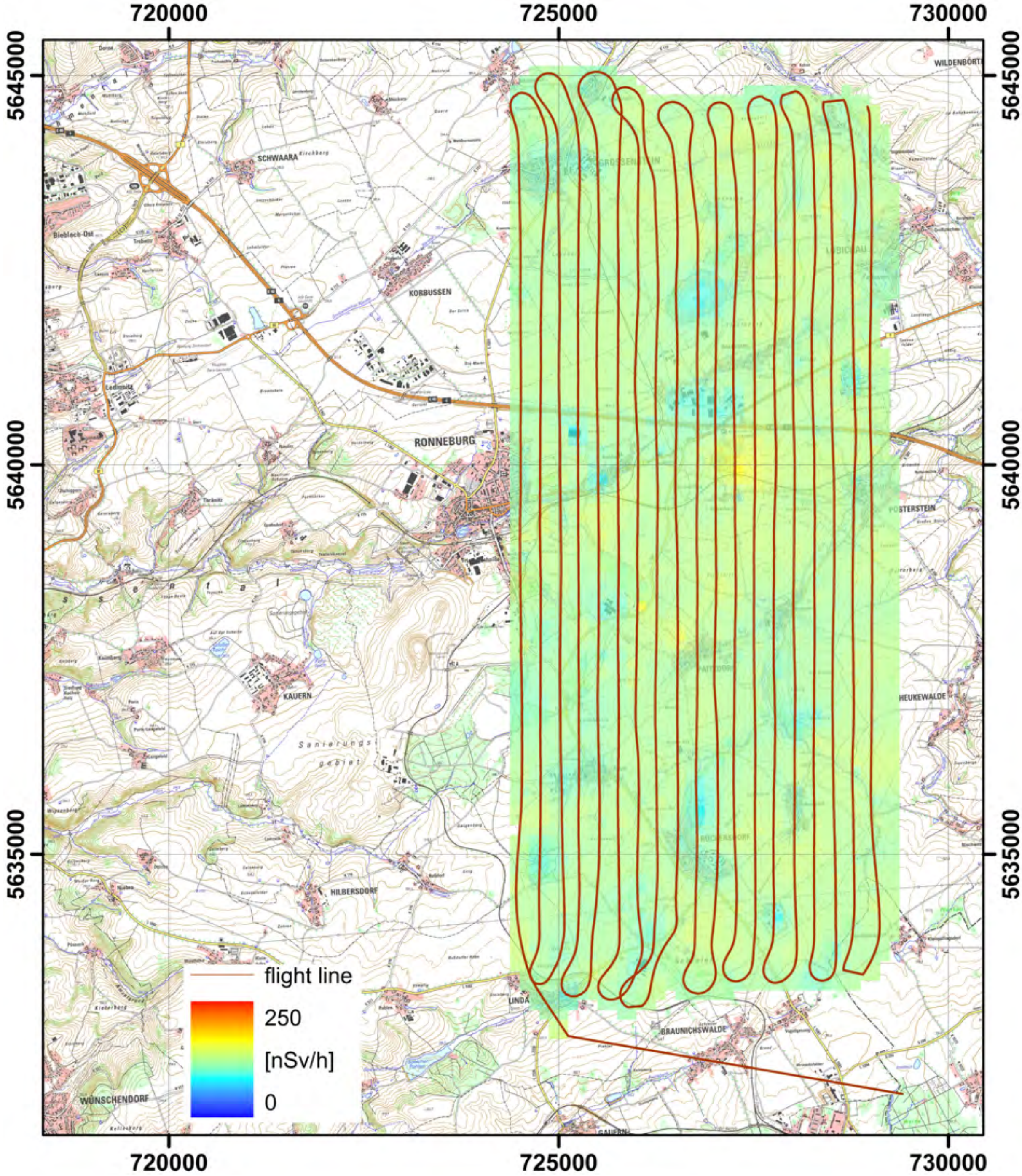

Figure 75: Dose rate over joint mapping area F. DTK25 ©Bundesamt für Kartographie und Geodäsie, Frankfurt a. M.

2.7.7 Joint mapping with team SURO

A third joint mapping exercise was planned with Czech colleagues from SURO in an area named D near Freital south of Dresden. Whereas the Swiss team could complete their flight, the flight of the Czech helicopter had to be cancelled due to unfavourable weather conditions. The map of the dose rate (Figure 76) shows elevated values over Burgk borough with values up to 280 nSv/h. The high values of the dose rate are associated with enhanced ^{238}U activity concentrations up to 430 Bq/kg (Figures 77 and 78). Separate and north of the uranium anomaly, elevated values of the ^{232}Th activity concentration are detected with activity concentrations up to 130 Bq/kg (Figure 79). The geological map (Figure 81) correlates the uranium anomaly with a sedimentary rock formation referred as "Schluffstein, Konglomerat, Kalkstein, Zauker..." in Figure 82, whereas the elevated thorium activity concentrations are found over a igneous monzonite body referred as "Monzonitoide" in Figure 82. The spatial pattern of the ^{40}K activity concentration (Figure 80) is distinct from the spatial patterns of uranium and thorium and associated with sandstone conglomerates (Figure 81) referred as "Konglomerat, Sandstein, Fanglomerat" in Figure 82.

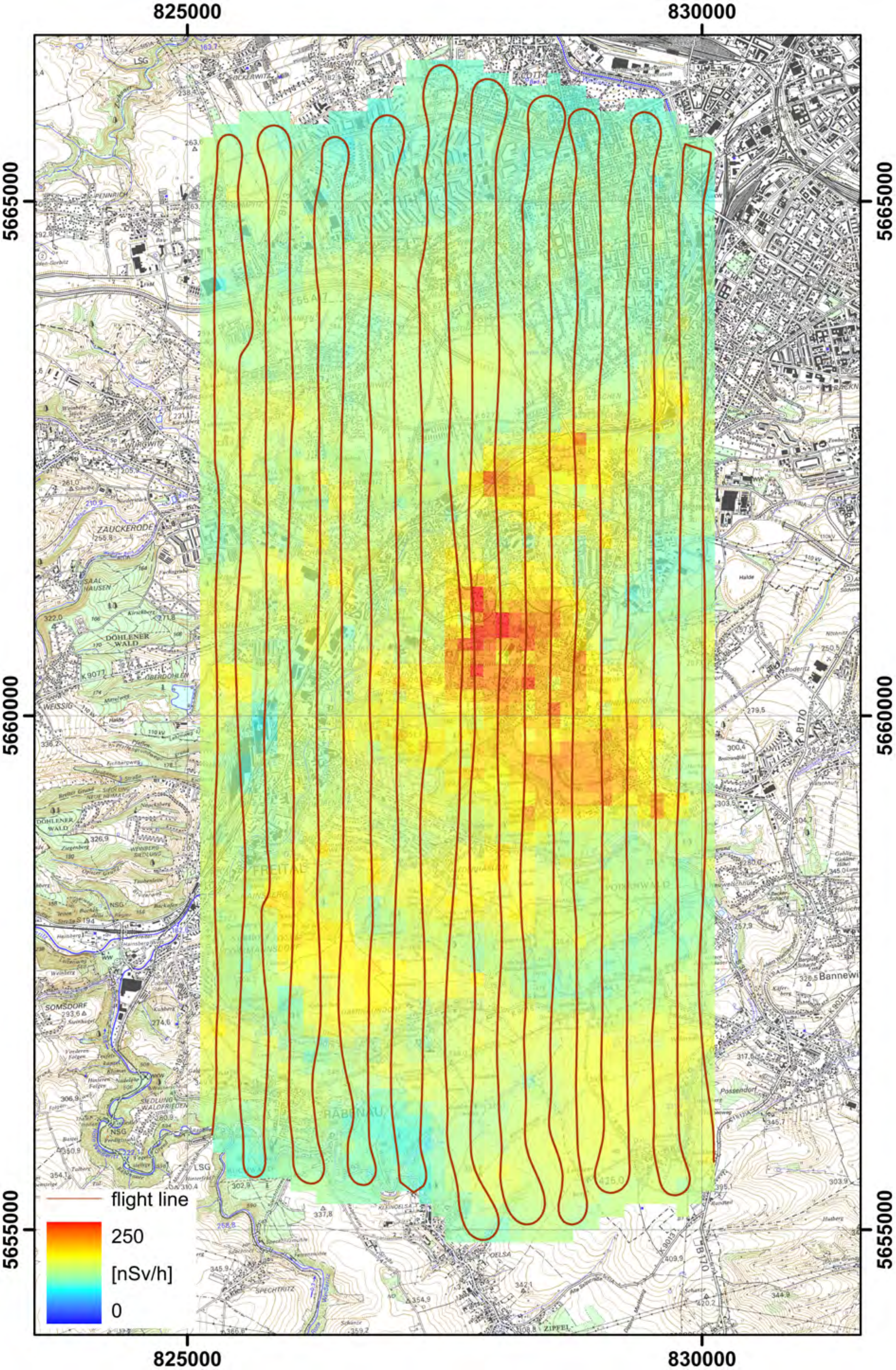

Figure 76: Dose rate over joint mapping area D. DTK25 ©Bundesamt für Kartographie und Geodäsie, Frankfurt a. M.

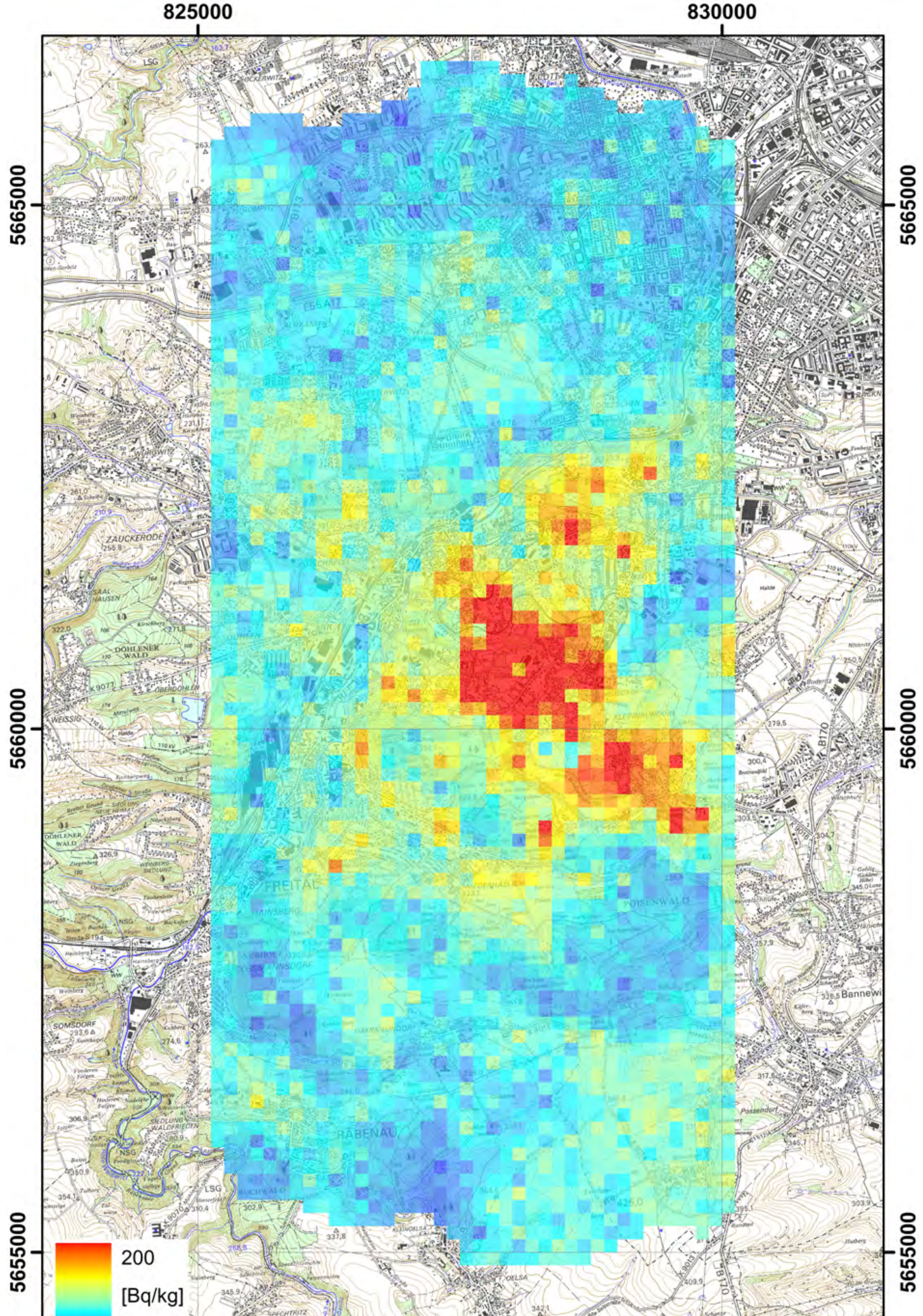

Figure 77: ^{238}U activity concentration of joint mapping area D. DTK25 ⓒBundesamt für Kartographie und Geodäsie, Frankfurt a. M.

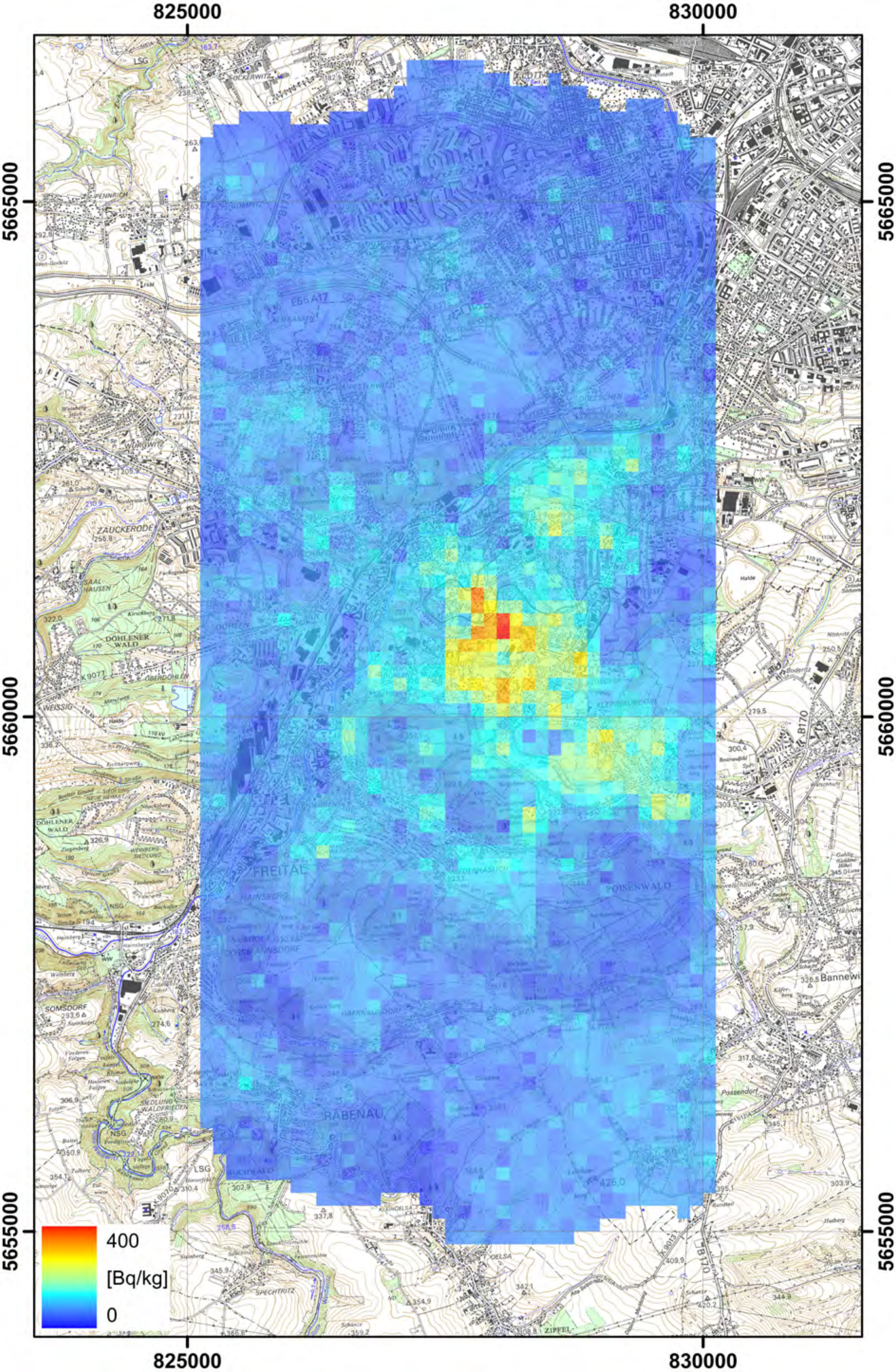

Figure 78: ^{238}U activity concentration of joint mapping area D (re-scaled). DTK25 ©Bundesamt für Kartographie und Geodäsie, Frankfurt a. M.

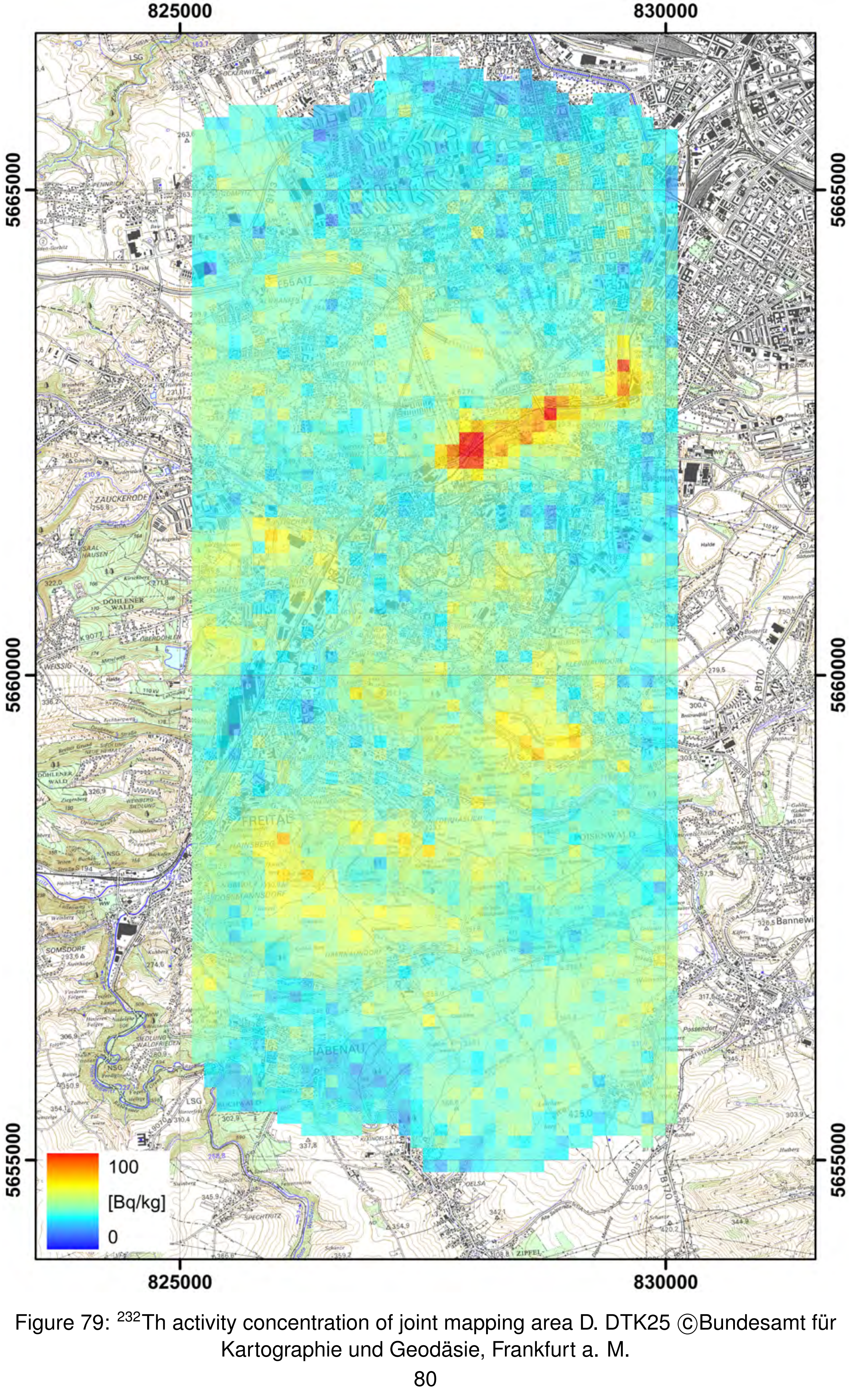

Figure 79: ^{232}Th activity concentration of joint mapping area D. DTK25 ©Bundesamt für Kartographie und Geodäsie, Frankfurt a. M.

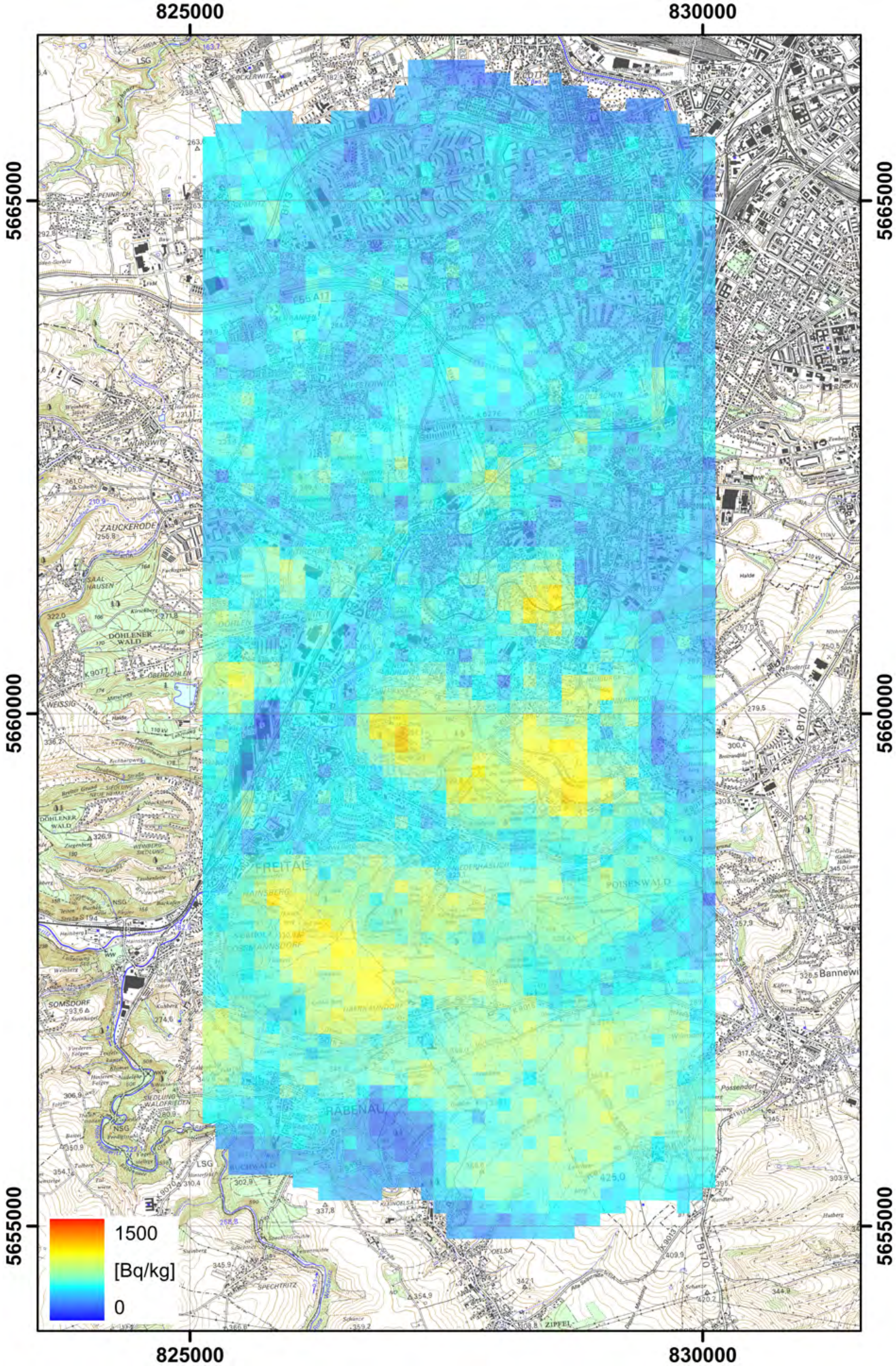

Figure 80: ^{40}K activity concentration of joint mapping area D. DTK25 ©Bundesamt für Kartographie und Geodäsie, Frankfurt a. M.

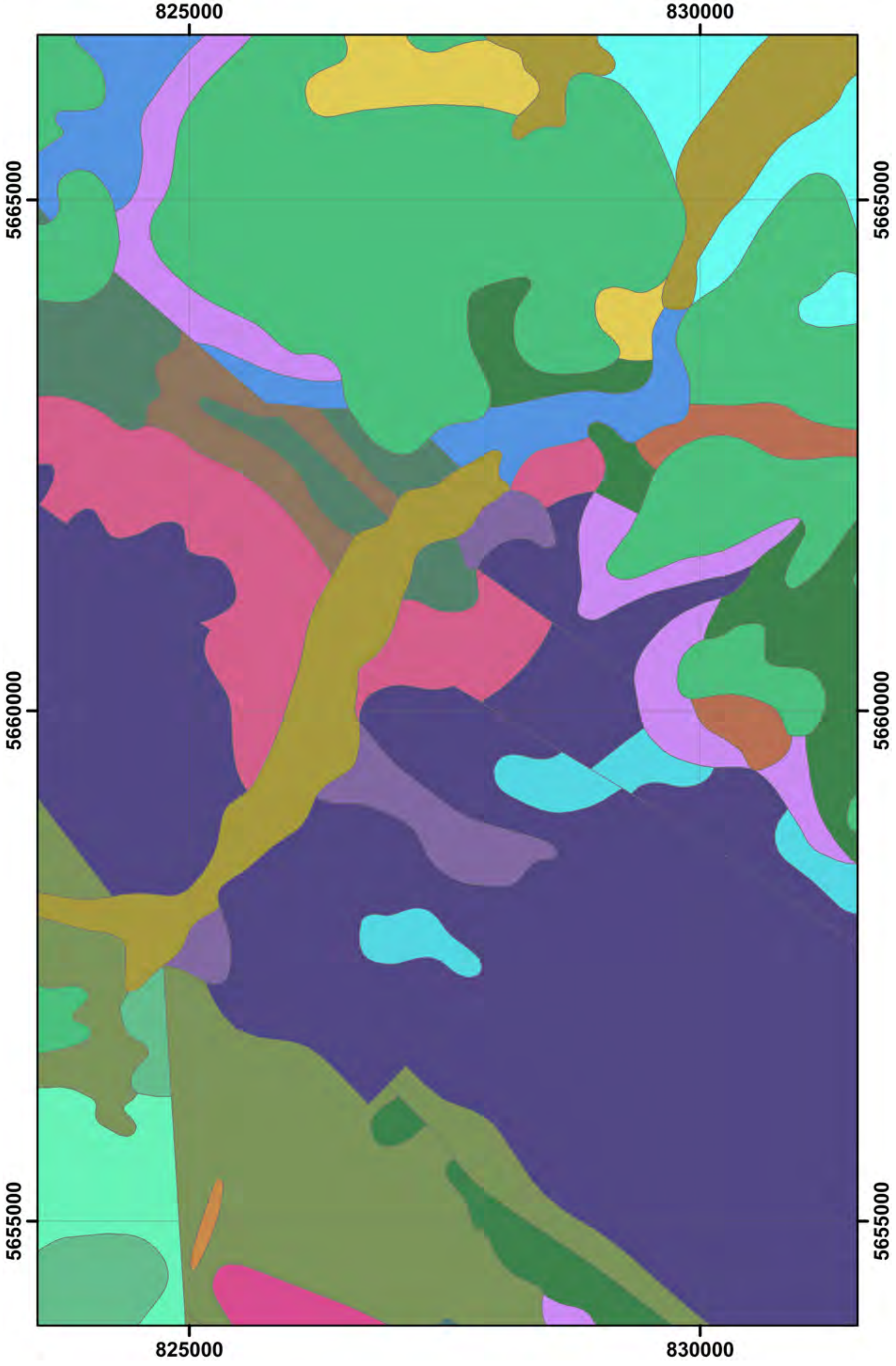

Figure 81: Geology of the joint mapping area D. GÜK200 ©Bundesamt für Kartographie und Geodäsie, Frankfurt a. M..

Figure 82: Legend for the geological map of the of the joint mapping area D (in German). GÜK200 ©Bundesamt für Kartographie und Geodäsie, Frankfurt a. M..

3 Conclusions

The survey of the environs of the Swiss nuclear power plants Mühleberg (KKM) and Gösgen (KKG) showed no artificial radionuclides outside of the plant premises. On behalf of the University of Basel, two alpine valleys were inspected. Elevated concentrations of natural radionuclides were found associated with detritus deposits at the slope of the mountains.
During these flights, problems in the spectrum acquisition were observed, which lead to a loss of about one percent of the data. The cause of the problems was a malfunction of a serial port and could be remediated utilising the redundant design of the data acquisition hardware.
As in the last year, the area of the Paul Scherrer Institut (PSI) was used as a testing field for a new airborne gammaspectrometry system (RLL) planned to be purchased by the Swiss army. Improvements of the performance of the new system were observed in intercomparison flights with the existing system (ARM), indicating further need for adapting the calibration parameters of the new system.
The focus of this years exercise was the participation in an international intercomparison exercise organised by Bundesamt für Strahlenschutz (BfS) in Germany. The measurements were performed in a former uranium mining district and gave the opportunity to measure at

dose rate and ^{238}U activity concentration levels which are not existing in Switzerland. The interaction and data exchange with the colleagues from Germany, France and the Czech Republic was pleasant and unproblematic. Data measured in adjacent sub-areas by the five teams could be compiled into consistent radiological maps in less than one day. The Swiss team thanks explicitly the organiser BfS and the colleagues from IRSN and SURO for an enjoyable and successful collaboration. A detailed analysis of the intercomparison exercise results will be published by BfS in 2016.

4 Literature

Schwarz, G. F.: Methodische Entwicklungen zur Aerogammaspektrometrie. Beiträge zur Geologie der Schweiz, Geophysik Nr. 23, Schweizerische Geophysikalische Kommission, 1991.

Rybach, L., Schwarz, G. F. and Medici, F.: Construction of radioelement and dose-rate baseline maps by combining ground and airborne radiometric data. IAEA-Tecdoc-980, 33-44, Vienna, 1996.

Schwarz, G.F., Rybach, L. and Klingelé, E.: Design, calibration and application of an airborne gamma spectrometric system in Switzerland. Geophysics 62, 1369-1378, 1997.

Bucher, B.: Methodische Weiterentwicklungen in der Aeroradiometrie. Dissertation Nr. 13973, ETH Zürich, 2001.

Butterweck, G. and Bucher B.: Evaluation of the intercomparison flights of March 18th 2015 with airborne gammaspectroscopy systems ARM and RLL, TM 96-15-08, Paul Scherrer Institut, 2015.

5 Previous reports

Schwarz, G. F., Klingelé, E. E., Rybach, L.: Aeroradiometrische Messungen in der Umgebung der schweizerischen Kernanlagen. Bericht für das Jahr 1989 zuhanden der Hauptabteilung für die Sicherheit der Kernanlagen (HSK). Interner Bericht, Institut für Geophysik, ETH Zürich, 1990.

Schwarz, G. F., Klingelé, E. E., Rybach, L.: Aeroradiometrische Messungen in der Umgebung der schweizerischen Kernanlagen. Bericht für das Jahr 1990 zuhanden der Hauptabteilung für die Sicherheit der Kernanlagen (HSK). Interner Bericht, Institut für Geophysik, ETH Zürich, 1991.

Schwarz, G. F., Klingelé, E. E., Rybach, L.: Aeroradiometrische Messungen in der Umgebung der schweizerischen Kernanlagen. Bericht für das Jahr 1991 zuhanden der Hauptabteilung für die Sicherheit der Kernanlagen (HSK). Interner Bericht, Institut für Geophysik, ETH Zürich, 1992.

Schwarz, G. F., Klingelé, E. E., Rybach, L.: Aeroradiometrische Messungen in der Umgebung der schweizerischen Kernanlagen. Bericht für das Jahr 1992 zuhanden der Hauptabteilung für die Sicherheit der Kernanlagen (HSK). Interner Bericht, Institut für Geophysik, ETH Zürich, 1993.

Schwarz, G. F., Klingelé, E. E., Rybach, L.: Aeroradiometrische Messungen in der Umgebung der schweizerischen Kernanlagen. Bericht für das Jahr 1993 zuhanden der Hauptabteilung für die Sicherheit der Kernanlagen (HSK). Interner Bericht, Institut für Geophysik, ETH Zürich, 1994.

Schwarz, G. F., Rybach, L.: Aeroradiometrische Messungen im Rahmen der Übung ARM94. Bericht für das Jahr 1994 zuhanden der Fachgruppe Aeroradiometrie (FAR). Interner Bericht, Institut für Geophysik, ETH Zürich, 1995.

Schwarz, G. F., Rybach, L.: Aeroradiometrische Messungen im Rahmen der Übung ARM95. Bericht für das Jahr 1995 zuhanden der Fachgruppe Aeroradiometrie (FAR). Interner Bericht, Institut für Geophysik, ETH Zürich, 1996.

Schwarz, G. F., Rybach, L., Bärlocher, C.: Aeroradiometrische Messungen im Rahmen der Übung ARM96. Bericht für das Jahr 1996 zuhanden der Fachgruppe Aeroradiometrie (FAR). Interner Bericht, Institut für Geophysik, ETH Zürich, 1997.

Bucher, B., Rybach, L., Schwarz, G., Bärlocher, C.: Aeroradiometrische Messungen im Rahmen der Übung ARM97. Bericht für das Jahr 1997 zuhanden der Fachgruppe Aeroradiometrie (FAR). Interner Bericht, Institut für Geophysik, ETH Zürich, 1998.

Bucher, B., Rybach, L., Schwarz, G., Bärlocher, C.: Aeroradiometrische Messungen im Rahmen der Übung ARM98. Bericht für das Jahr 1998 zuhanden der Fachgruppe Aeroradiometrie (FAR). Interner Bericht, Institut für Geophysik, ETH Zürich, 1999.

Bucher, B., Rybach, L., Schwarz, G., Bärlocher, C.: Aeroradiometrische Messungen im Rahmen der Übung ARM99. Bericht für das Jahr 1999 zuhanden der Fachgruppe Aeroradiometrie (FAR). Interner Bericht, Institut für Geophysik, ETH Zürich, 2000.

Bucher, B., Rybach, L., Schwarz, G., Bärlocher, C.: Aeroradiometrische Messungen im Rahmen der Übung ARM00. Bericht für das Jahr 2000 zuhanden der Fachgruppe Aeroradiometrie (FAR). Interner Bericht, Institut für Geophysik, ETH Zürich, 2001.

Bucher, B., Rybach, L., Schwarz, G., Bärlocher, C.: Aeroradiometrische Messungen im Rahmen der Übung ARM01. Bericht für das Jahr 2001 zuhanden der Fachgruppe Aeroradiometrie (FAR). Interner Bericht, Paul Scherrer Institut, Villigen, Schweiz, 2002.

Bucher, B., Rybach, L., Schwarz, G., Bärlocher, C.: Aeroradiometrische Messungen im Rahmen der Übung ARM02. Bericht für das Jahr 2002 zuhanden der Fachgruppe Aeroradiometrie (FAR). Interner Bericht, Paul Scherrer Institut, Villigen, Schweiz, 2003.

Bucher, B., Rybach, L., Schwarz, G.: Aeroradiometrische Messungen im Rahmen der Übung ARM03. PSI-Bericht 04-14, ISSN 1019-0643, Paul Scherrer Institut, Villigen, Schweiz, 2004.

Bucher, B., Butterweck, G., Rybach, L., Schwarz, G.: Aeroradiometrische Messungen im Rahmen der Übung ARM04. PSI-Bericht 05-10, ISSN 1019-0643, Paul Scherrer Institut, Villigen, Schweiz, 2005.

Bucher, B., Butterweck, G., Rybach, L., Schwarz, G.: Aeroradiometrische Messungen im Rahmen der Übung ARM05. PSI-Bericht 06-06, ISSN 1019-0643, Paul Scherrer Institut, Villigen, Schweiz, 2006.

Bucher, B., Butterweck, G., Rybach, L., Schwarz, G.: Aeroradiometrische Messungen im Rahmen der Übung ARM06. PSI-Bericht 07-02, ISSN 1019-0643, Paul Scherrer Institut, Villigen, Schweiz, 2007.

Bucher, B., Guillot, L., Strobl, C., Butterweck, G., Gutierrez, S., Thomas, M., Hohmann, C., Krol, I., Rybach, L., Schwarz, G.: International Intercomparison Exercise of Airborne Gammaspectrometric Systems of Germany, France and Switzerland in the Framework of the Swiss Exercise ARM07. PSI-Bericht Nr. 09-07, ISSN 1019-0643, Paul Scherrer Institut, Villigen, Schweiz, 2009.

Bucher, B., Butterweck, G., Rybach, L., Schwarz, G.: Aeroradiometrische Messungen im Rahmen der Übung ARM08. PSI-Bericht Nr. 09-02, ISSN 1019-0643, Paul Scherrer Institut, Villigen, Schweiz, 2009.

Bucher, B., Butterweck, G., Rybach, L., Schwarz, G., Strobl, C.: Aeroradiometrische Messungen im Rahmen der Übung ARM09. PSI-Bericht Nr. 10-01, ISSN 1019-0643, Paul

Scherrer Institut, Villigen, Schweiz, 2010.
Bucher, B., Butterweck, G., Rybach, L., Schwarz, G., Mayer, S.: Aeroradiometrische Messungen im Rahmen der Übung ARM10. PSI-Bericht Nr. 11-02, ISSN 1019-0643, Paul Scherrer Institut, Villigen, Schweiz, 2011.
Bucher, B., Butterweck, G., Rybach, L., Schwarz, G., Mayer, S.: Aeroradiometric Measurements in the Framework of the Swiss Exercise ARM11. PSI-Report No. 12-04, ISSN 1019-0643, Paul Scherrer Institut, Villigen, Switzerland, 2012.
Butterweck, G., Bucher, B., Rybach, L., Schwarz, G., Hödlmoser, H., Mayer, S., Danzi, C. Scharding, G.: Aeroradiometric Measurements in the Framework of the Swiss Exercise ARM12. PSI-Report No. 13-01, ISSN 1019-0643, Paul Scherrer Institut, Villigen, Switzerland, 2013.
Butterweck, G., Bucher, B., Rybach, L., Schwarz, G., Hohmann, E., Mayer, S., Danzi, C. Scharding, G.: Aeroradiometric Measurements in the Framework of the Swiss Exercise ARM13. PSI-Report No. 15-01, ISSN 1019-0643, Paul Scherrer Institut, Villigen, Switzerland, 2015.
Butterweck, G., Bucher, B., Rybach, L., Schwarz, G., Hohmann, E., Mayer, S., Danzi, C. Scharding, G.: Aeroradiometric Measurements in the Framework of the Swiss Exercises ARM14 and FTX14. PSI-Report No. 15-02, ISSN 1019-0643, Paul Scherrer Institut, Villigen, Switzerland, 2015.

The reports since 1994 can be found and downloaded from the FAR website `http://www.far.ensi.ch`.

6 Evaluation parameter files

The parameter files used for the evaluation of raw data in this report are listed below to improve the traceability of the presented results. The detector definition files have been re-evaluated for all detectors in 2014. A software modification was performed to take into account different formats of terrain model files used for topographic correction, leading to a change in the detector definition file. The increased background during some of the measuring flights was compensated with new background correction values.

6.1 DefinitionFile_Processing_ch.txt

This file defines the standard parameters used for the gridding of measured data used througout this report.

```
Definition file Swiss MGS32
"Windows"
10
Total    401.    2997.      0.   0
K-40    1369.    1558.   1460.   1
U-238   1664.    1853.   1765.   1
Th-232  2407.    2797.   2615.   1
Cs-137   600.     720.    660.   2
Co-60   1100.    1400.      0.   2
MMGC1    400.    1400.      0.   0
```

```
MMGC2   1400.    2997.      0.   0
LOW       40.     720.      0.   0
MID      720.    2997.      0.   0
"Ratios"
3
MMGCVerhältnis   MMGC1  MMGC2  Ratio_MMGC
LOWHigh          LOW    MMGC2  RatioLowHigh
LowMid           LOW    MID    RatioLowMid
"Conversion factors Activity to Dose Rate"
8
Total       0        NoCalibration   "     "   0
AD_K-40        0.044    DHSR            "nSv/h"   1
AD_U-238       0.55     DHSR            "nSv/h"   1
AD_Th-232      0.77     DHSR            "nSv/h"   1
AD_Cs-137      0.2      DHSR            "nSv/h"   2
Co-60       0        NoCalibration   "     "   0
MMGC1       0        NoCalibration   "     "   0
MMGC2       0        NoCalibration   "     "   0
"Typ des Darstellungsgrenzwertes"
1
Nachweistyp  0
"counts of spectra to stack"
1
Counts 1
"Auszugebende Werte"
30
"DHSR TOT            ","DHSR_TOT","nSv/h       ",0.00,250.00
"AP_Co-60            ","AP_Co-60","Bq       ",0.00,5000000.00
"AP_Cs-137           ","AP_Cs-137","Bq       ",0.00,5000000.00
"Terr. DL            ","DHSR_TOT","nSv/h     ",0.00,250.00
"CR_Caesium          ","CR_Cs-137","cps       ",20.00,120.00
"CR_Cobalt           ","CR_Co-60","cps       ",0.00,100.00
"NR_Caesium          ","NR_Cs-137","cps       ",0.00,120.00
"NR_Cobalt           ","NR_Co-60","cps       ",0.00,100.00
"AP_UT_Cs-137        ","AP_UT_Cs-137","Bq       ",0.00,5000000.00
"K-40                ","AD_K-40","Bq/kg     ",0.00,1000.00
"U-238               ","AD_U-238","Bq/kg     ",0.00,120.00
"Th-232              ","AD_Th-232","Bq/kg     ",0.00,120.00
"Cs-137              ","AD_Cs-137","Bq/kg     ",0.00,240.00
"Cobalt_CR           ","NR_Co-60","cps       ",0.00,120.00
"Nat.Terr.DL         ","DHSR_NAT","nSv/h     ",0.00,250.00
"Künst.DL            ","DHSR_ANT","nSv/h     ",0.00,250.00
"MMGC_Ratio          ","&MMGC_Ratio","%         ",400,600.00
"Cosmic DL           ","DHSR_COS","nSv/h     ",20.00,60.00
"Cosmic              ","CR_COS","cps       ",000.00,400.00
"Radar               ","PH","m         ",0.00,300.00
"ODL                 ","DHSR","nSv/h     ",0.00,250
"AD_UT_K-40          ","AD_UT_K-40","Bq/kg     ",0.00,200
"AD_UT_U-238         ","AD_UT_U-238","Bq/kg     ",0.00,50
```

```
"AD_UT_Th-232        ","AD_UT_Th-232","Bq/kg     ",0.00,40
"AD_UT_Cs-137        ","AD_UT_Cs-137","Bq/kg     ",0.00,20
"AP_UT_Co-60         ","AP_UT_Co-60","Bq       ",0.00,1000000
"Nachweis_Cs-137     ","CR_LD_Cs-137,"cps       ",0.00,100.00
"Nachweis_Co-60      ","CR_LD_Co-60","cps       ",0.00,100.00
"Cs-137 beta=0       ","AA_Cs-137","Bq/m2     ",0.00,50000.00
"AA_UT_Cs-137        ","AA_UT_Cs-137","Bq/m2     ",0.00,2000
```

6.2 DefinitionFile_Processing_de.txt

This file defines the parameters used for the gridding of measured data over German territory. The values are adapted to the reporting requisitions of the intercomparison organiser, for example the calculation of activity per wet weight. This parameter file was not used in this report.

```
Definition file Swiss MGS32
"Windows"
10
Total    401.    2997.      0.   0
K-40    1369.    1558.   1460.   1
U-238   1664.    1853.   1765.   1
Th-232  2407.    2797.   2615.   1
Cs-137   600.     720.    660.   2
Co-60   1100.    1400.      0.   2
MMGC1    400.    1400.      0.   0
MMGC2   1400.    2997.      0.   0
LOW       40.     720.      0.   0
MID      720.    2997.      0.   0
"Ratios"
3
MMGCVerhältnis   MMGC1  MMGC2  Ratio_MMGC
LOWHigh          LOW    MMGC2  RatioLowHigh
LowMid           LOW    MID    RatioLowMid
"Conversion factors Activity to Dose Rate"
8
Total       0        NoCalibration   "     "   0
AW_K-40        0.057    DHSR            "nSv/h"   1
AW_U-238       0.72     DHSR            "nSv/h"   1
AW_Th-232      1.00     DHSR            "nSv/h"   1
AW_Cs-137      0.26     DHSR            "nSv/h"   2
Co-60       0        NoCalibration   "     "   0
MMGC1       0        NoCalibration   "     "   0
MMGC2       0        NoCalibration   "     "   0
"Typ des Darstellungsgrenzwertes"
1
Nachweistyp  0
"counts of spectra to stack"
```

```
1
Counts 1
"Auszugebende Werte"
30
"DHSR TOT            ","DHSR_TOT","nSv/h       ",0.00,250.00
"AP_Co-60            ","AP_Co-60","Bq       ",0.00,1500000.00
"AP_Cs-137           ","AP_Cs-137","Bq       ",0.00,400000.00
"Terr. DL            ","DHSR_TOT","nSv/h     ",0.00,250.00
"CR_Caesium          ","CR_Cs-137","cps       ",20.00,120.00
"CR_Cobalt           ","CR_Co-60","cps       ",0.00,100.00
"Low-HighRatio       ","RatioLowHigh","%       ",0.00,1000.00
"Low-MidRatio        ","RatioLowMid","%       ",0.00,1000.00
"Total_CR_corr       ","NR_Total","cps       ",200.00,1200.00
"K-40                ","AW_K-40","Bq/kg     ",0.00,1000.00
"U-238               ","AW_U-238","Bq/kg     ",0.00,120.00
"Th-232              ","AW_Th-232","Bq/kg     ",0.00,120.00
"Cs-137              ","AW_Cs-137","Bq/kg     ",0.00,240.00
"Cobalt_CR           ","NR_Co-60","cps       ",0.00,120.00
"Nat.Terr.DL         ","DHSR_NAT","nSv/h     ",0.00,250.00
"Künst.DL            ","DHSR_ANT","nSv/h     ",0.00,250.00
"MMGC_Ratio          ","&MMGC_Ratio","%         ",400,600.00
"Cosmic DL           ","DHSR_COS","nSv/h     ",20.00,60.00
"Cosmic              ","CR_COS","cps       ",000.00,400.00
"Radar               ","PH","m         ",0.00,300.00
"ODL                 ","DHSR","nSv/h     ",0.00,250
"AW_UT_K-40          ","AW_UT_K-40","Bq/kg     ",0.00,200
"AW_UT_U-238         ","AW_UT_U-238","Bq/kg     ",0.00,50
"AW_UT_Th-232        ","AW_UT_Th-232","Bq/kg     ",0.00,40
"AW_UT_Cs-137        ","AW_UT_Cs-137","Bq/kg     ",0.00,20
"Err_Co-60           ","NR_UT_Co-60","cps       ",0.00,40
"Nachweis_Cs-137     ","CR_LD_Cs-137,"cps       ",0.00,100.00
"Nachweis_Co-60      ","CR_LD_Co-60","cps       ",0.00,100.00
"Cs-137 beta=0       ","AA_Cs-137","Bq/m2     ",0.00,20000.00
"AA_UT_Cs-137        ","AA_UT_Cs-137","Bq/m2     ",0.00,20
```

6.3 Processing_Quellensuche_de.txt

This file defines the parameters used for a source search over German territory.

```
Definition file Swiss MGS32
"Windows"
10
Total    401.    2997.      0.   0
K-40    1369.    1558.   1460.   1
U-238   1664.    1853.   1765.   1
Th-232  2407.    2797.   2615.   1
Cs-137   600.     720.    660.   2
```

```
Co-60   1100.    1400.      0.   2
MMGC1    400.    1400.      0.   0
MMGC2   1400.    2997.      0.   0
LOW       40.     720.      0.   0
MID      720.    2997.      0.   0
"Ratios"
3
MMGCVerhältnis   MMGC1  MMGC2  Ratio_MMGC
LOWHigh          LOW    MMGC2  RatioLowHigh
LowMid           LOW    MID    RatioLowMid
"Conversion factors Activity to Dose Rate"
8
Total       0        NoCalibration   "     "   0
AW_K-40        0.057    DHSR            "nSv/h"   1
AW_U-238       0.72     DHSR            "nSv/h"   1
AW_Th-232      1.00     DHSR            "nSv/h"   1
AW_Cs-137      0.26     DHSR            "nSv/h"   2
Co-60       0        NoCalibration   "     "   0
MMGC1       0        NoCalibration   "     "   0
MMGC2       0        NoCalibration   "     "   0
"Typ des Darstellungsgrenzwertes"
1
Nachweistyp  2
"counts of spectra to stack"
1
Counts 1
"Auszugebende Werte"
30
"CR_total            ","CR_Total","cps       ",200.00,1200.00
"CR_Kalium           ","CR_K-40","cps       ",0.00,150.00
"CR_Uranium          ","CR_U-238","cps       ",0.00,40.00
"CR_Thorium          ","CR_Th-232","cps       ",0.00,40.00
"CR_Caesium          ","CR_Cs-137","cps       ",20.00,120.00
"CR_Cobalt           ","CR_Co-60","cps       ",0.00,100.00
"Low-HighRatio       ","RatioLowHigh","%        ",0.00,1000.00
"Low-MidRatio        ","RatioLowMid","%        ",0.00,1000.00
"Total_CR_corr       ","NR_Total","cps       ",200.00,1200.00
"K-40                ","AW_K-40","Bq/kg     ",0.00,1000.00
"U-238               ","AW_U-238","Bq/kg     ",0.00,120.00
"Th-232              ","AW_Th-232","Bq/kg     ",0.00,120.00
"Cs-137_Net_CR       ","NR_Cs-137","cps       ",0.00,240.00
"Co-60_Net_CR        ","NR_Co-60","cps       ",0.00,120.00
"Terr.DL             ","DHSR_TOT","nSv/h     ",0.00,250.00
"Künst.DL            ","DHSR_ANT","nSv/h     ",0.00,250.00
"MMGC_Ratio          ","&Ratio_MMGC","%         ",400,600.00
"Cosmic DL           ","DHSR_COS","nSv/h     ",20.00,60.00
"Cosmic              ","CR_COS","cps       ",000.00,400.00
"Radar               ","PH","m         ",0.00,300.00
"ODL                 ","DHSR","nSv/h     ",0.00,250
```

```
"AW_UT_K-40          ","AW_UT_K-40","Bq/kg     ",0.00,200
"AW_UT_U-238         ","AW_UT_U-238","Bq/kg     ",0.00,50
"AW_UT_Th-232        ","AW_UT_Th-232","Bq/kg     ",0.00,40
"AW_UT_Cs-137        ","AW_UT_Cs-137","Bq/kg     ",0.00,20
"Err_Co-60           ","NR_UT_Co-60","cps       ",0.00,40
"Nachweis_Cs-137     ","CR_LD_Cs-137,"cps       ",0.00,100.00
"Nachweis_Co-60      ","CR_LD_Co-60","cps       ",0.00,100.00
"Cs-137 beta=0       ","AA_Cs-137","Bq/m2     ",0.00,20.00
"AA_UT_Cs-137        ","AA_UT_Cs-137","Bq/m2     ",0.00,20
```

6.4 DefinitionFile_DetD_ch.txt

This file defines the parameter set used for detector D over Swiss territory.

```
Definition file System
"Koordinaten"
WGS84
"Non-linearity"
4
a0  0.0
a1  0.083333
a2  0.0
a3  0.0
"Recorder old RDT-Files"
8
Radar  0.00   -61.00
Baro   0.74   457.14
Cosm   0.00   1.00
Dead   5.00   0.00
Time   0.00   1.00
Temp   0.00   1.00
Pitch  0.00   76.20
Roll   0.00   90.91
"Background/Cosmic"
10
Total      98.1000       1.041      0.032
K-40        12.100       0.050      0.004
U-238        2.700       0.043      0.002
Th-232       3.400       0.044      0.001
Cs-137      15.500       0.102      0.005
Co-60       13.900       0.100      0.004
MMGC1       79.540       0.771      0.019
MMGC2       18.500       0.270      0.007
LOW          0.          0.         0.
MID          0.          0.         0.
"Stripping Coefficients"
10
```

```
1.000  0.000  0.000  0.000  0.000  0.000  0.000  0.000  0.000  0.000
0.000  1.000  1.003  0.461 -0.001  0.104  0.000  0.000  0.000  0.000
0.000 -0.030  1.000  0.359 -0.001  0.004  0.000  0.000  0.000  0.000
0.000 -0.020  0.054  1.000  0.000  0.002  0.000  0.000  0.000  0.000
0.000  0.323  4.013  2.392  1.000  0.225  0.000  0.000  0.000  0.000
0.000  0.649  2.534  0.695 -0.002  1.000  0.000  0.000  0.000  0.000
0.000  0.000  0.000  0.000  0.000  0.000  1.000  0.000  0.000  0.000
0.000  0.000  0.000  0.000  0.000  0.000  0.000  1.000  0.000  0.000
0.000  0.000  0.000  0.000  0.000  0.000  0.000  0.000  1.000  0.000
0.000  0.000  0.000  0.000  0.000  0.000  0.000  0.000  0.000  1.000
"Converted Stripping Coefficients Matrix"
10
1.000  0.000  0.000  0.000  0.000  0.000  0.000  0.000  0.000  0.000
0.000  1.042 -0.774 -0.130  0.000 -0.105  0.000  0.000  0.000  0.000
0.000  0.027  1.005 -0.371  0.001 -0.006  0.000  0.000  0.000  0.000
0.000  0.021 -0.064  1.017  0.000 -0.004  0.000  0.000  0.000  0.000
0.000 -0.323 -3.181 -0.971  0.997 -0.175  0.000  0.000  0.000  0.000
0.000 -0.759 -2.006  0.317 -0.001  1.086  0.000  0.000  0.000  0.000
0.000  0.000  0.000  0.000  0.000  0.000  1.000  0.000  0.000  0.000
0.000  0.000  0.000  0.000  0.000  0.000  0.000  1.000  0.000  0.000
0.000  0.000  0.000  0.000  0.000  0.000  0.000  0.000  1.000  0.000
0.000  0.000  0.000  0.000  0.000  0.000  0.000  0.000  0.000  1.000
"Sigma of Converted Stripping Coefficients Matrix"
10
0.000  0.000  0.000  0.000  0.000  0.000  0.000  0.000  0.000  0.000
0.000  0.000 -0.040 -0.017  0.000 -0.016  0.000  0.000  0.000  0.000
0.000  0.000  0.000 -0.028  0.000  0.000  0.000  0.000  0.000  0.000
0.000  0.000 -0.009  0.000  0.000  0.000  0.000  0.000  0.000  0.000
0.000 -0.080 -0.103 -0.037  0.000 -0.008  0.000  0.000  0.000  0.000
0.000 -0.140 -0.068  0.013  0.000  0.000  0.000  0.000  0.000  0.000
0.000  0.000  0.000  0.000  0.000  0.000  0.000  0.000  0.000  0.000
0.000  0.000  0.000  0.000  0.000  0.000  0.000  0.000  0.000  0.000
0.000  0.000  0.000  0.000  0.000  0.000  0.000  0.000  0.000  0.000
0.000  0.000  0.000  0.000  0.000  0.000  0.000  0.000  0.000  0.000
"Attenuation Coefficients"
10
Total       0.00600    1.00000   0.0003
K-40        0.00800    1.00000   0.0008
U-238       0.00550    1.00000   0.0114
Th-232      0.00600    1.00000   0.0044
Cs-137      0.01000    1.00000   0.0100
Co-60       0.00800    1.00000   0.0080
MMGC1       0.00600    1.00000   0.0060
MMGC2       0.00650    1.00000   0.0065
LOW         0.02000    1.00000   0.01
MID         0.01500    1.00000   0.005
"3D Attenuation Coefficients"
10
Total       0.00350    2.00000
```

```
K-40         0.00420    2.00000
U-238        0.00320    2.00000
Th-232       0.00350    2.00000
Cs-137       0.00800    2.00000
Co-60        0.00800    1.00000
MMGC1        0.00600    1.00000
MMGC2        0.00650    1.00000
LOW          0.02000    1.00000
MID          0.01500    1.00000
"Conversion factors Counts to Activity"
11
Total        0        NoCalibration   "     "
K-40         7.95     AD_K-40         "Bq/kg"
U-238        3.87     AD_U-238        "Bq/kg"
Th-232       1.62     AD_Th-232       "Bq/kg"
Cs-137       1.88     AD_Cs-137       "Bq/kg"
Cs-137       32.96    AA_Cs-137       "Bq/m2"
Cs-137       7200     AP_Cs-137       "Bq   "
Co-60        2500     AP_Co-60        "Bq   "
Co-60        0        NoCalibration   "     "
MMGC1        0        NoCalibration   "     "
MMGC2        0        NoCalibration   "     "
"Radon"
1
0            0
"Hoehenkorrektur"
4
AltMethod   0
GroundAltDGM  1
DGMType     0
PfadDHM25   C:\DATEN\Aeroradiometrie\Daten\DHM25\
"SDI Constants"
7
Aten         0.0053
Convert      0.00096
CosmicKorr   95.5
Back         12640.0
Gain         12.0
referenz_alt 100.0
Threshold    240.0
```

6.5 DefinitionFile_DetD_de_oBat.txt

This file defines the parameter set used for detector D with normal intrinsic backgroundover German territory. The output was adjusted for this report to the standard Swiss measurment quantities instead of the requirement of the intercomparison organiser.

```
Definition file System
```

```
"Koordinaten"
WGS84
"Non-linearity"
4
a0  1.8745
a1  0.082009
a2  0.00000012708
a3  0.0
"Recorder old RDT-Files"
8
Radar  0.00   -61.00
Baro   0.74   457.14
Cosm   0.00   1.00
Dead   5.00   0.00
Time   0.00   1.00
Temp   0.00   1.00
Pitch  0.00   76.20
Roll   0.00   90.91
"Background/Cosmic"
10
Total      98.1000       1.041      0.032
K-40        12.100       0.050      0.004
U-238        2.700       0.043      0.002
Th-232       3.400       0.044      0.001
Cs-137      15.500       0.102      0.005
Co-60       13.900       0.100      0.004
MMGC1       79.540       0.771      0.019
MMGC2       18.500       0.270      0.007
LOW          0.          0.         0.
MID          0.          0.         0.
"Stripping Coefficients"
10
1.000  0.000  0.000  0.000  0.000  0.000  0.000  0.000  0.000  0.000
0.000  1.000  1.025  0.461  0.000  0.106  0.000  0.000  0.000  0.000
0.000 -0.029  1.000  0.347  0.000  0.004  0.000  0.000  0.000  0.000
0.000 -0.020  0.055  1.000  0.000  0.002  0.000  0.000  0.000  0.000
0.000  0.328  3.235  1.604  1.000  0.202  0.000  0.000  0.000  0.000
0.000  0.637  2.485  0.670  0.001  1.000  0.000  0.000  0.000  0.000
0.000  0.000  0.000  0.000  0.000  0.000  1.000  0.000  0.000  0.000
0.000  0.000  0.000  0.000  0.000  0.000  0.000  1.000  0.000  0.000
0.000  0.000  0.000  0.000  0.000  0.000  0.000  0.000  1.000  0.000
0.000  0.000  0.000  0.000  0.000  0.000  0.000  0.000  0.000  1.000
"Converted Stripping Coefficients Matrix"
10
1.000  0.000  0.000  0.000  0.000  0.000  0.000  0.000  0.000  0.000
0.000  1.042 -0.795 -0.133  0.000 -0.106  0.000  0.000  0.000  0.000
0.000  0.026  1.007 -0.358  0.000 -0.006  0.000  0.000  0.000  0.000
0.000  0.021 -0.067  1.016  0.000 -0.005  0.000  0.000  0.000  0.000
0.000 -0.310 -2.498 -0.488  1.000 -0.158  0.000  0.000  0.000  0.000
```

```
0.000 -0.742 -1.950  0.294 -0.001  1.085  0.000  0.000  0.000  0.000
0.000  0.000  0.000  0.000  0.000  0.000  1.000  0.000  0.000  0.000
0.000  0.000  0.000  0.000  0.000  0.000  0.000  1.000  0.000  0.000
0.000  0.000  0.000  0.000  0.000  0.000  0.000  0.000  1.000  0.000
0.000  0.000  0.000  0.000  0.000  0.000  0.000  0.000  0.000  1.000
"Sigma of Converted Stripping Coefficients Matrix"
10
0.000  0.000  0.000  0.000  0.000  0.000  0.000  0.000  0.000  0.000
0.000  0.000 -0.040 -0.017  0.000 -0.016  0.000  0.000  0.000  0.000
0.000  0.000  0.000 -0.028  0.000  0.000  0.000  0.000  0.000  0.000
0.000  0.000 -0.009  0.000  0.000  0.000  0.000  0.000  0.000  0.000
0.000 -0.080 -0.103 -0.037  0.000 -0.008  0.000  0.000  0.000  0.000
0.000 -0.140 -0.068  0.013  0.000  0.000  0.000  0.000  0.000  0.000
0.000  0.000  0.000  0.000  0.000  0.000  0.000  0.000  0.000  0.000
0.000  0.000  0.000  0.000  0.000  0.000  0.000  0.000  0.000  0.000
0.000  0.000  0.000  0.000  0.000  0.000  0.000  0.000  0.000  0.000
0.000  0.000  0.000  0.000  0.000  0.000  0.000  0.000  0.000  0.000
"Attenuation Coefficients"
10
Total        0.00600    1.00000   0.0003
K-40         0.00800    1.00000   0.0008
U-238        0.00550    1.00000   0.0114
Th-232       0.00600    1.00000   0.0044
Cs-137       0.01000    1.00000   0.0100
Co-60        0.00800    1.00000   0.0080
MMGC1        0.00600    1.00000   0.0060
MMGC2        0.00650    1.00000   0.0065
LOW          0.02000    1.00000   0.01
MID          0.01500    1.00000   0.005
"3D Attenuation Coefficients"
10
Total        0.00350    2.00000
K-40         0.00420    2.00000
U-238        0.00320    2.00000
Th-232       0.00350    2.00000
Cs-137       0.00800    2.00000
Co-60        0.00800    1.00000
MMGC1        0.00600    1.00000
MMGC2        0.00650    1.00000
LOW          0.02000    1.00000
MID          0.01500    1.00000
"Conversion factors Counts to Activity"
11
Total        0         NoCalibration    "      "
K-40         7.95      AD_K-40          "Bq/kg"
U-238        3.87      AD_U-238         "Bq/kg"
Th-232       1.62      AD_Th-232        "Bq/kg"
Cs-137       1.88      AD_Cs-137        "Bq/kg"
Cs-137       32.96     AA_Cs-137        "Bq/m2"
```

```
Cs-137      7200     AP_Cs-137       "Bq    "
Co-60       2500     AP_Co-60        "Bq    "
Co-60       0        NoCalibration   "      "
MMGC1       0        NoCalibration   "      "
MMGC2       0        NoCalibration   "      "
"Radon"
1
0           0
"Hoehenkorrektur"
4
AltMethod   1
GroundAltDGM  1
DGMType     1
PfadDHM25   C:\Daten\Aeroradiometrie\ARM2015\Karten_DE\dgm200utm32\dgm200_utm32s.asc
"SDI Constants"
7
Aten         0.0053
Convert      0.00096
CosmicKorr   95.5
Back         12640.0
Gain         12.0
referenz_alt 100.0
Threshold    240.0
```

6.6 DefinitionFile_DetD_de_BackNeu.txt

This file defines the parameter set used for detector D with elevated intrinsic background over German territory. The output was adjusted for this report to the standard Swiss measurment quantities instead of the requirement of the intercomparison organiser.

```
Definition file System
"Koordinaten"
WGS84
"Non-linearity"
4
a0  1.8745
a1  0.082009
a2  0.00000012708
a3  0.0
"Recorder old RDT-Files"
8
Radar  0.00   -61.00
Baro   0.74   457.14
Cosm   0.00   1.00
Dead   5.00   0.00
Time   0.00   1.00
Temp   0.00   1.00
```

```
Pitch  0.00   76.20
Roll   0.00   90.91
"Background/Cosmic"
10
Total     125.8000       2.091      0.032
K-40        23.900       0.121      0.004
U-238        1.454       0.081      0.002
Th-232       0.979       0.099      0.001
Cs-137      17.986       0.283      0.005
Co-60       14.164       0.207      0.004
MMGC1       97.012       1.647      0.019
MMGC2       30.190       0.442      0.007
LOW          0.          0.         0.
MID          0.          0.         0.
"Stripping Coefficients"
10
1.000  0.000  0.000  0.000  0.000  0.000  0.000  0.000  0.000  0.000
0.000  1.000  1.025  0.461  0.000  0.106  0.000  0.000  0.000  0.000
0.000 -0.029  1.000  0.347  0.000  0.004  0.000  0.000  0.000  0.000
0.000 -0.020  0.055  1.000  0.000  0.002  0.000  0.000  0.000  0.000
0.000  0.328  3.235  1.604  1.000  0.202  0.000  0.000  0.000  0.000
0.000  0.637  2.485  0.670  0.001  1.000  0.000  0.000  0.000  0.000
0.000  0.000  0.000  0.000  0.000  0.000  1.000  0.000  0.000  0.000
0.000  0.000  0.000  0.000  0.000  0.000  0.000  1.000  0.000  0.000
0.000  0.000  0.000  0.000  0.000  0.000  0.000  0.000  1.000  0.000
0.000  0.000  0.000  0.000  0.000  0.000  0.000  0.000  0.000  1.000
"Converted Stripping Coefficients Matrix"
10
1.000  0.000  0.000  0.000  0.000  0.000  0.000  0.000  0.000  0.000
0.000  1.042 -0.795 -0.133  0.000 -0.106  0.000  0.000  0.000  0.000
0.000  0.026  1.007 -0.358  0.000 -0.006  0.000  0.000  0.000  0.000
0.000  0.021 -0.067  1.016  0.000 -0.005  0.000  0.000  0.000  0.000
0.000 -0.310 -2.498 -0.488  1.000 -0.158  0.000  0.000  0.000  0.000
0.000 -0.742 -1.950  0.294 -0.001  1.085  0.000  0.000  0.000  0.000
0.000  0.000  0.000  0.000  0.000  0.000  1.000  0.000  0.000  0.000
0.000  0.000  0.000  0.000  0.000  0.000  0.000  1.000  0.000  0.000
0.000  0.000  0.000  0.000  0.000  0.000  0.000  0.000  1.000  0.000
0.000  0.000  0.000  0.000  0.000  0.000  0.000  0.000  0.000  1.000
"Sigma of Converted Stripping Coefficients Matrix"
10
0.000  0.000  0.000  0.000  0.000  0.000  0.000  0.000  0.000  0.000
0.000  0.000 -0.040 -0.017  0.000 -0.016  0.000  0.000  0.000  0.000
0.000  0.000  0.000 -0.028  0.000  0.000  0.000  0.000  0.000  0.000
0.000  0.000 -0.009  0.000  0.000  0.000  0.000  0.000  0.000  0.000
0.000 -0.080 -0.103 -0.037  0.000 -0.008  0.000  0.000  0.000  0.000
0.000 -0.140 -0.068  0.013  0.000  0.000  0.000  0.000  0.000  0.000
0.000  0.000  0.000  0.000  0.000  0.000  0.000  0.000  0.000  0.000
0.000  0.000  0.000  0.000  0.000  0.000  0.000  0.000  0.000  0.000
0.000  0.000  0.000  0.000  0.000  0.000  0.000  0.000  0.000  0.000
```

```
0.000  0.000  0.000  0.000  0.000  0.000  0.000  0.000  0.000  0.000
"Attenuation Coefficients"
10
Total       0.00600    1.00000   0.0003
K-40        0.00800    1.00000   0.0008
U-238       0.00550    1.00000   0.0114
Th-232      0.00600    1.00000   0.0044
Cs-137      0.01000    1.00000   0.0100
Co-60       0.00800    1.00000   0.0080
MMGC1       0.00600    1.00000   0.0060
MMGC2       0.00650    1.00000   0.0065
LOW         0.02000    1.00000   0.01
MID         0.01500    1.00000   0.005
"3D Attenuation Coefficients"
10
Total       0.00350    2.00000
K-40        0.00420    2.00000
U-238       0.00320    2.00000
Th-232      0.00350    2.00000
Cs-137      0.00800    2.00000
Co-60       0.00800    1.00000
MMGC1       0.00600    1.00000
MMGC2       0.00650    1.00000
LOW         0.02000    1.00000
MID         0.01500    1.00000
"Conversion factors Counts to Activity"
11
Total       0        NoCalibration   "     "
K-40        7.95     AD_K-40         "Bq/kg"
U-238       3.87     AD_U-238        "Bq/kg"
Th-232      1.62     AD_Th-232       "Bq/kg"
Cs-137      1.88     AD_Cs-137       "Bq/kg"
Cs-137      32.96    AA_Cs-137       "Bq/m2"
Cs-137      7200     AP_Cs-137       "Bq   "
Co-60       2500     AP_Co-60        "Bq   "
Co-60       0        NoCalibration   "     "
MMGC1       0        NoCalibration   "     "
MMGC2       0        NoCalibration   "     "
"Radon"
1
0           0
"Hoehenkorrektur"
4
AltMethod   1
GroundAltDGM  1
DGMType     1
PfadDHM25   C:\Daten\Aeroradiometrie\ARM2015\Karten_DE\dgm200utm32\dgm200_utm32s.asc
"SDI Constants"
7
```

Aten	0.0053
Convert	0.00096
CosmicKorr	95.5
Back	17459.0
Gain	12.0
referenz_alt	100.0
Threshold	240.0

Paul Scherrer Institut :: 5232 Villigen PSI :: Switzerland :: Tel. +41 56 310 21 11 :: Fax +41 56 310 21 99 :: www.psi.ch